AD-A286 990

1. AGENC... USE ONLY (Leave blank)	2. REPORT DATE	3. REPORT TYPE AND DATES COVERED
	1995	Final Report

4. TITLE AND SUBTITLE

Development of Algorithms and Programs for the Ray Nonlinear Radiotomography of the Ionosphere and Radiotomography Using Middle and High-Orbital Satellites

5. FUNDING NUMBERS

F6170894W0904

6. AUTHOR(S)

Dr Viatcheslav Kunitsyn

7. PERFORMING ORGANIZATION NAME(S) AND ADDRESS(ES)

Moscow State University
Physics Dept
Moscow 119899
Russia

8. PERFORMING ORGANIZATION REPORT NUMBER

N/A

9. SPONSORING/MONITORING AGENCY NAME(S) AND ADDRESS(ES)

EOARD
PSC 802 BOX 14
FPO 09499-0200

10. SPONSORING/MONITORING AGENCY REPORT NUMBER

SPC 94-4066

11. SUPPLEMENTARY NOTES

12a. DISTRIBUTION/AVAILABILITY STATEMENT

Approved for public release; distribution is unlimited.

12b. DISTRIBUTION CODE

A

13. ABSTRACT (Maximum 200 words)

This report results from a contract tasking Moscow State University as follows: Develop algorithms for the ray nonlinear radiotomography of the ionosphere and radiotomography using middle and high-orbital satellites.

19990311028

14. SUBJECT TERMS	15. NUMBER OF PAGES
EOARD	98
	16. PRICE CODE N/A

17. SECURITY CLASSIFICATION OF REPORT	18. SECURITY CLASSIFICATION OF THIS PAGE	19. SECURITY CLASSIFICATION OF ABSTRACT	20. LIMITATION OF ABSTRACT
UNCLASSIFIED	UNCLASSIFIED	UNCLASSIFIED	UL

99-00034

A-1

Development of Algorithms and Programs for the Ray Nonlinear Radiotomography of the Ionosphere and Radiotomography using middle and high-orbital satellites

Final report (EOARD SPC 94-4066)

Principal Investigator

Professor V.E.Kunitsyn

List of Investigators:

Dr. E.S.Andreeva
Dr. I.Yu.Zhidovlenko
Dr. A.B.Usachev
O.G.Razinkov
A.Yu.Popov
L.D.Bigvava
I.A.Nesterov

Contents.

1. Introduction

The past decade witnessed an extensive development in the field of satellite radiotomography (RT) of the ionosphere, which significantly extends the capabilities of research of the nearspace environment. Some experimental teams in many countries have been working on the problem of reconstruction of ionospheric sections by means of ray RT methods. Since 1990 a number of experimental studies in this direction have been reported in the literature [1-17]. Some comparisons with the data from incoherent scattering radars and ionosondes have generally shown an acceptable quality of tomographic reconstructions [12-14]. All the shown experiments were realized by middle-orbit navigation satellites (1000 km, like "Transit"-USA and "Cikada"-Russia). Surely the development of these data by means of high-orbital navigation satellites is of great interest (for example, like "GPS"-USA and "GLONASS"-Russia (20,000 km)). The consideration of a combination of middle and high-orbital satellites is usefull, too. Such radiotomographic systems allow to search the structure of magnetosphere, protonosphere, etc, and to study the influence of these mediums on navigation and connection systems in details.

In connection with the experiments performed the questions arise concerning the data quality, the accuracy of tomographic reconstruction. Given strong gradient of electron density, one of substantial contraints imposed on ray radiotomography is the ray refraction. Ignoration of refraction limits the resolving power of RT systems. Taking the refraction into account, it allows to increase the possible resolving power, but it transforms to more complex problems of nonlinear RT. Supposed that the set of integrals over refractable rays, which curvature is determined by the propagating medium are known. That is why the exploration of abilities of nonlinear RT is seems important.

The aim of this work is to develop algorithms and programs for the ray nonlinear (with refraction) Radiotomography of the Ionosphere and Radiotomography using middle and high-orbital satellites.

Part 1.

Algorithms and Programs for Radiotomography using middle and high-orbital satellites.

1.1. Description variants of satellite Radiotomography using middle and high-orbital satellites of opportunity.

As modern navigation systems on high-orbital satellites (like "GPS" - USA and "GLONASS" - Russia) are operated on a frequency of 1 GHz, in this case it is enough to consider problems of linear tomography ignoring the ray refraction. The ray refraction is a factor at a frequency of hundreds of MHz. Such problems of radiotomography would be considered in the second part. Modern navigation systems on high-orbital satellites mentioned in the first part ("GPS" or "GLONASS") are supposed to operate on frequences nearly 1.2 and 1.5 GHz.

Firstly let us remind the main relationships which connect the experimentally measured physical values with the parameters of propagating medium. Known is [18-20] the differential phase between the two L-band carriers, at f_1 = 1.575 GHz and f_2 = 1.227 GHz can be used to make precise relative total electron content (TEC) measurements. The differential group delay between the 10.23 MHz modulation on the two L-band carriers is used to fit these precise relative TEC measurements to an absolute scale.

The difference of simultaneous dual-frequency GPS code measurements P_1, P_2 (in meter) equals the TEC along the transmitter-receiver ray [18-20].

$$TEC \equiv \int Nd\sigma = S(P_2 - P_1) + e_p \tag{1}$$

Where $\int Nd\sigma$ denotes the integration of the electron density N along the signal path. Merging all bias terms (differential instrumental group delays in the receiver and in the satellite, and multipath and observation noise) yields the error $e_p[m^{-2}]$.

The scaling factor S converts units of distance [m] to units of TEC (electrons/m^2) and is derived from the GPS frequencies with:

$$S = 0.025 \frac{f_1^2 * f_2^2}{f_1^2 - f_2^2} = 9.52 * 10^{16} \, m^{-3}$$

The observation equation for the TEC from phase measurements (phase puth) Φ_1, Φ_2 [m] looks similar [18-20]. The error e_Φ [m^{-2}] include the differential instrumental biases of the phases and additional bias term exist due to the carrier phase ambiguities M_1, M_2.

$$TEC \equiv \int N d\sigma = S(\Phi_2 - \Phi_1) + S(M_1 \lambda_1 - M_2 \lambda_2) + e_\Phi \qquad (2)$$

Where the λ_1, λ_2 denotes the wavelengths of sounding waves.

Thus phase and group delay measurements by means of modern navigation systems GPS and GLONASS allow to find linear integrals of the electron concentration. The following fact is of great importance for further consideration of radiotomographic problems by means of GPS and GLONASS. TEC can be measured to a relative accuracy of approximately $3*10^{14} el / m^2$, and absolute values can be determined to approximately $(1 - 2)*10^{16} el / m^2$, plus any unknown GPS satellite differential code offsets [21-24]. In other words given methods allow to determine relative TEC precisely enough, but they showed unacceptable mistake in determination of absolute TEC. This case is similar to the situation in Transit-Cikada RT systems where major difficulty is that the linear integral of the electron concentration is proportional to the absolute phase Φ, whose accurate determination is practically impossible, but the differences of linear integrals (phase difference) are measured with high precision. That is why the new approach was taken earlier to determine the difference of linear integrals [1-3, 25], which (approach) brought satisfyed results [1-3, 13, 14, 17]. Further the same approach would be taken to determine the difference of linear integrals.

Let us consider possible variants of using of midlle and high-orbital satelittes for radiotomographic purposes. Mostly geometry of experiments is essential for qualitative radiotomographic reconstruction: the correlation of receivers and transmitters, the way of crossing the reconstrtuctive area by rays, angle between rays. The program "SATTOMO" was worked out to make geometrical analysis of registration scheme. Given program allows to analyze radiotomographic registration schemes, which use ground receivers and measuring systems on satelittes with cyclic

orbits, such as Transit, Cikada, GPS, GLONASS, Microlab, etc. The description of this program is cited in the end of this article.

Heights of orbits of satellites in program SATTOMO can be varyed, respectively the period and the rotating angular velocity is changing. Zero height is corresponded to receivers on the Earth, whose angular velocity is supposed to be zero. Given critical altitude is the minimum height of passage of rays over the Earth . This height can be chosen equal to zero. In other cases the choise of this height limits the range of ray registration, and, for example, limits the rays passing through lower ionosphere. If the number of satellites is given, it is possible to determine the direction of satellites rotation in any of two orbits (+ counterclockwise, - clockwise) Angular location in the initial moment of time is given in degrees in polar coordinate system where the zero angle is corresponded to horisontal X-coordinate. Program also includes the setable time of tomographic measurments T_m in seconds, time interval between drawing of two neiboring rays (convenient time is 30-60 s , if the less time interval is chosen, the picture of rays will be too densely) and time of drawing of the total picture on the screen in seconds. The last is wished to be little (5-10 seconds) to have an opportunity to examine the satellite motion.

The use of the only high-orbital navigation system like GPS-GLONASS with the ground receivers for purposes of radiotomography of ionosphere and protonosphere appears to be unperspective with the respect to little angular velocity of high-orbital satellites. Indeed, for example, the GPS angular velocity is equal to $\omega = 0.0001456 \, rad \, / \, sec$, what is seven times less than the middle-orbital satellite angular velocity equal to $0.0009966 \, rad \, / \, sec$. Such satellites pass small distances in tens of minutes (20-40) and fill a small angle. The use of a greater time intervals is almost impossible because of the time change in ionosphere. In fig.1a shown $\Delta\theta$ - is the angle of filling the space by rays over the ground receiver during the GPS fly over the head. This angle $(\Delta\theta \cong \Delta\alpha(1 + R / H))$ is close to polar angle of satellite $\Delta\alpha$, as the height of satellite is H = 20200 km what is essentially exceeds the Earth radius R = 6370 km. Polar angle is changes proportionally to the time $\Delta\alpha = \omega t$. For example, in one hour (equal to 1/12 of period of rotating) the polar angle will change only for $2\pi / 12 = 30°$. The intersection of the rays (fig.1b) for receivers located at a distance of $\Delta\tau$ (on the Earth) occurs on the height $h_0 \approx \Delta\tau / 2 \tan(\Delta\theta / 2) \approx \Delta\tau / 2 \tan(\omega t / 2)$, what is (for $t \approx 1800s$) $h_0 \approx 12\Delta\tau / \pi$. If the distance between receivers is greater than 250 km, than the rays of neiboring receivers are intersected on heights more than 1000 km. To make the rays intersect in the lower boundary of ionosphere (150 km), receivers should be located densely
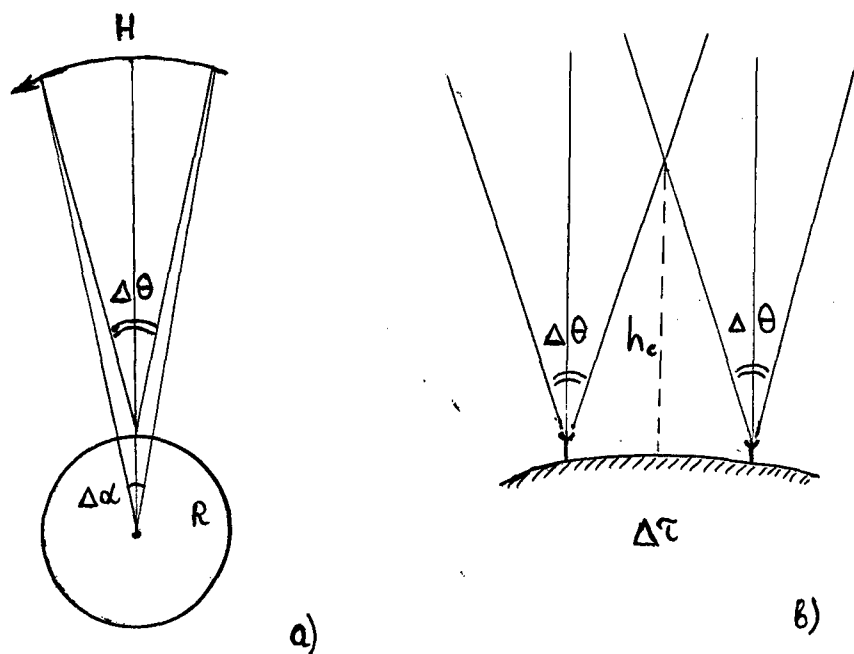
Fig. 1

The Geometry of the RT Measurements
Relative time 01:00:00
1st orbit (4): 0 km, T = 5066.1 sec, w = 0.0000000 rad/sec
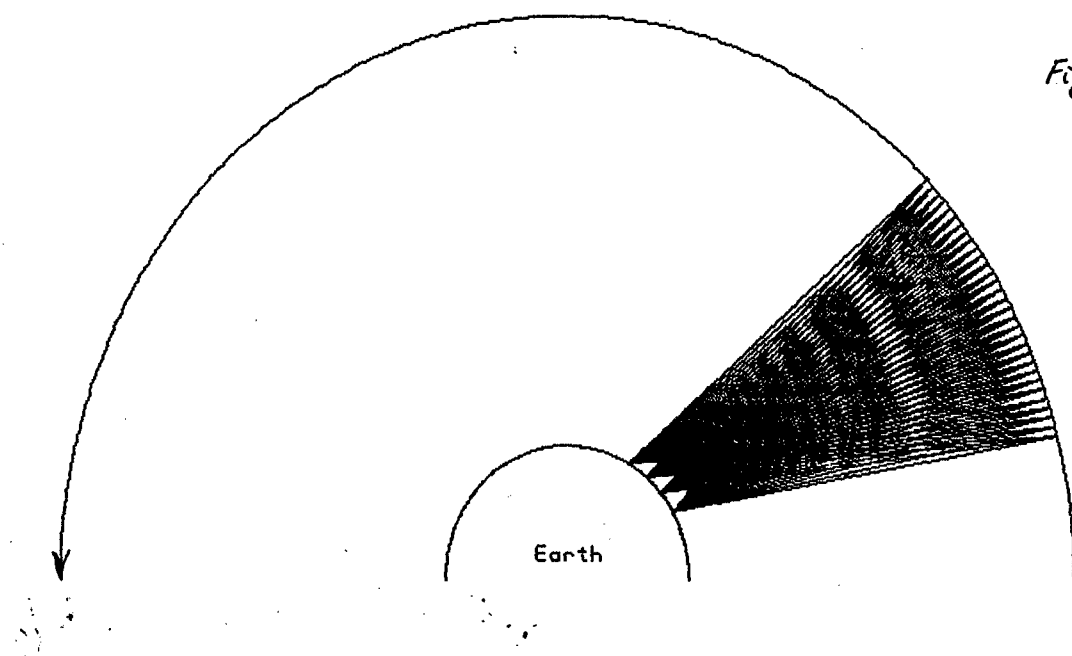2nd orbit (1): 20200 km, T = 43149.0 sec, w = 0.0001456 rad/sec
Critical altitude: 0 km

Fig. 2

($\Delta \tau \leq 60km$). Fig.2 describes the geometry of radiotomographic experiment with one and four receivers on the Earth (angular location $30°,40°,50°,60°$). Even after an hour of measurings the essential "holes" were taken place, where the rays didn't get into. The chosen distance between receivers was too great to examine the details in such a scale. Picture didn't change high-quality , as the receivers have been coming together, only the size and height of "holes" were reduced. Geometry of experiments appears to be unsuitable for qualitative radiotomographic reconstruction with the use of high-orbital satellites and receivers on the Earth. Next two pictures show bad geometry and the existance of "holes" for four ground receivers (T_m =3600 s) and for two GPS satellites (fig.3). The same for two GLONASS satellites (fig.4). However the use of network of ground receivers on the given square, each of that registrates signals simultaniously from GPS and GLONASS satellites in various directions is waited to be perspective. Such a system allows to determine parameters of ionosphere in three-dimensional area over the given region.

The using of combination of different satellite systems appears to be more perspective for radiotomography. Similar satellite systems were already worked out for scientific investigations. Recently, on April, 3, 1995 Orbital Sciences Corporation successfully launched the Microlab-1 scientific spacecraft (with altitude 600 km). However the only middle-orbital satellite (with altitude equal to 500-2000 km) also does not give the good geometry of experiment. Fig.5-6 show the schemes of experiments with one middle-orbital satellite $(T_m = 1800s)$ in combination with high-orbital satellites: one Microlab with two GPS (angular location of GPS in the initial time moment - 20, 110 degree) and Microlab (25 degree) (pic.5), and one Transit (30 degree) with three GLONASS (angular locaton in the initial time moment - 15 , 60 , 105 degree) (pic.6). These pictures show slight intersection of rays. With the help of such a scheme it is possible to explore only part of protonosphere, where rays are intersecting, under the condition that this area has strong enough local disturbance and the contribution of inside areas of protonosphere is negligible.

The geometry of experiment is essentially better if the combination of a few middle-orbital satellites on the orbit with high-orbital satellites is used. Fig.7 gives the scheme of an experiment with three satellites Transit (angular location of the initial time moment - 0, 30, 60 degree) and one GPS (15 degree). It is seen that thirty minutes measurements allow to reconstruct the structure of protonosphere on a wide enough band. Fig.8 describes the scheme of radiotomographic registration with three Transit (angular locations in the initial time moment 0, 30, 60 degree) and three GLONASS satellites (angular locations in the initial time moment 15, 60, 105 degree). Here thirty minutes measurements allow to reconstruct the structure of protonosphere

The Geometry of the RT Measurements
Relative time 00:30:00
1st orbit (4): 0 km, T = 5066.1 sec, w = 0.0000000 rad/sec
2nd orbit (2): 20200 km, T = 43149.0 sec, w = 0.0001456 rad/sec
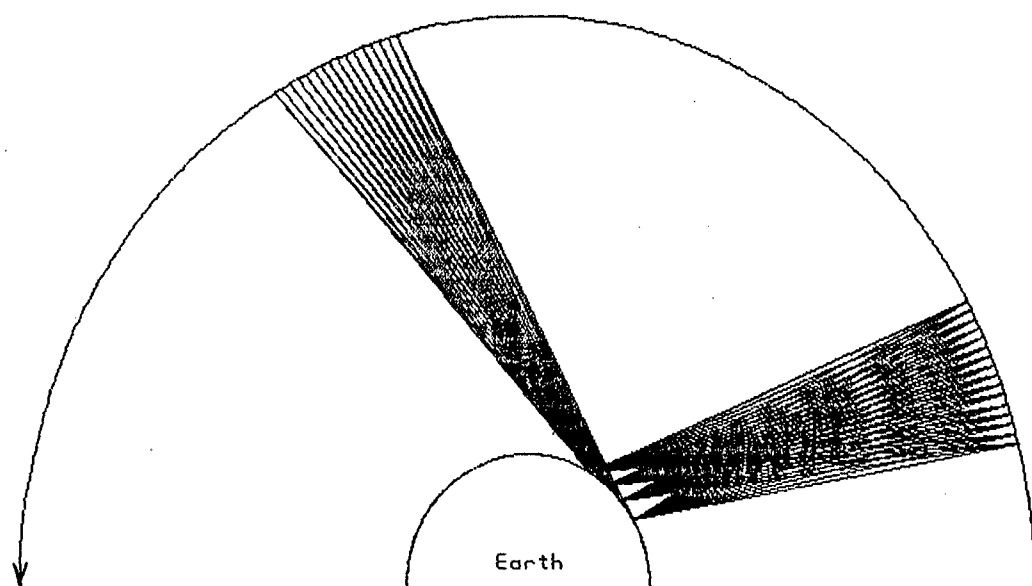Critical altitude: 0 km

Earth

Fig. 3

The Geometry of the RT Measurements
Relative time 00:30:00
1st orbit (4): 0 km, T = 5066.1 sec, w = 0.0000000 rad/sec
2nd orbit (2): 19100 km, T = 40497.5 sec, w = 0.0001551 rad/sec
Critical altitude: 0 km

Earth
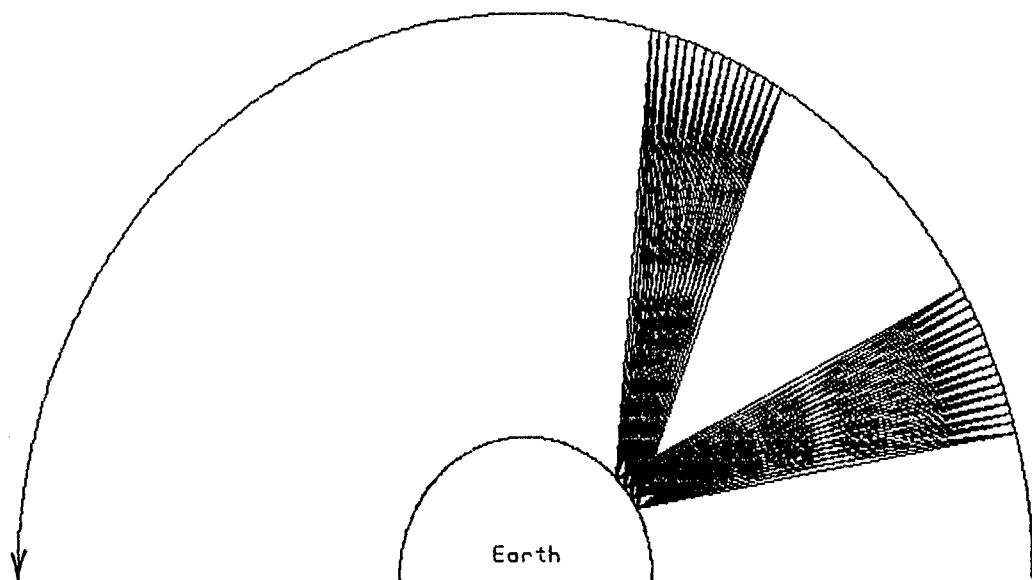
Fig. 4

The Geometry of the RT Measurements
Relative time 00:30:00
1st orbit (1): 600 km, T = 5798.3 sec, w = 0.0010836 rad/sec
2nd orbit (2): 20200 km, T = 43149.0 sec, w = 0.0001456 rad/sec
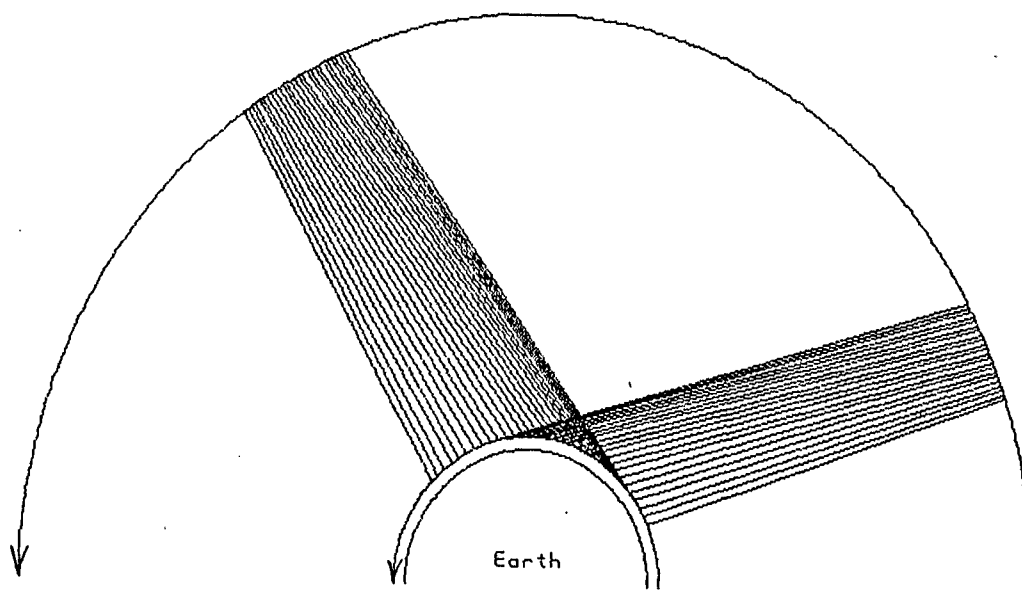Critical altitude: 600 km

Earth

Fig. 5

The Geometry of the RT Measurements
Relative time 00:40:00
1st orbit (1): 1000 km, T = 6304.5 sec, w = 0.0009966 rad/sec
2nd orbit (3): 19100 km, T = 40497.5 sec, w = 0.0001551 rad/sec
Critical altitude: 1000 km

Earth

Fig. 6

The Geometry of the RT Measurements
Relative time 00:30:00
1st orbit (3): 1000 km, T = 6304.5 sec, w = 0.0009966 rad/sec
2nd orbit (1): 20200 km, T = 43149.0 sec, w = 0.0001456 rad/sec
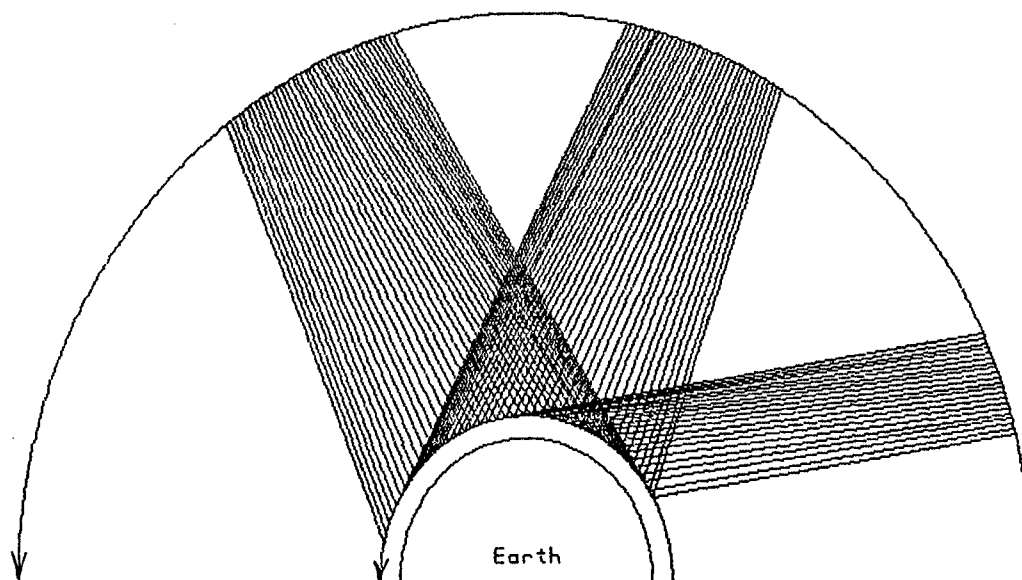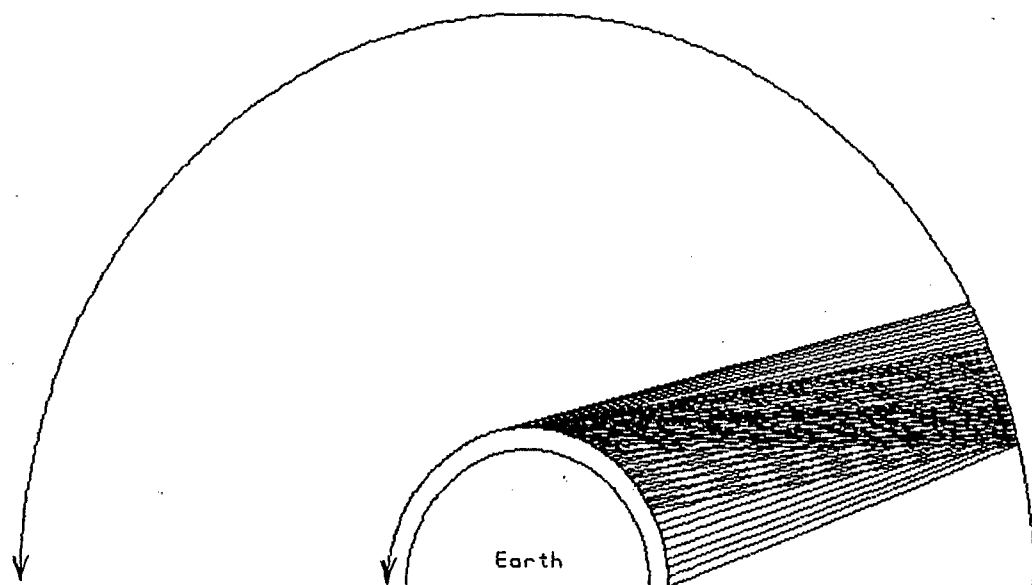Critical altitude: 1000 km

Earth

Fig. 7

The Geometry of the RT Measurements
Relative time 00:30:00
1st orbit (3): 1000 km, T = 6304.5 sec, w = 0.0009966 rad/sec
2nd orbit (3): 19100 km, T = 40497.5 sec, w = 0.0001551 rad/sec
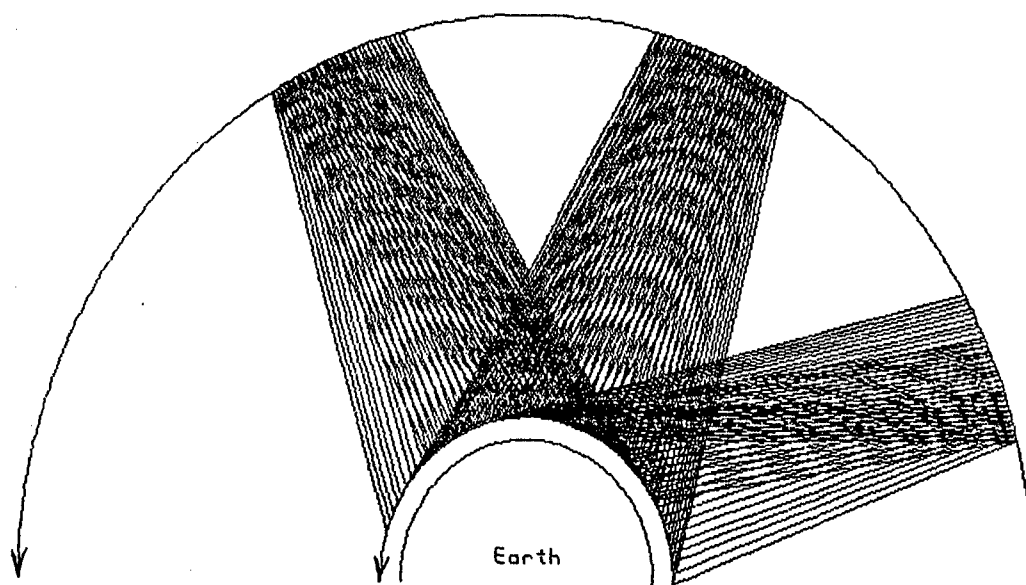Critical altitude: 1000 km

Earth

Fig. 8

in three intersective bands. Though this geometry is worse than a typical geometry of experiments on satellites Cikada and Transit [1-17], as the range of angles of intersection between rays is smaller, nevertheless, as it would be shown lower, it allows to get radiotomographic cross-sections of protonosphere.

It is a remarkable fact that the use of several middle-orbital satellites, rotating in the opposite direction, gives a good geometry with a set of fan beams. Fig.9 shows the scheme of experiment with one GPS and three Microlab satellites (angular location in the initial time moment   90, 120, 150 degree), rotating in the opposite to GPS (80 degree) direction. After the registration period of twenty minutes ($T_m = 1200s$) the ray structure, which consists of three beams is seen well. Fig.10 shows one of such a beam with the height of "focus" multiplicity of 12000 km for one Microlab satellite. Let us cite one more interesting example of using of combination of middle and high-orbital satellites. Fig.11 shows the scheme of fifteen minutes ($T_m = 900s$) measurings between one Transit satellite (angular location in the initial time moment 90 degree) and one GPS (25 degree). Such satellite orientation allows to fill the area of nearearth ionosphere by quasiparallel rays. Fig.12 describes analogious scheme ($T_m = 960s$) with one Transit satellite (angular location in the initial time moment 90 degree) and two GLONASS (0, 45 degree). This geometry allows to fill the area around all the Earth by quasiparallel rays.

First of all we want to remind the geometrical equations, which connect the transmitters and recievers locations [3,6,8]. Here we will conditionally indicate the locations of transmitters and recievers on the concrete orbits, meaning that the observing result will not depend on changing this locations. We introduce a series of parameters characterizing the geometry of the recording scheme in polar coordinates (r, α). In Fig.13 (R_1, α_i) - are the coordinates of one of the receivers located on the first orbit $r = R_1$ (also the reciever can locate on the Earth surface - $R_1 = R$ - Earth radius); (R_2, α_0) - are the coordinates of the satellite with transmitter on the second orbit $r = R_2, R_2 > R_1$; β is the elevation of the R_2 satellite; $\varphi = \beta - \pi / 2$ is the angle to the satellite measured from vertical; O is the center of the earth; axis O-O' is axis of the polar coordinate system. We consider here, that satellites rotate in single or nearer planes, what is important for RT purposes. On the basis of simple geometrical relations for any point in the ionosphere with coordinates (r, α) located at the distance of l from the receiver the following equations are satisfied:

The Geometry of the RT Measurements
Relative time 00:20:00
1st orbit (3): 600 km, T = 5798.3 sec, w = 0.0010836 rad/sec
2nd orbit (1): 22000 km, T = 47607.0 sec, w = 0.0001320 rad/sec
Critical altitude: 600 km

Earth

Fig. 9
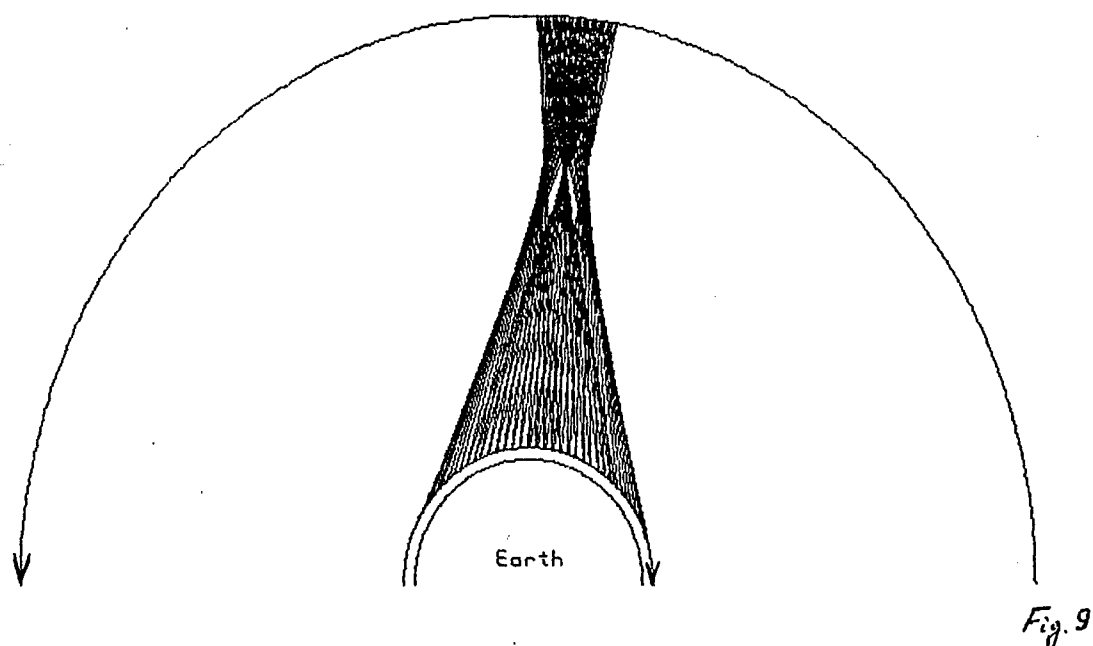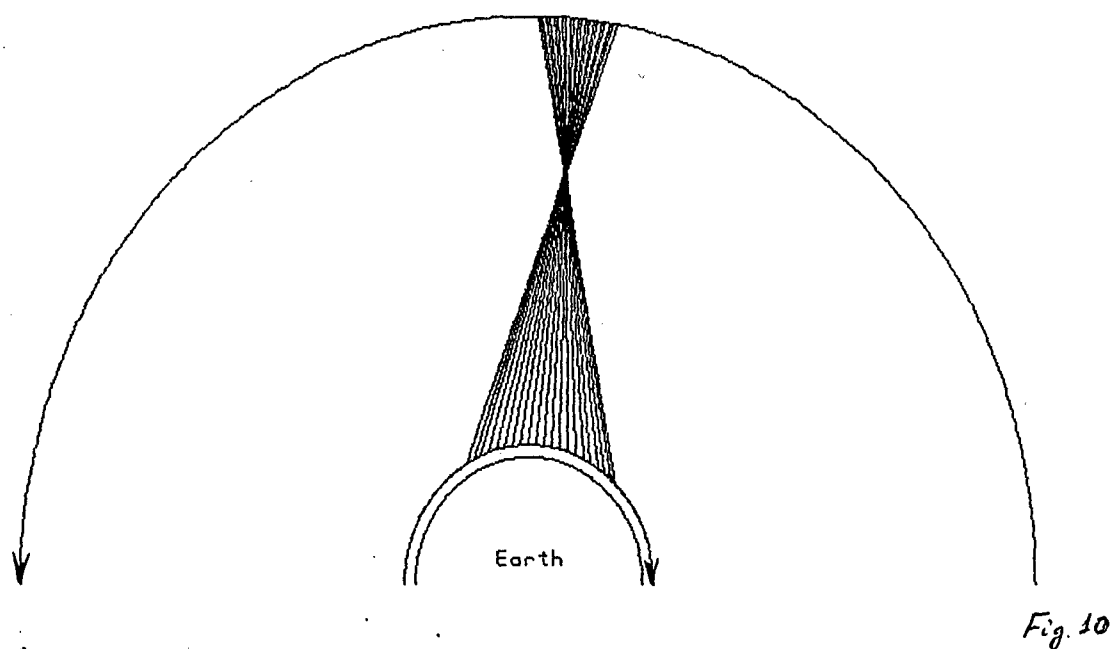
The Geometry of the RT Measurements
Relative time 00:20:00
1st orbit (1): 600 km, T = 5798.3 sec, w = 0.0010836 rad/sec
2nd orbit (1): 22000 km, T = 47607.0 sec, w = 0.0001320 rad/sec
Critical altitude: 600 km

Earth

Fig. 10

The Geometry of the RT Measurements
Relative time 00:15:00
1st orbit (1): 1000 km, T = 6304.5 sec, w = 0.0009966 rad/sec
2nd orbit (1): 20200 km, T = 43149.0 sec, w = 0.0001456 rad/sec
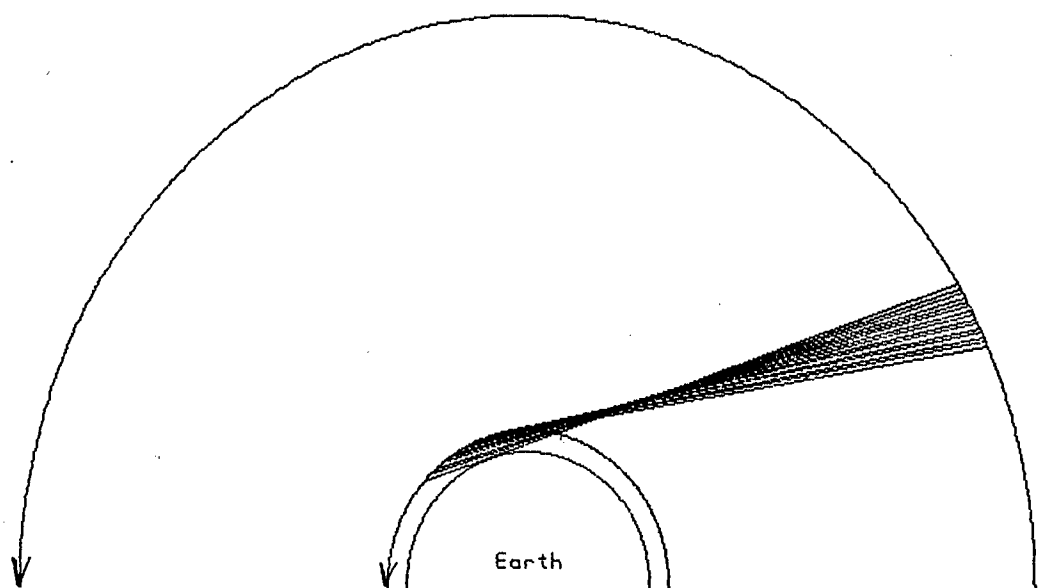Critical altitude: 0 km

Earth

Fig. 11

The Geometry of the RT Measurements
Relative time 00:21:00
1st orbit (1): 1000 km, T = 6304.5 sec, w = 0.0009966 rad/sec
2nd orbit (2): 19100 km, T = 40497.5 sec, w = 0.0001551 rad/sec
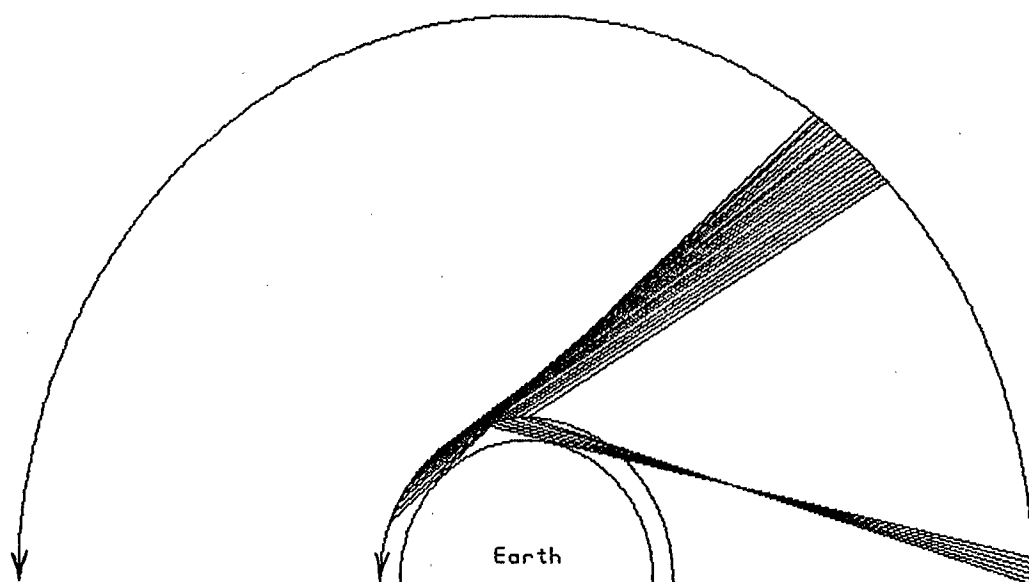Critical altitude: 0 km

Earth

Fig. 12

$$\frac{l}{\sin(\alpha_i - \alpha)} = \frac{r}{\sin(\pi / 2 + \beta)} = \frac{R_1}{\sin(\pi - (\pi / 2 + \beta) - (\alpha_i - \alpha))}.$$

From this, we obtain an equation for $r(\alpha)$ of the straight (β =const) ray

$$r(\alpha) = R_1 \cos(\beta) / (\cos(\beta + \alpha_i - \alpha)) \tag{4}$$

and the relation which is inverse of it

$$\alpha(r) = \alpha_i + \beta - \arccos(\frac{R_1}{r} - \cos \beta) \tag{5}$$

The relation between β and α, r follows from (4):

$$\tan \beta = (\cos(\alpha_i - \alpha) - R_1 / r) / (\sin(\alpha_i - \alpha)) \tag{6}$$

Using (5), we obtain a formula for an element of the ray of length $d\sigma$:

$$d\sigma^2 = [1 + r^2 (\frac{d\alpha}{dr})^2] * dr^2 = \frac{r^2}{r^2 - R_1^2 \cos^2 \beta} * dr^2 \tag{7}$$

Then, the relation for the measured linear integrals (1,2) with respect to the electron concentration will have the form

$$\text{TEC} = \int \frac{N(r, \alpha) r dr}{\sqrt{r^2 - R_1^2 \sin^2 \varphi}}.$$

In the place of the polar coordinates (r, α), hereafter it is convenient to use the orthogonal system $(h, \tau): h = (r - R_1)$ is the height above the first orbit or above the earth's surface and $\tau = \alpha R_1$ is the "transverse" (horizontal) distance along first orbit. Here, ray equation (4) will no longer be a straight line

$$h(\tau) = R_1 [\frac{\cos \beta}{\cos(\beta + (\tau_i - \tau) / R_1)} - 1] \tag{8}$$

Here, $(\tau_i, h = 0)$ are the coordinates of the receivers. The relation which is the inverse of (8) is similar to (5).

$$\tau - \tau_i = R_1[\beta - \arccos(\frac{R_1}{R_1 + h}\cos\beta)] \qquad (9)$$

In this case, subject to (7), the linear integrals of type (1-2) have the form

$$\int_0^{h_0} \frac{F(h,\tau)(R_1 + h)dh}{\sqrt{R_1^2 \sin^2\beta + 2R_1 h + h^2}} = I(\beta, \tau_i) \qquad (10)$$

Integration with respect to the ray connecting receiver i $(\tau_i = \alpha_i R_1)$ to the satellite is replaced according to (7) by integration with respect to the height above the first orbit to the height of the satellite h_0. The elevation β is determined (6) by position of the satellite (h_0, τ_0). The linear integral $I(\beta, \tau_i)$ is dependent on the coordinate of the receiver τ_i and the elevation of the satellite β. The linear integral is the TEC here, the reconstructed function F will be proportional to N. Since there cannot be a large number of receivers and the range of angles β is limited, it is inadvisable to examine methods for analytical inversion of such linear integrals and methods for integral transformations. In given case small-positions (smallforeshortening) tomography is intended from the start to solve the problem in discrete form and to use algebraic reconstruction algorithms or methods for expansion into finite series.

Description of the the programm "sattomo" for vizualisation geometry of satellite RT experiments.

This program allow to view on the screen the different versions of the radiotomography measurements geometry for the one- and two-orbit satellite configurations.

Input parameters and files.

Command line format is: SAT2.exe <config_file_name> [p]. First parameter - the name of file that defines all the input parameters for RT system geometry.

Second parameter (optional), if set, allow to print geomerty picture on the EPSON-compatible printer.

The configuration file has the following format: several lines started at 1st position in form: PAR1,PAR2,.... [; comments]:

Line 1:   H_low H_high H_crit

Line 2:   NSat1[+ or -] NSat2[+ or -]

Line 3:   Pos1(1) Pos1(2) ..... Pos1(NSat1)

Line 4:   Pos2(1) Pos2(2) ..... Pos2(NSat2)

Line 5:   PassTime Step DrawTime

The above mentioned parameters are:

- H_low, H_high - orbit heights (kilometers) of 2 groups of satellites. H_low=0 defines the receiver on the Earth's surface. - H_crit - minimum height for the ray traectory. If H_crit=0, the ray may touch the Earth's surface.

- NSat1, NSat2 - the number of satellites on the heights H_low, H_high. The signs '+' or '-' are optional, but if they are set, must follow immediately after this numbers and define the direction of the satellite moving (clockwise or opposite). If no sign character set, '+' assumed.

- The arrays of Pos1 and Pos2 define the initial positions of satellites. Must be set in degrees.

- PassTime - full time of real measurements.

- Step - the ray drawing step time.

- DrawTime - time that needs to draw picture on the screen.

The tree last parameters must be set in seconds.

1.2. The solution of the direct problem of TEC calculation for high-orbital satellites Radiotomography.

The purpose of this section is to describe the technique and program for solving the direct problem of ionosphere radio probing, i.e. the problem of obtaining the TEC and the TEC difference from the data on the electron density distribution. In view of calculation the direct problem solution amounts to calculatiry the integral (10), i.e. the TEC or the TEC difference of such integrals for a small variations of the satellite positions. For the computer modeling of RT

problems it is necessary to calculate a series of such integrals for arbitrary positions of the receivers and the transmitters on the satellites, therefore we accomplished the program for calculating TEC and the TEC difference for arbitrary positions of the receivers and the transmitters on the satellites.

Since the integrand has no peculiarities, the calculation can be performed using the rectangle technique or the Simpson method. Let us evaluate the necessary step of numerical integration and the accuracies obtained in this way. It is well known that errors of numerical integration by the rectangle method ε_r and the Simpson method ε_s are equal to:

$$\varepsilon_r = \frac{S^3 F^{(2)}}{12 m^2}, \qquad \varepsilon_s = \frac{S^5 F^{(4)}}{2880 m^4} \qquad (11)$$

where S is the integration interval length (the distance between satellites), m is the number of the integral discretization elements. Integration errors made using the rectangle and Simpson methods are proportional to the values of the second and fourth derivatives, respectively, of the integrand at a certain point within the integration interval. For an approximate estimation of errors it is sufficient to evaluate the second and fourth derivatives as a result of dividing a characteristic value of the function F by the square or the fourth power "a", respectively, of the structural irregularities of F. Limitations associated with diffraction effects as well as those of the linear tomography problem make it impossible to reconstruct details smaller than 10-20 km using the method of linear ray RT [3,8], therefore $a \geq 10 - 20km$ The value of m is equal to the result of dividing S by the integration step Δs. Hense the estimations of absolute and relative errors are:

$$\varepsilon_r \leq \frac{SF}{12}(\Delta h / a)^2, \qquad \varepsilon_s \leq \frac{SF}{2880}(\Delta h / a)^4.$$

$$(12)$$

$$\frac{\varepsilon_r}{I} \approx \frac{\varepsilon_r}{SF} \leq (\Delta h / a)^2 / 12, \qquad \frac{\varepsilon_s}{I} \approx \frac{\varepsilon_s}{SF} \leq (\Delta h / a)^4 / 2880.$$

When the integration step $\Delta s = 0.5km$ and a=20km the relative error of the rectangle method is $0.5*10^{-4}$ (for the Simpson method it is smaller than 10^{-11}) which is quite satisfactory for RT applications.

Description of the program for calculation TEC and TEC-difference for the high-orbit RT measurements

System Requirements

- Computer: IBM AT-486 or compatible (with coprocessor)
- Operating System: MS-DOS or PC-DOS version 3.0 and later
- Memory: at least Extended memory 8 Mbytes
                   (depends on geometry and type of
                   approximation reconstructed function)
- Hard Disk Space: 35 Mbytes
- Software: NDP-FORTRAN-486 Compiler Ver.3.1
                   NDPLink Ver.3.0 (C) MicroWay, Inc.

1. Program <dir_rth1.for>

This program solves direct problem for high-orbit RT measurements, namely, determines the model structure and calculates the TEC or TEC-difference integrals on the model structure.

Input parameters and files:

When starting program, you may choose the type of RT measurements (TEC or TEC-difference). Then program asks about inegrals to calculate. If you need only model structure you can answer 'No'.

Input file <task.dir> contains information about RT measurements geometry and defines the names for output files. The example of this file is enclosed. It contains the following lines:

'model.fun' - input file that describes model structure

'model.grd' - output file with model structure (GRD-format)

NF   NR - number of discrets on the horizontal and vertical grid

0.   H_GPS - high orbit altitude (GPS satellites) over low orbit in km

TFIST TFIN - size of reconstructed area in km on the low orbit height

STEPS   - number of the discrete steps along the ray

Nrec   - number of receivers

LOs LOe HOs HOe Nrays - Nrec lines with initial and final positions of
                satellites on the low and high orbits in km and number of

rays for this couple of satellites

'lin_int' - Nrec lines with the names of output files for integrals

for each receiver

The model structure is determined by function <FMODEL> which uses functions <HOMCOS>. Function parameters are defined in file <model.fun>. The example of this file is enclosed.

Output files:

MODEL.GRD - file with model structure (GRD-format)

Files <lin_int> - arrays of either TEC or TEC-difference integrals

Compilation

mf77 dir_rth1.for -ol -486

RUN

ndprun dir_rth1.ltl

1.3. The construction of the projection operators for the high-orbital RT measurements using various approximation methods.

In this section we consider the various methods to constuct the projection operator L that translates the sought function of the electron concentration distribution F into a set of integrals (TEC) I:

$$LF = I$$

First of all we shell perform the discretization procedure for equations (1) to prepare the numerical calculations. We shall use the orthogonal coordinate system (h, τ), where h - is the height above the low satellite orbit and τ - is transverse distance along this orbit. To digitize the sought function $F(h, \tau)$ in a fixed rectangular $(m_o * n_o)$ grid we divide the rectangular reconstruction region into m_0 heights (m < m_0) and n_0 horizontal samples (1 < n < n_0) and replace function by a piecewise-constant approximation, or to represent F by a system of $(m_0 * n_0)$ basis

functions equal to unity in certain rectangle and zero in all others. The value of the function $F(h, \tau)$ in a fixed ($m*n$) rectangle we define as F_{mn}.

We perform digitization of the linear TEC integrals $I(\beta, \tau_i)$ (10) according to the initial direction to the satellite on the high orbit from receiver number i placed on the low orbit satellite with current coordinate τ_i. The set of elevation β_{ij} (6) of all moving receivers define a series of discrete values of the linear integrals (10) $I_{ij} \equiv I(\beta_{ij}, \tau_i)$, where i - receiver number, j - ray number from set for receiver i. The number of rays is determined by the parameters of the recording system. The point in the rectangles at which the samples of $F(h, \tau)$ are selected is not especially important; this may be at the middle of the rectangles or nodes of the grid.

The simplest method of project operator discretization is piecewise-constant approximation, when the coefficients of matrix A are proportional to the ray length in elements of the discrete grid. Designating the length of ray (i,j) in cell (m,n) as $L_{i,j}^{m,n}$, we obtain the system of linear equations

$$L_{i,j}^{m,n} F_{m,n} = I_{i,j}$$

or after "renumbering" of the ray (i,j) - J and the cells of the ionosphere (m,n) - M

$$L_J^M F_M = I_J \tag{13}$$

System (13) may be either overdetermined or sub-definite. The problem of high-orbit tomographic reconstruction according to TEC measurements is to determine the set of discrete samples $\{F_{mn}\}$ in the known grid according to the set $\{I_{ij}\}$.

This simple method of projection operator constructing, however, gives the high error value of the direct problem solution (particulary for the small number of discrete elements). Besides that the piecewise-constant approximation is invalid for the problem of high-orbit RT according to TEC-difference measurements. The fact is that the data here will be derivatives of linear integrals of type (10): $D = dI / d\alpha_0$, or finite-difference ratios of the increment ΔI of the linear integrals to the increment $\Delta \alpha_0$ of the satellite coordinate. The difference of TEC measured in the experiment can be determined by the TEC (1) derivative. Because the satellites move uniformly along a circular orbits it is possible to express the difference of TEC by means of the derivative with respect to the angle of the satellite on the

high orbit α_0 and, hence, TEC-difference tomography data are proportional to $\Delta I / \Delta \alpha_0$. The derivatives of the linear integrals in a piecewise-constant approximation of the sought function F will be discontinuous. This is because each linear integral is the sum of integrals over the set of cells. As the elevation of the high orbit satellite changes, the ray encounters a new cell; the integral with respect to every of this cells is a continuous function of the angle of the satellite α_0, but the derivative of the linear integral with respect to α_0 will contain a discontinuity when the ray contacts the corner of each cell. Therefore, the piecewise-constant representation of the function to be reconstructed is not appropriate to solve the TEC-difference problem correctly.

To ensure continuity of linear TEC integrals with respect to the coordinates of the both satellites α_0 (or elevation β) the matrix L_{JM} for transition from the function to be reconstructed to linear integrals should be calculated differently. The main idea of other methods of RT operators (matrices) design is the increase of the approximation order for the reconstructed function and, hence, for the matrix L. We used the piecewise-planar approximation based on the triangular elements, product of linear approximations, product of local spline approximations and the modification of the last method also including derivatives of the function on the discrete grid. The accuracy of the direct problem solution is increased with the higher approximations and the distinction between constructed and the real "natural" operators is reduced. The matrix of the direct problem constructed by these methods $L_{JM}: F_M \rightarrow I_J$ is continuous with respect to the angle of the satellite on the high orbit α_0, hence, in place system (13) it is possible to obtain a system for TEC-difference data by differentiating (13) with respect to the angle α_0:

$$A_{JM} F_M = D_J \tag{14}$$

Here, $D_J \equiv \Delta I_J / \Delta \alpha_0$ are TEC-difference data and $A_{JM} \equiv \Delta L_M / \Delta \alpha_0$ is finite - difference ratio (or derivative) of the matrix L_{JM} to the increment of the angle.

In this section we consider examples of constructing smooth projection operators of the direct problem wich are smooth by the satellite angle. The examples of constructing the L_{JM} matrices of the transition from the reconstructed function to the linear integrals (matrices of projection operators) are useful for both TEC-difference RT and for the TEC RT but the first is preferable. The advantages of the

first method was repeatedly shown on the example of phase-difference RT [6,8,25].

One must construct such a L_{JM} matrix that would provide the smooth of linear integral over the satellite angle using the piecewise-planar approximation of the sought function on the basis of triangular elements. Such approximation ensures the smoothness of the matrix L_{JM} to be constructed. The smooth function $F(h, \tau)$ is replaced by a continuous polyhedral approximation surface, according to which the derivative with respect to the satellite angle of the linear integrals is already a continuous function. Triangular elements are obtained naturally from a grid of rectangles: each cell (m,n)

$$(\tau_m, \tau_{m+1}) * (h_n, h_{n+1}) = \Delta\tau * \Delta h$$

is divided by a diagonal $(\tau_m, h_{n+1}) - (\tau_{m+1}, h_n)$ running downward and left -to-right, into two triangular elements: the "lower" and "upper" elements. The function $F(h, \tau)$ within each triangular element is replaced by linear approximation

$$F(h, \tau) = a + b\tau + ch \qquad (15)$$

The values of the coefficients (a, b, c) in each finite element are determined from system of three equations for three boundary points. It is simple to immediately write expressions for the function presentation in the lower (m,n) element

$$F(h, \tau) = F_{m,n} + \frac{F_{m+1,n} - F_{m,n}}{\Delta\tau}(\tau - \tau_m) + \frac{F_{m,n+1} - F_{m,n}}{\Delta h}(h - h_n) \qquad (16)$$

and in the upper (m,n) element

$$F(h, \tau) = F_{m+1,n+1} + \frac{F_{m+1,n+1} - F_{m,n+1}}{\Delta\tau}(\tau - \tau_{m+1}) + \frac{F_{m+1,n+1} - F_{m+1,n}}{\Delta h}(h - h_{n+1}) \qquad (17)$$

As before, to simplify the notation we will renumber the values of the samples below: $F_{m,n} \to F_M$,

$$(m+1, n) \to (M+1), (m, n+1) \to (M + \Delta M), (m+1, n+1) \to (M + \Delta M + 1),$$

where ΔM is the number of cells horizontally in one row. Now we can define the result of integration of such an approximation in lower element M

$$\int w(h)Fdh = J_0 F_M + J_\tau (F_{M+1} - F_M) + J_h (F_{M+\Delta M} - F_M) \tag{18}$$

and in upper triangular element M

$$\int w(h)Fdh = J_0' F_{M+\Delta M+1} + J_\tau' (F_{M+\Delta M+1} - F_{M+\Delta M}) + J_h' (F_{M+\Delta M+1} - F_{M+1}) \tag{19}$$

Here

$$J_\tau = \frac{1}{\Delta \tau} \int_{h_n}^{h} w(h)[\tau(h) - \tau_m]dh, \quad J_\tau' = \frac{1}{\Delta \tau} \int_{h}^{h_{n+1}} w(h)[\tau(h) - \tau_{m+1}]dh,$$

$$\tag{20}$$

$$J_h = \frac{1}{\Delta h} \int_{h_n}^{h} w(h)[h - h_n]dh, \quad J_h' = \frac{1}{\Delta h} \int_{h}^{h_{n+1}} w(h)[h - h_{n+1}]dh$$

where $w(h) = (R+h)[R^2 \sin^2 \beta + 2Rh + h^2]^{-1/2}$, $F(h, \tau)$ is represented in the form of piecewise-planar approximations (16),(17) in each finite element, h_n - lower boundary of the cell in row n, h - height,where the ray leaves the lower element and enters into upper. After integration (18) with respect to ray J in the lower element M the value $(J_0 - J_\tau - J_h)$ is entered into the coefficient L_{JM} , since it is a coefficient for F_M. Correspondingly, J_τ is entered into $L_{J,M+1}$ and J_h into $L_{J,M+\Delta M}$. The complete value of the coefficient L_{JM} is the sum of integration result with respect to the ray J in six around triangular elements. The integrals with respect to all rays of type (20) can be calculated by various numerical methods, and, in each integration step Δh it is necessary to verify that the ray does not exceed the limits of the finite element. After complete numerical integration with respect to all rays, we obtain the matrix L_{JM}. The matrix L_{JM} is related to the set $\{\alpha_0\}$ of positions of the satellite on the high orbit and the corresponding series of rays. To determine the matrix for TEC-difference tomography problem A_{JM} one must calculate the matrix L' for another set of close positions of the satellites with a fixed increment $\{\alpha_0 + \Delta\alpha_0\}$ for the first satellite and $\{\alpha_1 + \Delta\alpha_1\}$ for the second one and to find the difference between them: $A_{JM} = (L'_{JM} - L_{JM}) / \Delta\alpha_0$. Because all circular satellites positions are proportional to time it is equivalent to time derivitivies or finite-differences.

To construct the projection operator using product of linear approximations one can define two-dimensional function $F(h, \tau)$ as the following sum [25]:

$$F(h, \tau) = a_{00} + a_{01}h + a_{10}\tau + a_{11}\tau h$$

This formula defines the function inside an arbitrary (m,n) rectangle through the values of the function at the four angular points (x,y)= {(0,0); (0,1); (1,0); (1,1)}, where x, y are normalized coordinates $x = (\tau - \tau_m) / \Delta\tau, y = (h - h_n) / \Delta h$.

The next example of projection operator design is based on the product of local cubic splines [25]. Then the function $F(h, \tau)$ takes the form

$$F(h, \tau) = \sum_{m,n=0}^{3} a_{mn}\tau^m h^n \tag{21}$$

As it was described above the function represented through the normalized coordinates $x = (\tau - \tau_m) / \Delta\tau, y = (h - h_n) / \Delta h$, inside an arbitrary (m,n) rectangle, can be obtained through the values of the function at the four angular points (x,y)= {(0,0); (0,1); (1,0); (1,1)}:

$$F(x, y) = F_{00}P_{00} + F_{00}^x P_{00}^x + F_{00}^y P_{00}^y + F_{00}^{xy} P_{00}^{xy} + F_{01}P_{01} + \ldots$$

Here F^X, F^Y are the values of the function partial derivatives with respect to x,y, F_{00}^{xy} is the value of the function partial derivative of the second order with respect to x and y. The total sum (21) will contain 16 summands, $P_{\alpha\beta}^Y(x, y)$ are corresponding polynomials of the power up to three. Two exaples of coefficient calculation are

$$P_{00} = 4x^3y^3 - 6x^2y^3 - 6x^3y^2 + 9x^2y^2 + 2y^3 - 3y^2 + 2x^3 - 3x^2 + 1$$
$$P_{00}^x = 2x^3y^3 - 4x^2y^3 - 3x^3y^2 + 6x^2y^2 + 2xy^3 - 3xy^2 + x^3 - 2x^2 + x$$

Then, integrating in each cell of the given polynomials we can produce the corresponding elements of the matrix, as in the case (16-20). The cubic spline approximation is differ from the described above. Such representation makes it possible to find not only the function but also its first derivatives.

Now we have describe four methods of the RT projection operators constructing. As it was mentioned above, the projection operators with approximations of higher orders allow a better approximation of the operator of the direct problem, i.e. they enable us to come closer to the true operator of the direct problem [25].

Description of the program for calculation of the different versions of the RT matrices (operators) for the high-orbit RT measurements

2. Program <mat_rth1.for>

This program designs different versions of the operators (matrices) for the TEC and TEC-difference high-orbit RT measurements.

Input parameters and files:

When starting program, you may choose the type of RT measurements (TEC or TEC-difference) and the order of approximation (one of four mentioned above approximation methods).

File <task.dir> contains the same parameters as the input file for the dir_rth1.for program. It was described in chapter 1.

File <name_F.mat> contains names of output files with parameters of matrix, nonzero matrix items and they positions in matrix. All this files are need as input files for program of the inverse problem solution. The example of <name_F.mat> file for two-receiver configuration is enclosed.

Output files:

Files <F_matr> - arrays of matric of corresponding approximation
for each receiver

File <Fparam> - parameters of matrices for each receiver

Files <F_int> - results of multiplications of calculated matric
and model structure

File <F_st> - array (LST) of number of all rays which cross the
corresponding discret of model (SIRT algorithm)

Compilation

mf77 mat_rth1.for -ol -486

RUN

ndprun mat_rth1.ltl

1.4. The solution of the inverse problem for satellite RT using middle and high-orbital satellites of opportunity.

For futher computer modeling of the RT problems using middle and high-orbital satellites of opportunity it is necessary to use a set of appropriate electron density distributions models of the protonosphere. We have less information about structure and dinamic of magnetosphere and protonosphere. Now there are no detailed and precise models of magnetosphere and protonosphere, however as for ionosphere , too. But there is no need in it for estimation of possibilities of radiotomography of the magnetosphere and protonosphere. To solve this problem the simple models of magnetosphere and protonosphere are required, which include the main structural features (plasmasphere and localized natural or man-made irregularities and groups of irregularities). However, the presented package of programs makes it easy to design many other structural types and to extend this "ZOO" as far as possible using the available "detailes". Here we will use the simple protonospheric model , which is based on the idea, that electron density distribution is determined mainly by geomagnetic L shells. Fig.14 illustrates a cutaway view of geomagnetic L shells from the northen mid-latitude station [23]. The L shells greater than 4 are considered to be open field lines, and consequently almost do not contents the electrons. In addition supposed is the possibility of existance of localized natural or man-made irregularities and groups of irregularities. In coordinate system τ is counted from horisontal axis - counterclockwise), such electron density distribution, set by the state L=4 shells, may be assigned by the following model function:

$$N = N_0 + N_1(1 - h / h_1) + N_2 \cos^2(\frac{\pi}{2}(\frac{h^2}{h_2^2} + \frac{\tau^2}{\tau_2^2}))$$

(22)

First two items describe the background density (interplanet plasma, solar wind, etc.) and the last item describes the plasmosphere. In computer modelling we will suppose that (if there are no another values)

$N_0 = 10^1 cm^{-3}; N_1 = 10^2 cm^{-3}; N_2 = 5*10^3 cm^{-3}; h_1 = 20000km;$

$h_2 = 20000km; \tau_2 = 5000km.$ Let us underline one more time that precise functional dependencies, describing the structure and location of L shells, are unimportant for RT modelling. The qualitative congruence of reconstructed "pictures" is quite sufficient. The electron density distribution, setting by model 22 is cited in fig.15, where h and τ are measuring in km.

Let us turn to the description of computer modelling results. We wil consider three main experimental geometries, which were chosen from data of the section 1.1: I - three middle-orbital and one high-orbital satellites (fig.7), II - one middle-orbital

Fig. 13

L SHELLS

Fig.14. Cutaway view of the earth along the station meridian, showing the magnetic L shells and the station elevation angles, both north and south of the station. Dashed line represents GPS orbital height. [23].
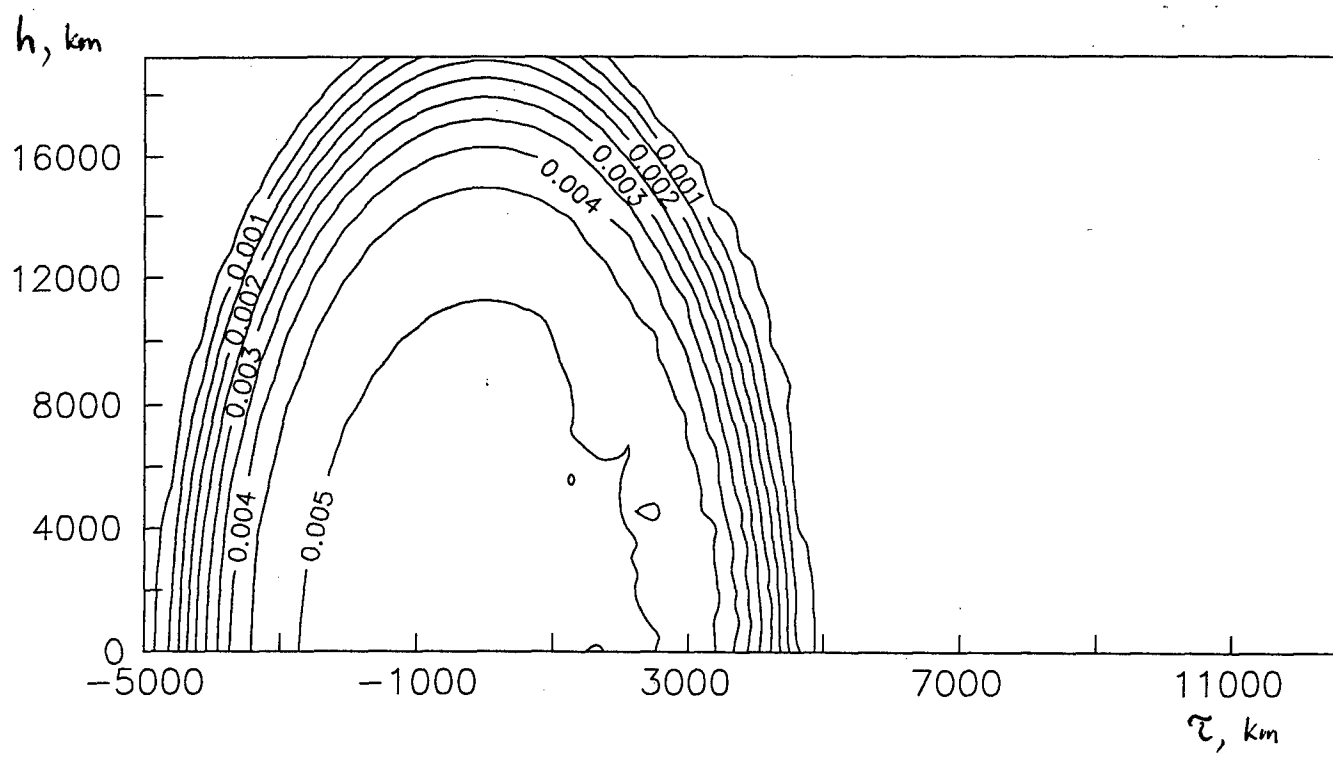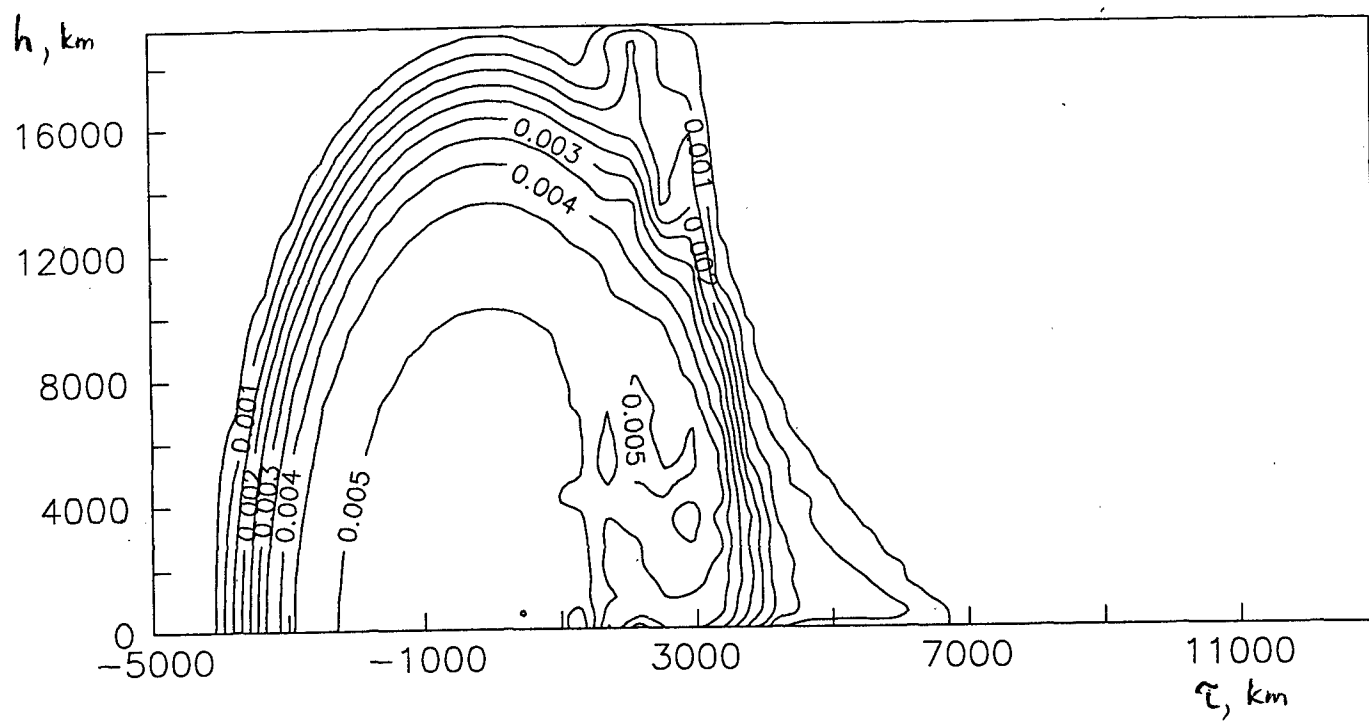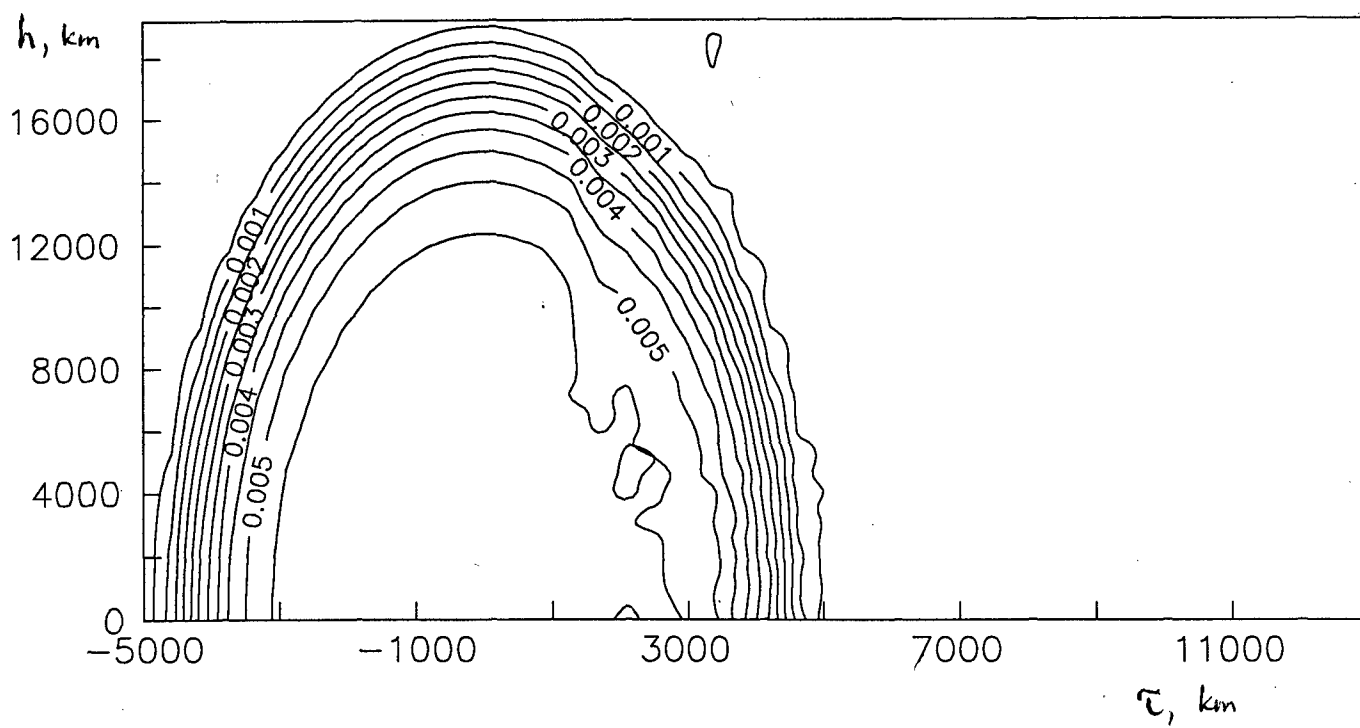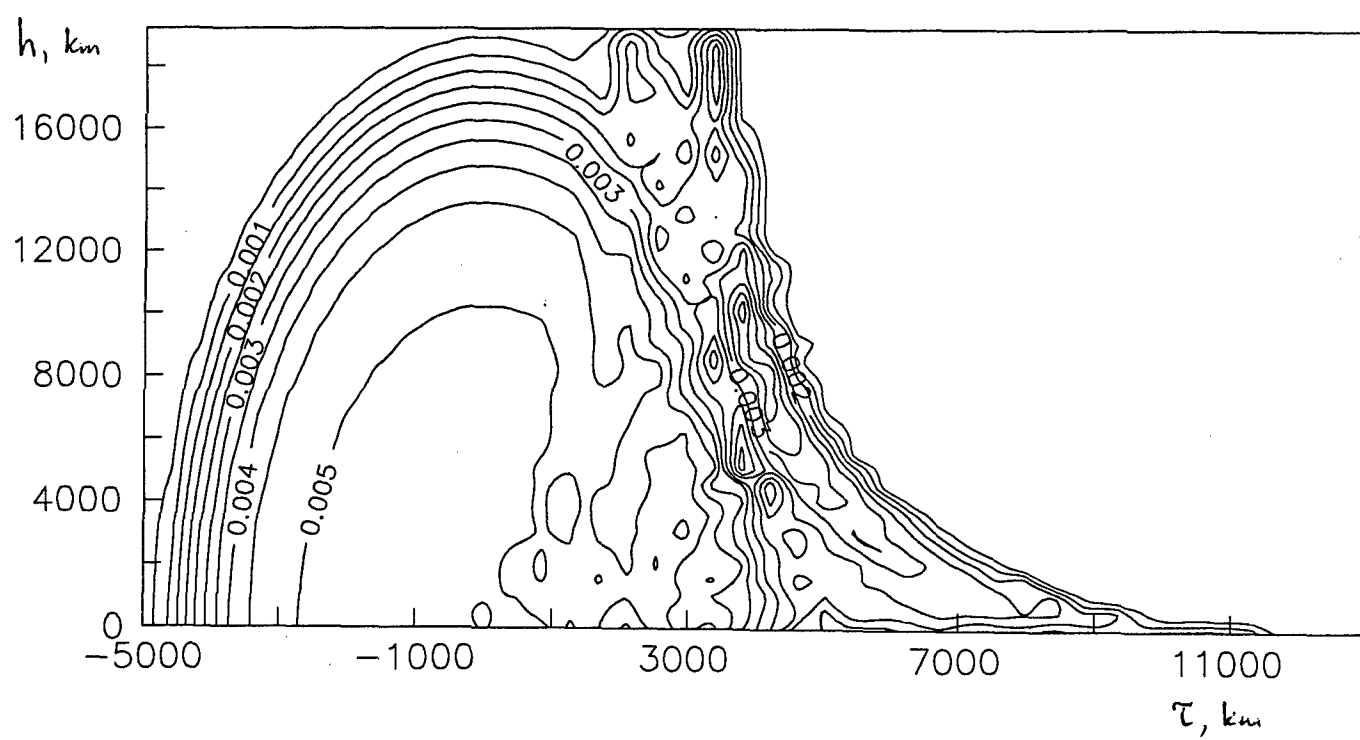
fig. 15

Fig. 16

Fig. 17

Fig. 18

Fig. 19
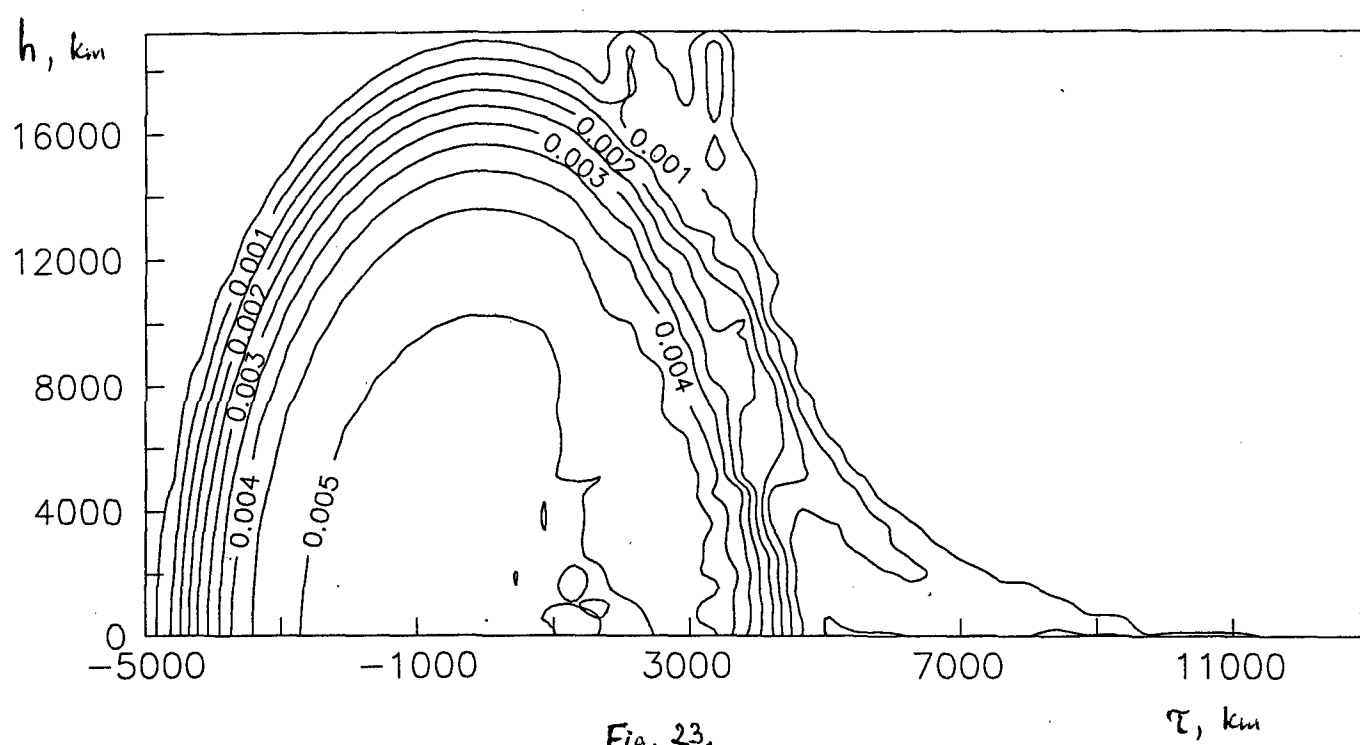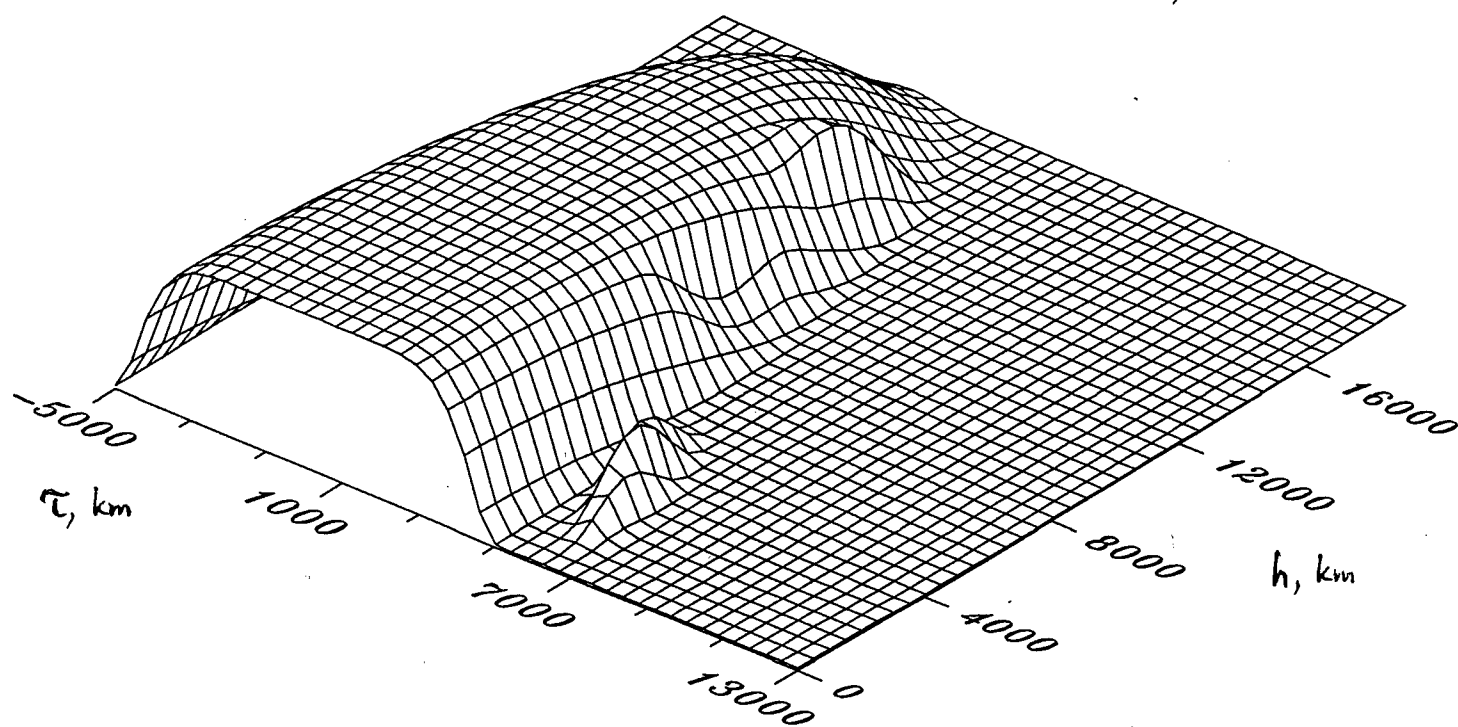

Fig. 20

Fig. 21.

Fig. 22

Fig. 23.

Fig. 24.

Fig. 25.

Fig. 26.

Fig. 27.

Linear RT, Real Geometry (h,tau)
Model area: X=[-5000.0,13000.0], Y=[0.0,19200.0], Grid 44x39 = 1716 items
Receivers at altitude 0.0, orbit height 19200.0

Nreceiver	Nrays	Positions		Orbit	
1	5	0.0 —> 13223.0		1930.0 —> 3861.0	
2	5	3860.0 —> 12674.0		1930.0 —> 3217.0	
3	5	7719.0 —> 11685.0		1930.0 —> 2509.0	

Fig. 28

and two high-orbital satellites (as first two satellites in fig.6), III - one high- orbital and three middle-orbital satellites, rotating in opposite direction (fig.9). Other experimental schemes are either unusefull for reconstruction of two-dimensional crosses (contribution of high-orbital satellites and onearth receivers), or give the same results.

RT reconstruction of plasmaspheric structure or location of L shells boundaries gives quite good results for all three schemes under the condition, that we have a priori information about electron density magnitude, location and sizes of desired structure. However, here the sufficient accuracy of this a priori information is required to be 30-50%. According to the comparison of TEC, restored by reconstruction and real TEC, it is possible to chose appropriate initial approximations and finite results, varying different initial approximations. Fig.16-17 show the results of RT reconstruction model (22) according to scheme 1, where the initial approximation contain the mistakes in determination of real distribution parameters: fig.16 (the mistake in estimation of vertical size h_2 is +10%), fig.17 (the mistake in estimation of the size τ_2 is - 15%), fig.18 (the mistake in estimation of electron density maximum N_2 is +15%). The experimental scheme was made in following way: the area of positive τ can be seen, that is why we can observe the only initial approximation from the left of reconstruction.

The quality of RT reconstructions of smaller structures with localized irregularities is notably worse according to scheme I. The results of RT reconstruction model (22) with additional localized irregularities are cited in fig.19-27. The localized irregularity of the model from fig.19 under reconstruction (fig.20) is extracting and distoring. The irregularities located on the border of L=4 shell, like model from fig.21, are reconstructed badly. The results of RT plasmaspheric reconstruction with such a irregularity with different magnitudes of local electron density maximum N_m of irregularity are cited in fig.22 ($N_m = 5*10^9 m^{-3}$), fig.23 ($N_m = 10*10^9 m^{-3}$), fig.24 ($N_m = 25*10^9 m^{-3}$). It is seen that even the irregularities of quite high concentration exceeding maximum inside L=4 shell in 2-5 times, practically can not be reconstructed. Under the reconstruction , the local irregularity is only "spreading" along the enclosing space. The same picture is observed under the reconstruction of more complex model with three local irregularities (fig.25,26). Here also (fig.27) the "internal" irregularities practically are not reconstructed, and the "external" are distorting under the reconstruction. Such a lower quality of reconstructions is connected with bad experimental geometry (fig.7), which is cited in coordinates (h, τ) in fig.28. The crossing angles of probing rays are small in this scheme, what leads to strong expansion and deformation of localized objects under the reconsruction.

The scheme II also leads to the "spreading" of reconstructed objects. It can be seen well, if we cite an example of restoration of model structure (22) with localized irregularity in its center (fig.29), which practically is not selected being reconstructed. The same pictire of "spreading" can be observed on fig.31-32 under the reconstruction of a pair of localized irregularities. However there is another cause of such "spreading" for experimental geometry II, than it was in I geometry. In fact it can be seen from experimental scheme in coordinates (h, τ), that the cross angles of probing rays are varying in a wide range, but , unfortunately, there (in this scheme) exist no extensive areas of uncrossed rays, which contain the rays of the only one satellite. The existance of such areas leads, while reconstruction, to the "spreading" of restored object from the crossing ray area to the area of uncrossed rays. It is easy to understand, that if there exist the localized irregularity (shaded in fig.33) in the crossing ray area, than the algorithms will localize and select this irregularity correctly in the crossing ray area under the reconstruction, but will leave its traces (shaded horisontally in fig.33) in the uncrossing ray area. To illustrate this thesis let us consider the simple model of one localized irregularity (fig.34), the result of its reconstruction is cited in fig.35, where extensive traces of such a "spreading" can be seen from the crossing ray area to uncrossing ray area. However such a "spreading" can be avoided if we have a priori information about negligibly small electron density in the uncrossing ray area, that is the irregularities are located only in the crossing probing ray area. The example of RT reconstruction of tha same model (fig.34) with the use of such a priori information is cited in fig.36.

The results of RT reconstructions for scheme III with satellites, rotating in the opposite directions, and with quasifan beams are little bit better. The odd figures (fig.37-48) show the protonospheric models with various localized irregularities, even figures show the results of RT reconstructions. Here, as usual, the localized irregularities are selected under the reconstruction though the distortions and attefacts are significant. The higher quality of RT reconstructions of scheme III is explained by the better experimental geometry (fig.9, cited in fig.33, in coordinates (h, τ), from which the large crossing angles of probing rays and small uncrossing ray areas on the border of reconstruction area can be seen. Surely, large ray curvature on borders of reconstruction area, the existence of upper and lower ray beams lead to corresponded distortions and artefacts in RT reconstructions. However the development of effective methods and algorithms of RT reconstructions in connection with the similar certain schemes makes it possible to improve the results.
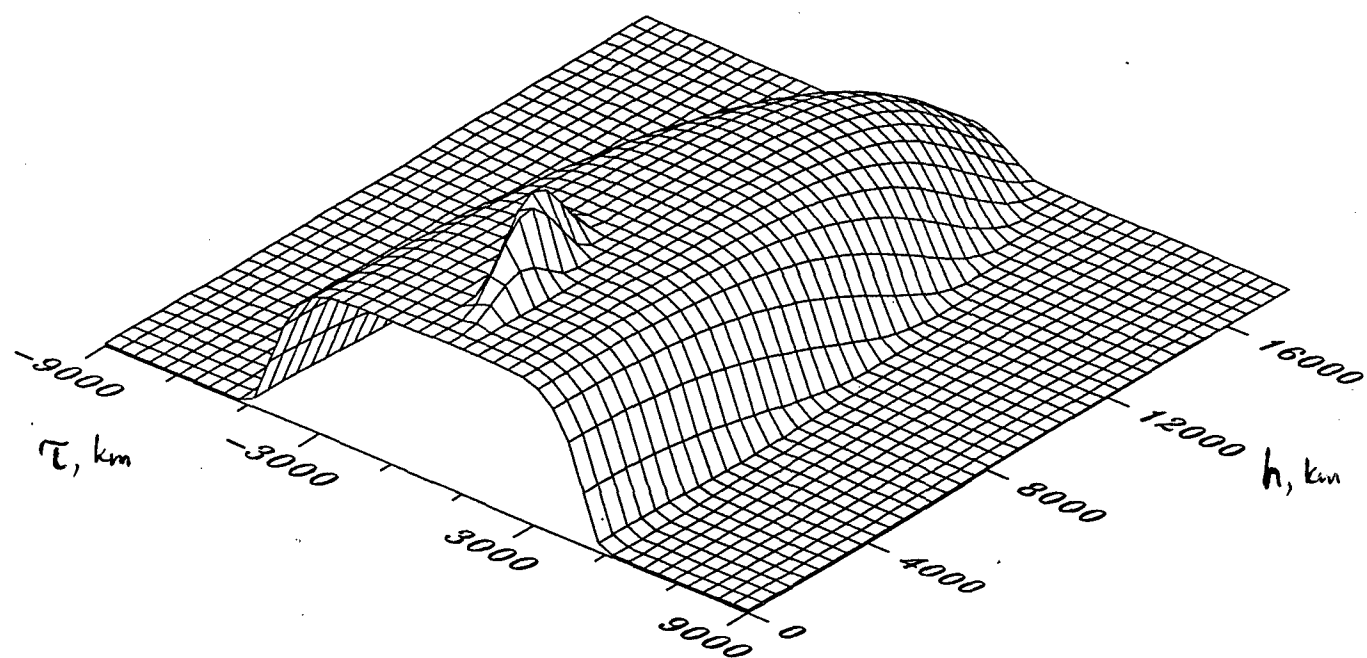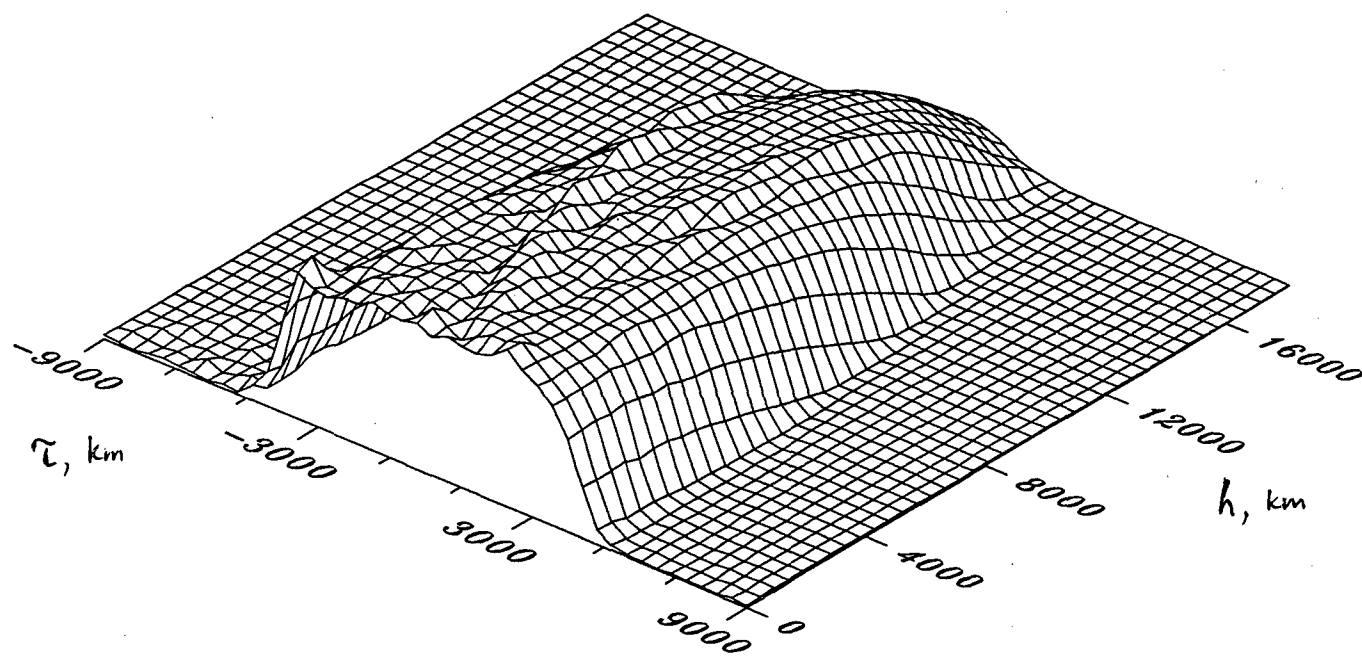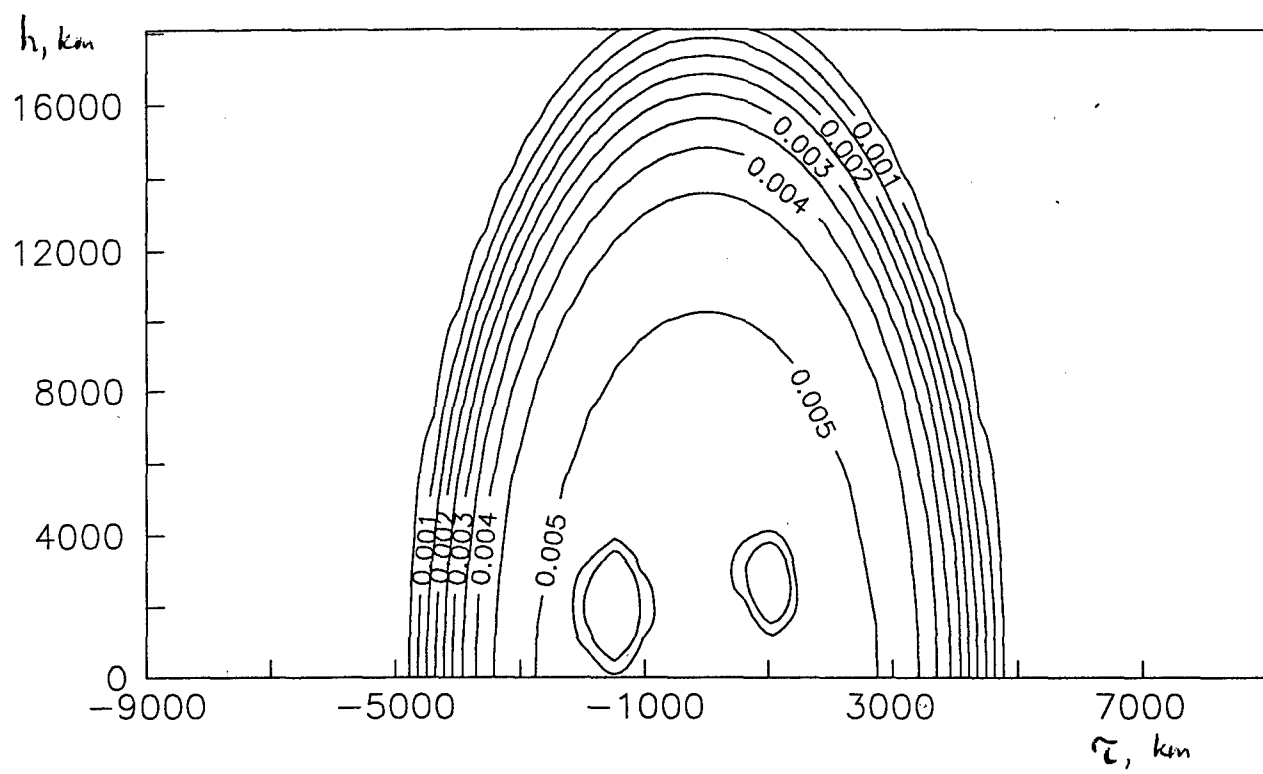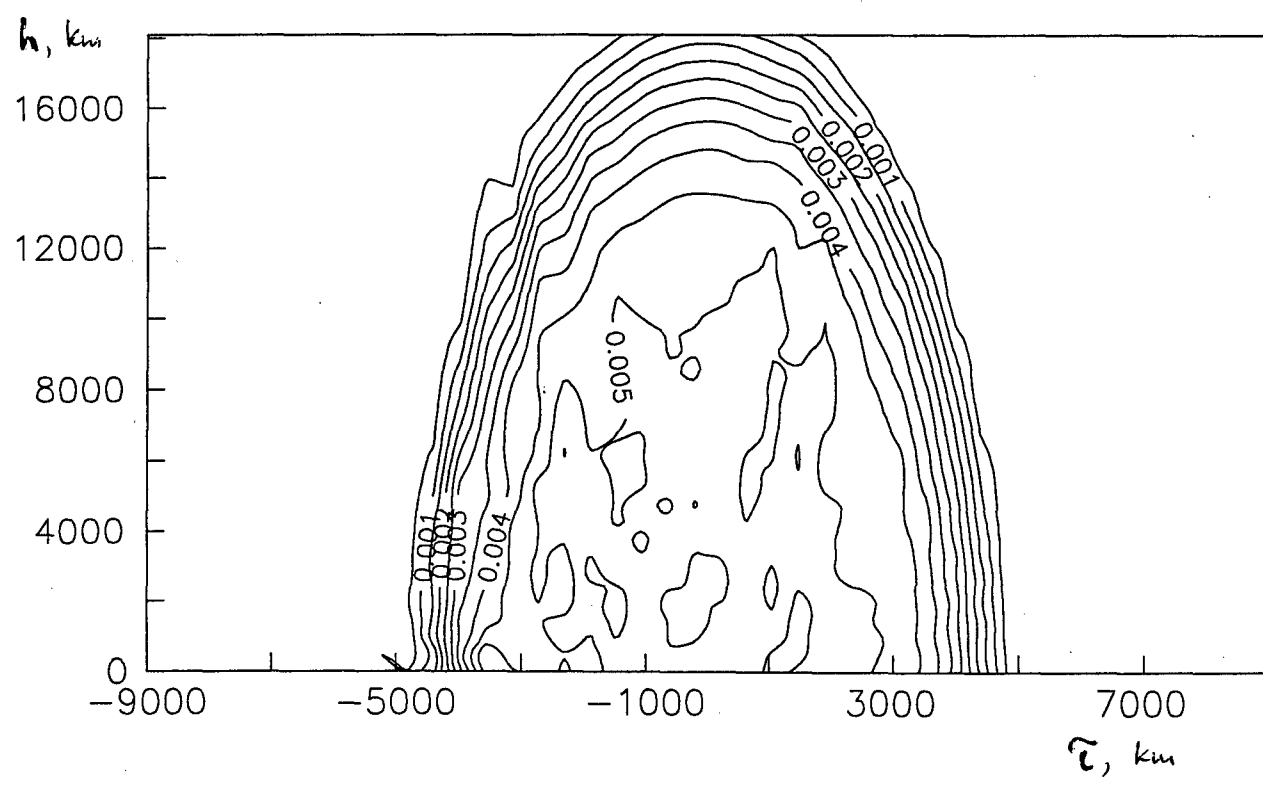
Fig. 29.

Fig. 30.

Fig. 31.

Fig. 32

Linear RT, Real Geometry (h,tau)
Model area: X=[-9000.0,9000.0], Y=[0.0,18100.0], Grid 44x39 = 1716 items
Receivers at altitude 0.0, orbit height 18100.0

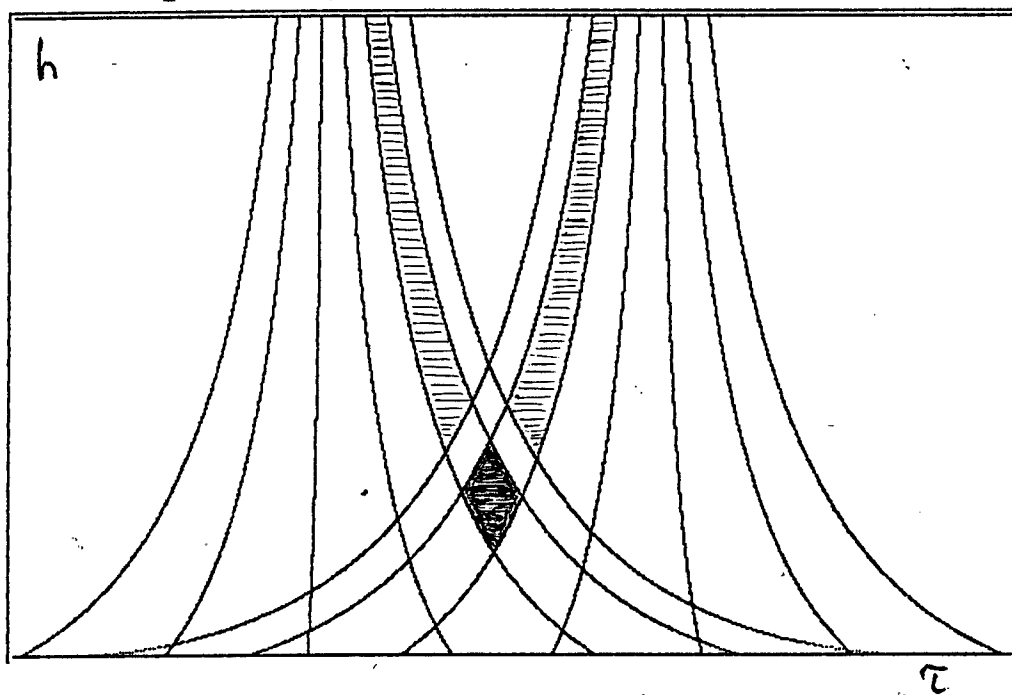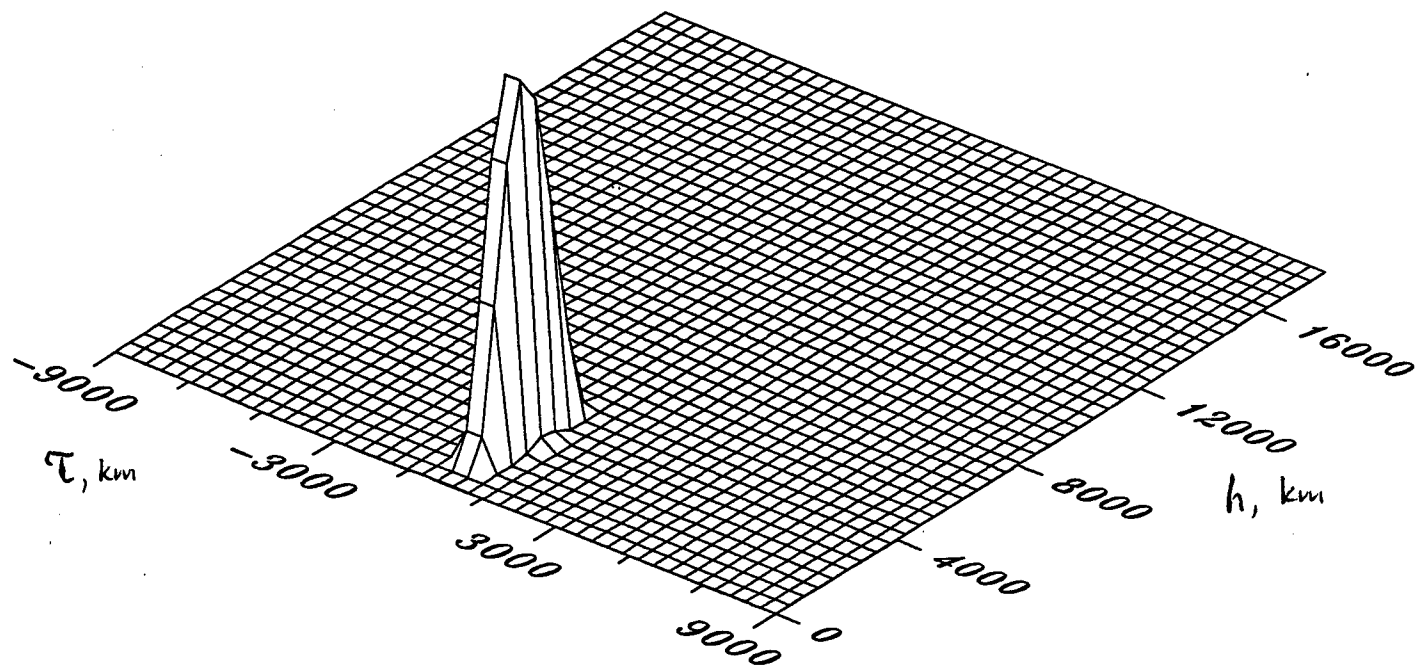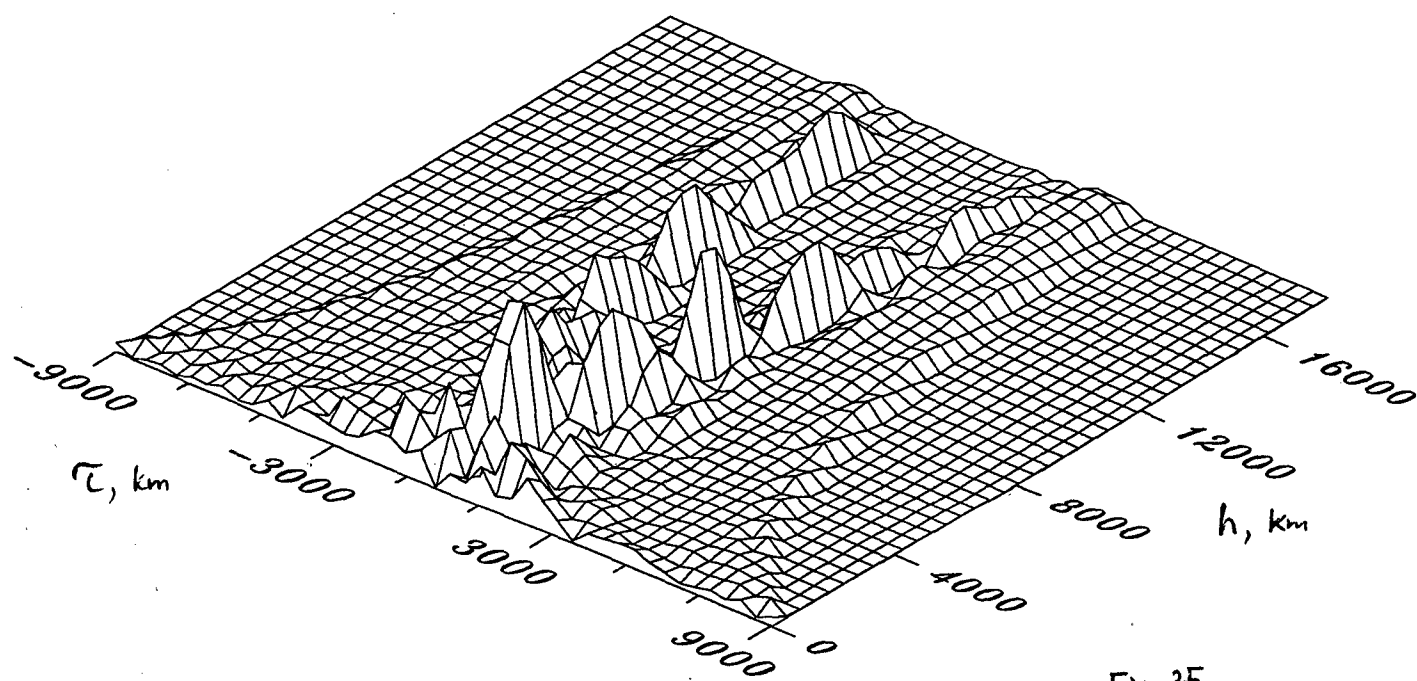| Nreceiver	Nrays	Positions	Orbit
1	7	-8815.0 —> 6611.0	-4266.0 —> -1865.0
2	7	-7374.0 —> 8815.0	1000.0 —> 3519.0

Fig. 33.

Fig. 34.

Fig. 35.
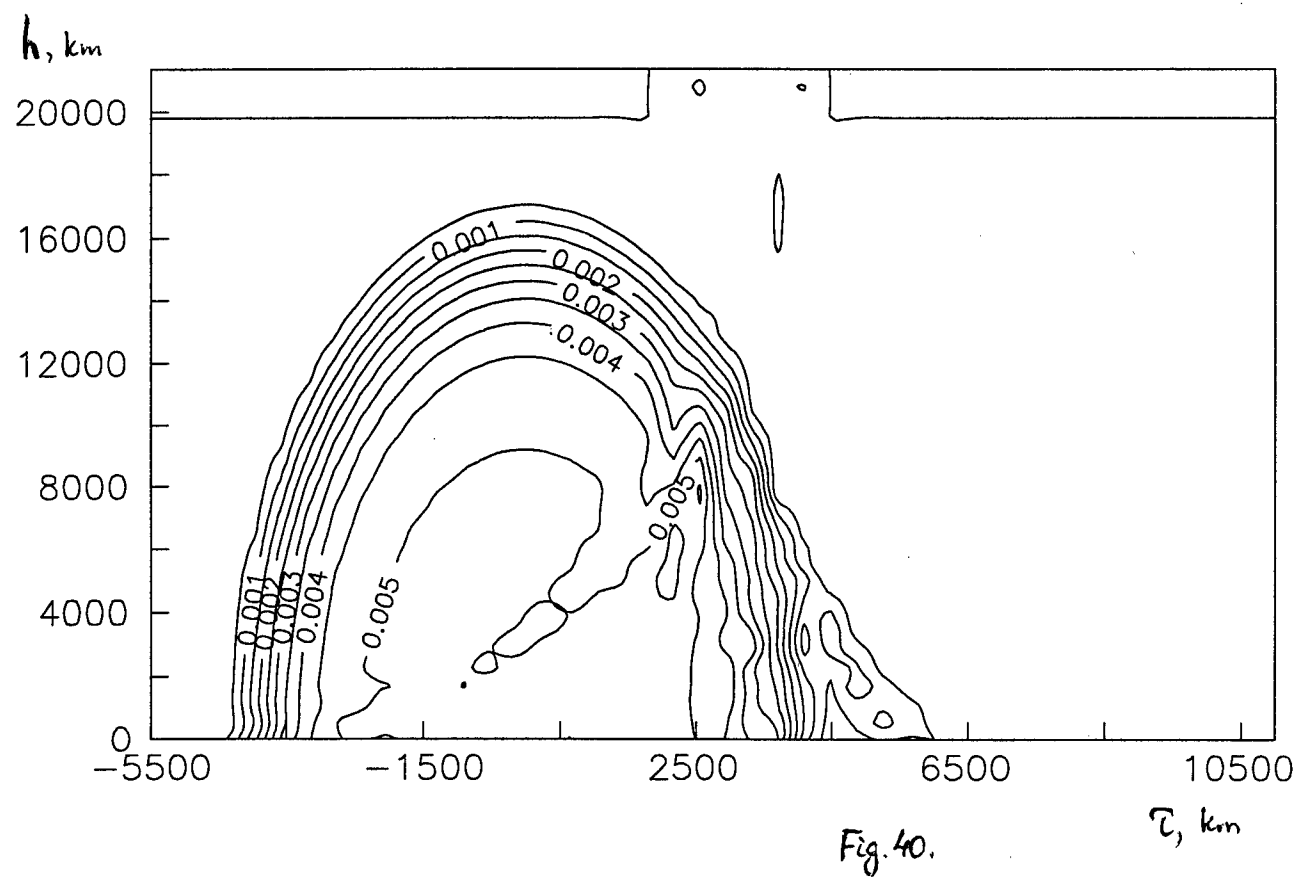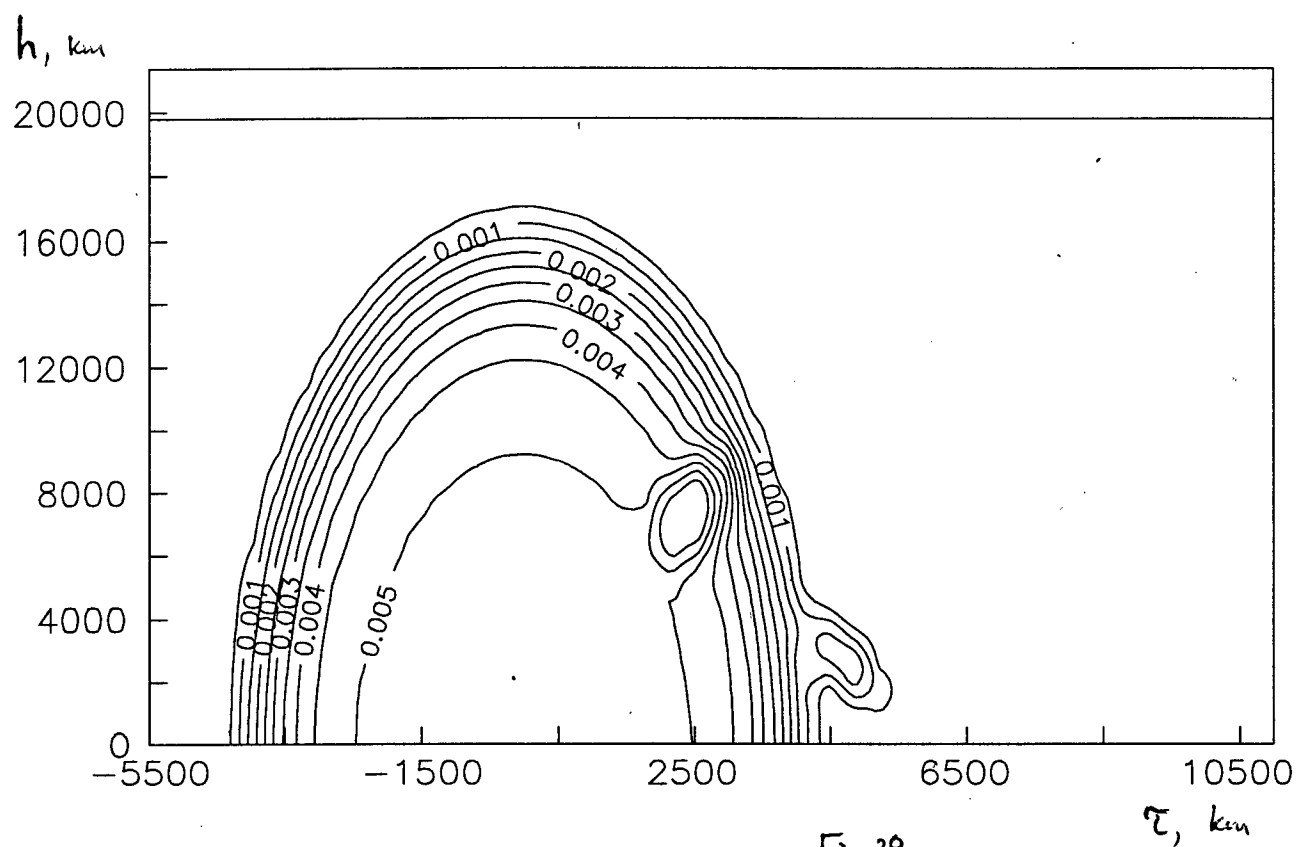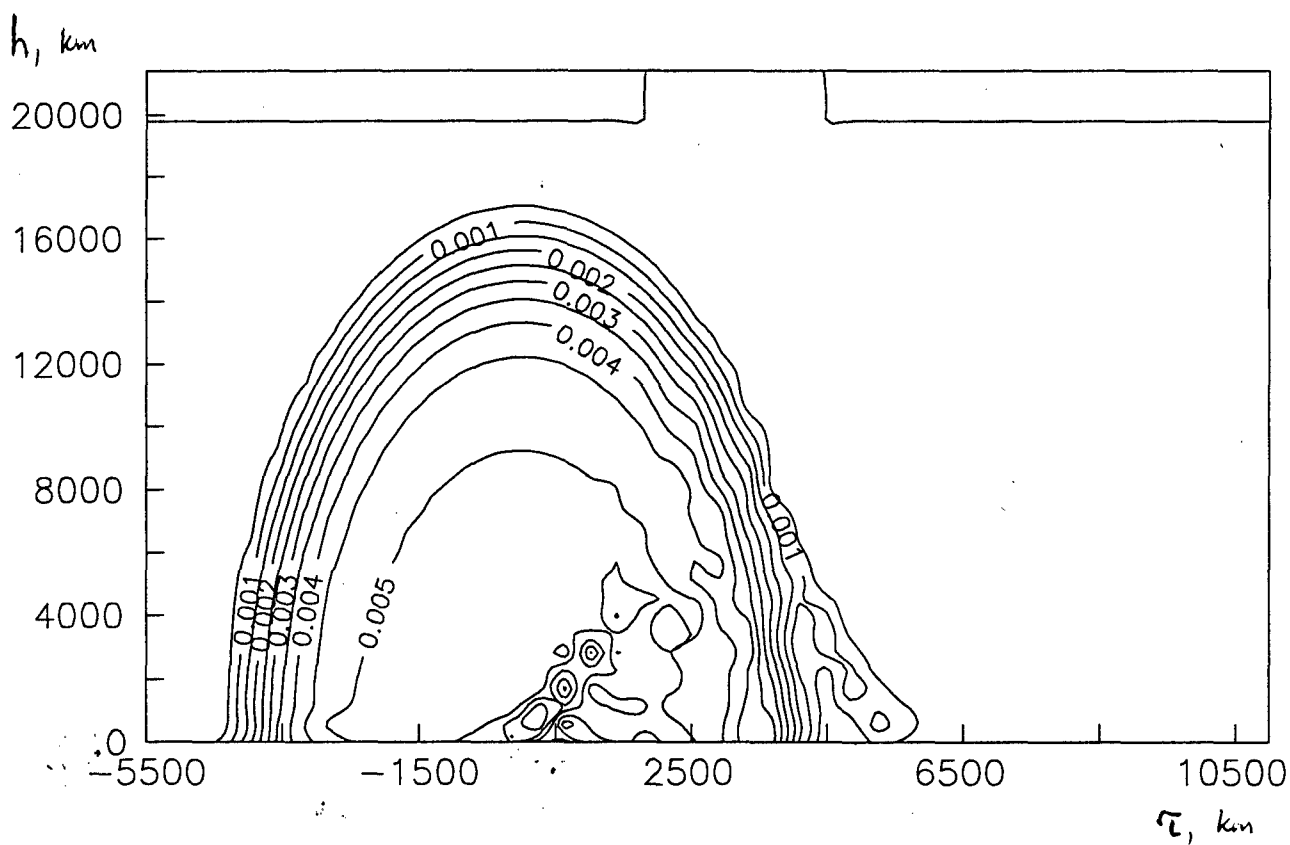

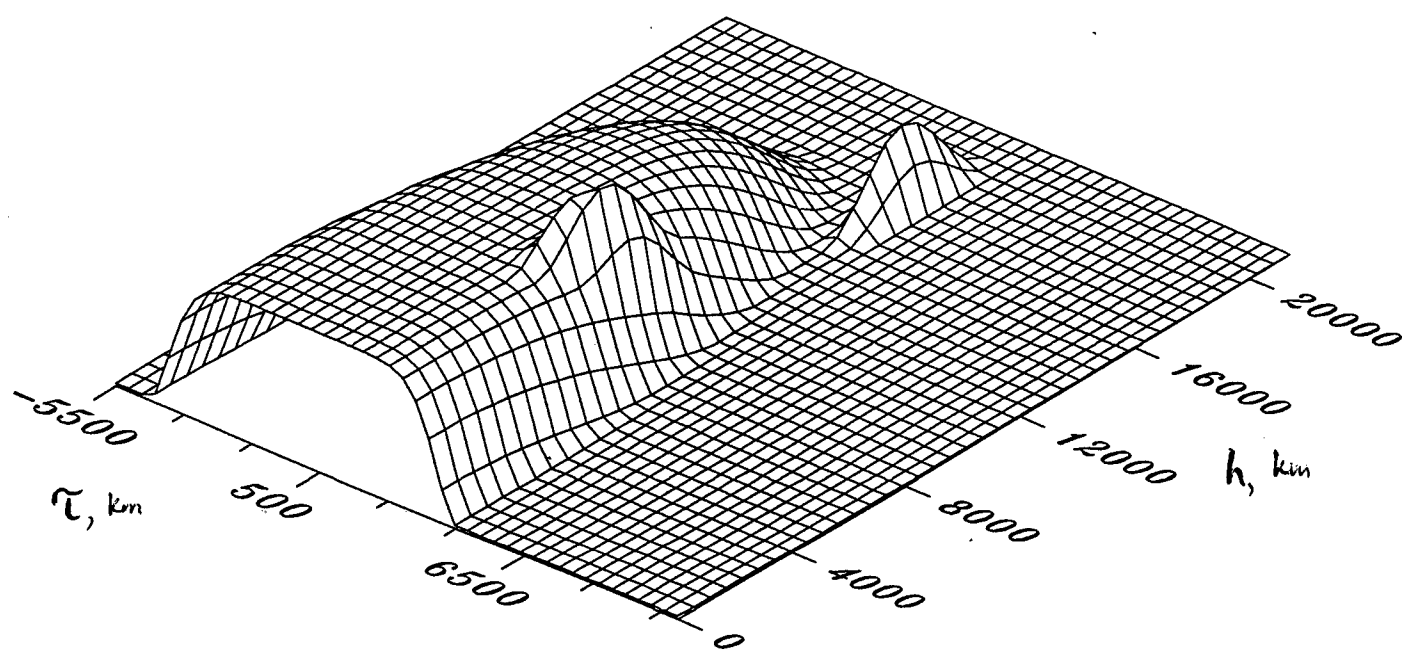
Fig. 36.
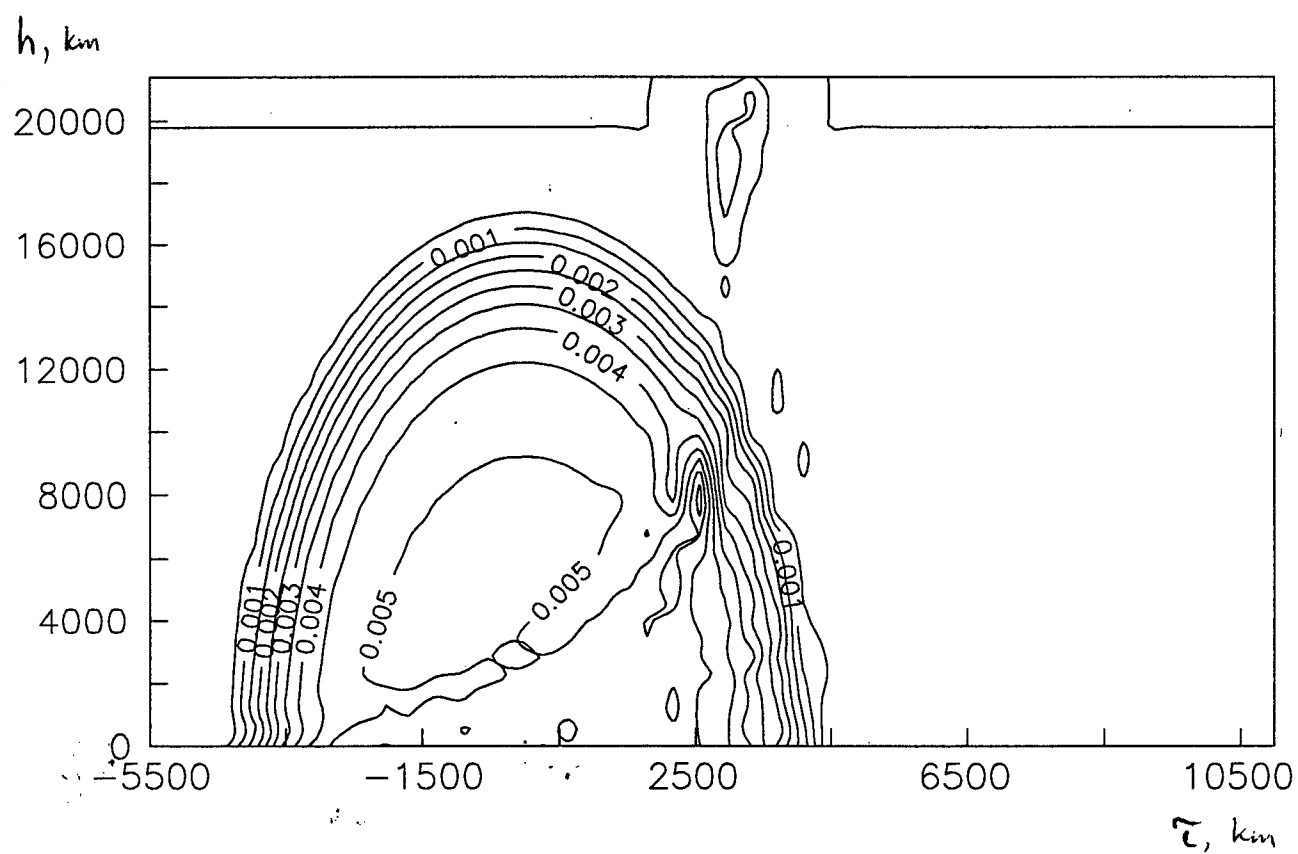
Fig. 37.

Fig. 38.

Fig. 39.

Fig. 40.

Fig. 41.

Fig. 42.
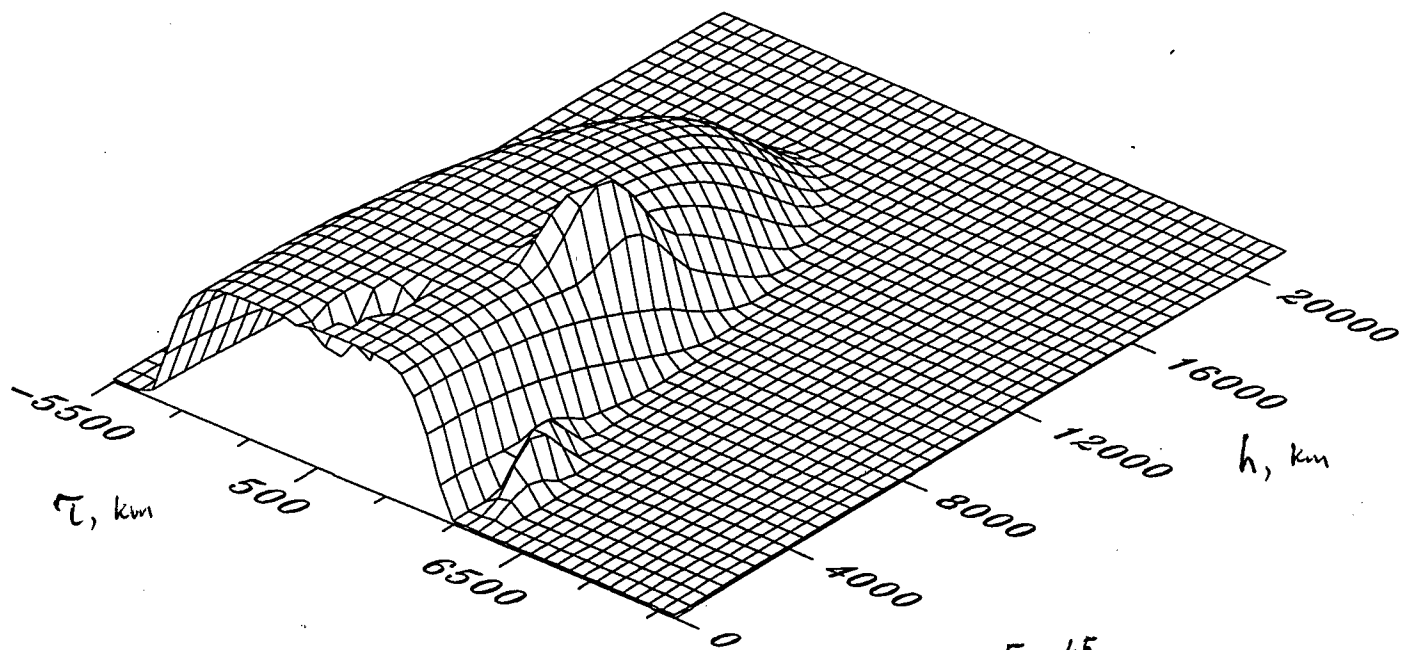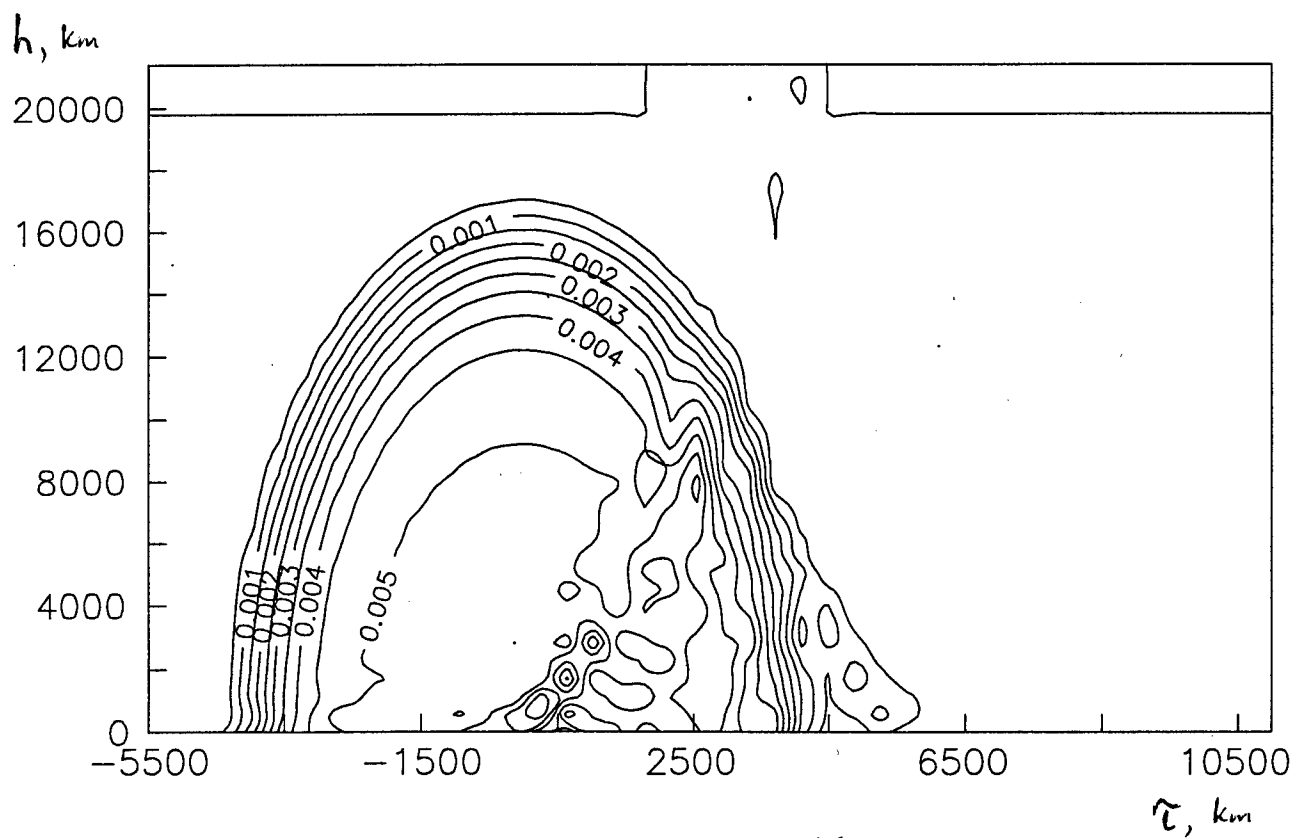
Fig. 43.

Fig. 44.

Fig. 45.

Fig. 46.

Fig. 47.
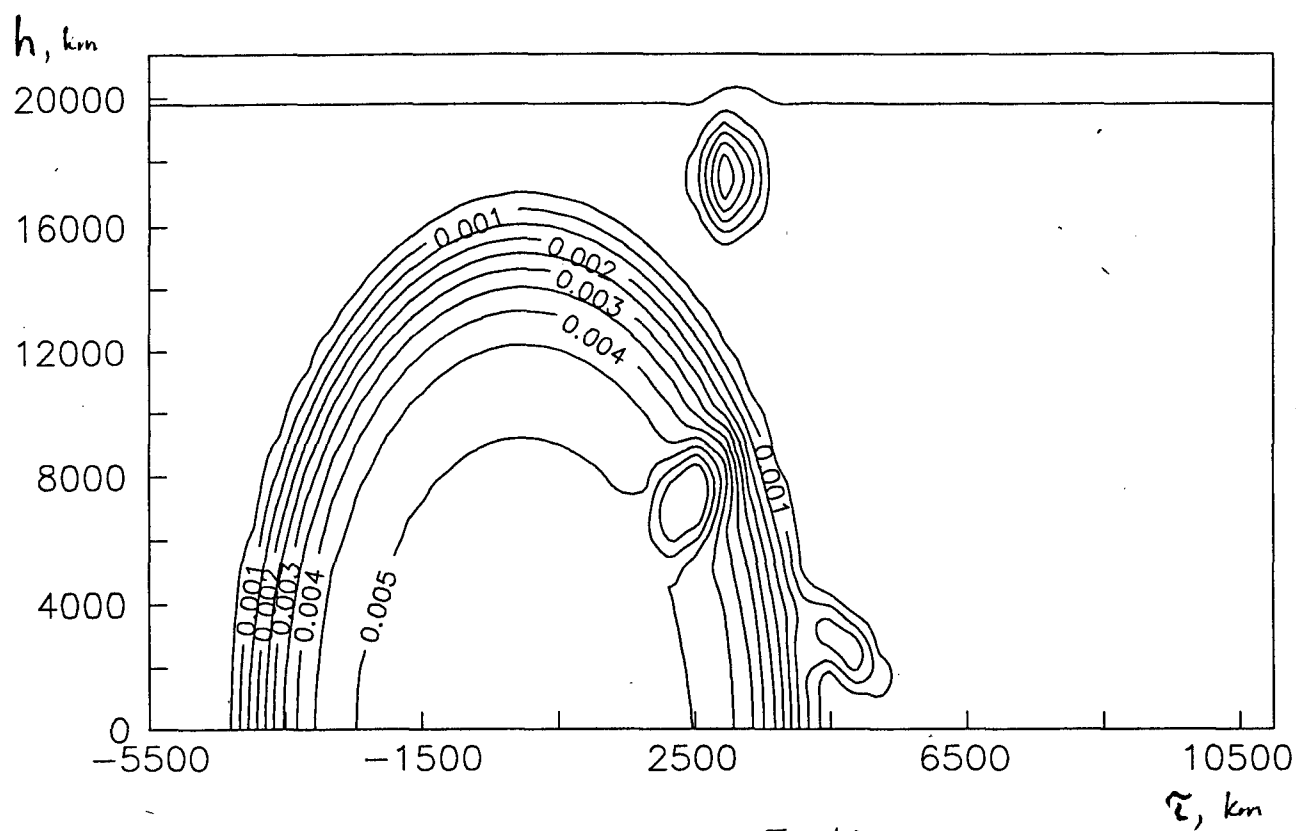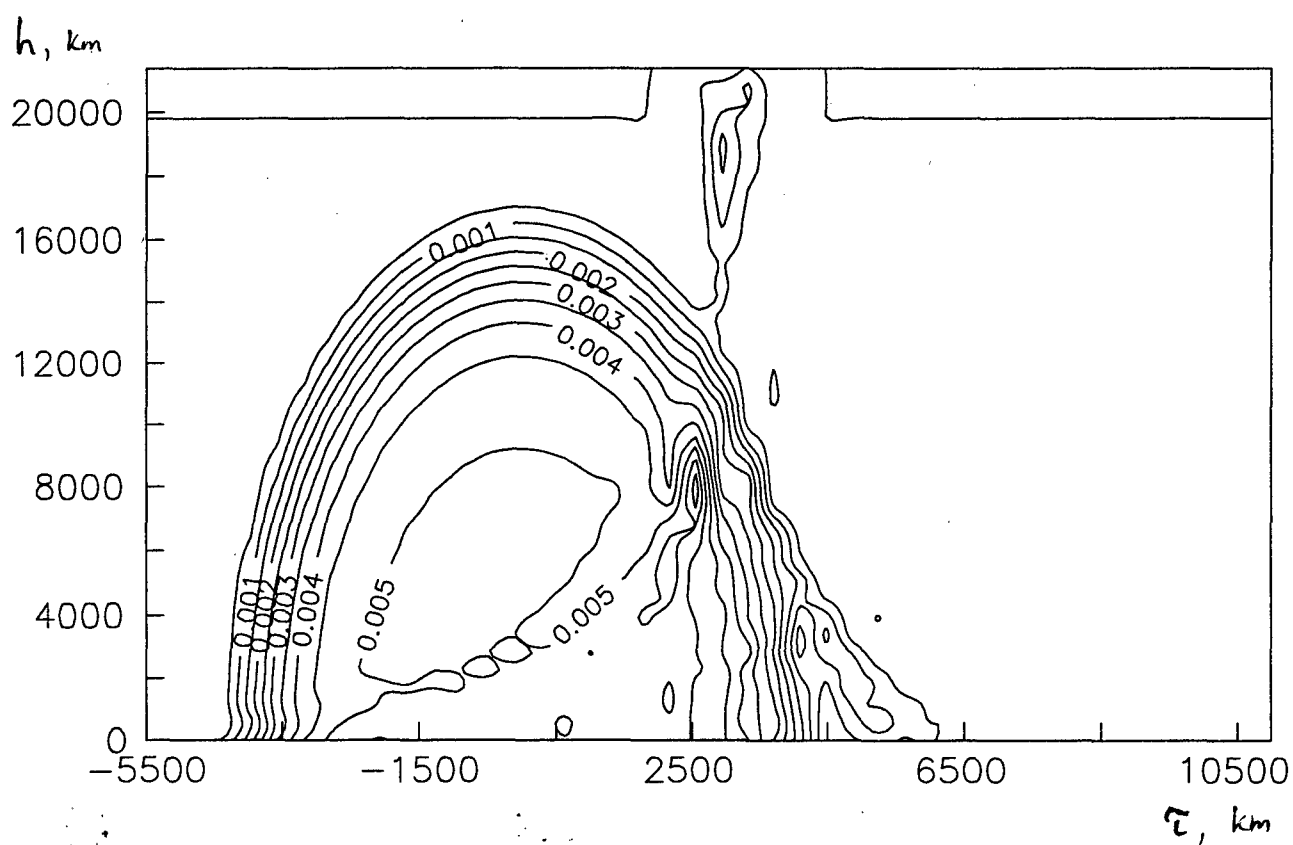

Fig. 48.

Linear RT, Real Geometry (h,tau)
Model area: X=[-5500.0,11000.0], V=[0.0,21400.0], Grid 44x39 = 1716 items
Receivers at altitude 0.0, orbit height 21400.0

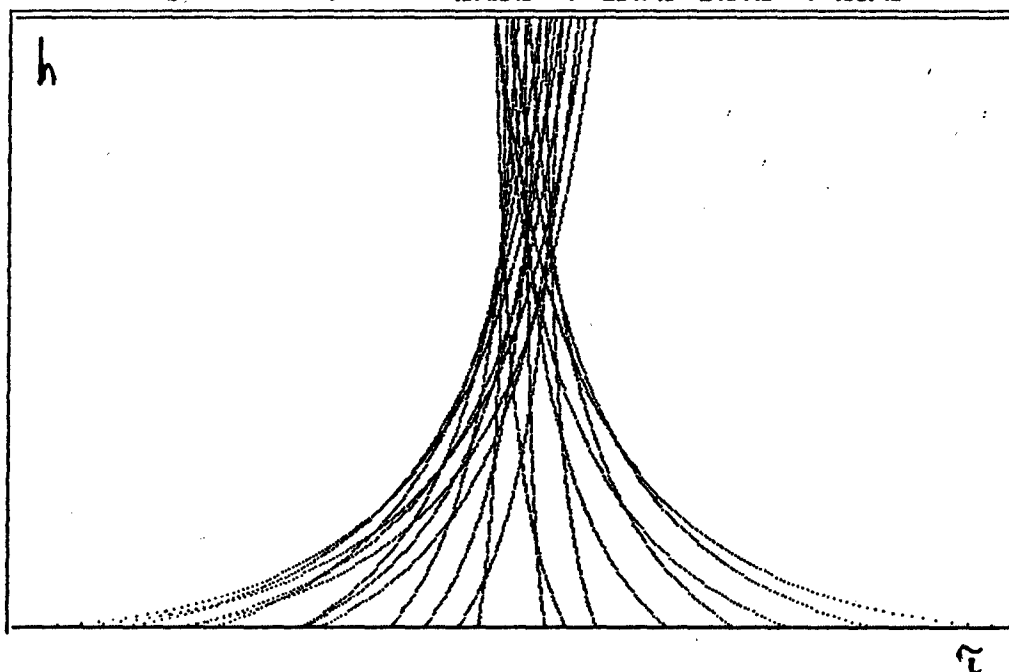| Nreceiver	Nrays	Positions	Orbit
1	7	3650.0 —> -5014.0	2434.0 —> 3537.0
2	7	7300.0 —> -4637.0	2434.0 —> 3923.0
3	7	10950.0 —> -2647.0	2434.0 —> 4009.0

h

τ

Fig. 49.

Description of the program for solution inverse problem for TEC RT or TEC-difference for high orbital RT .

Program <slv_rth1.for>

Input parameters and files.
When starting program, you may choose the type of RT measurements.
Answer = 1 : TEC RT
Answer = 2 : TEC-difference RT
NF, NR - number of discrets on the horizontal and vertical grid
NREC - number of receivers
'F_MOD' - input file of model structure (program <dir_rth1.for>)
'F_X0' - input file of initial guess
        (program <dir_rth1.for> or function <guess>)
'Fparam' - input file with parameters of matrix
XIST - model structure from input file 'F_MOD'
File 'name_F.slv' containes Nrec lines with names of input and output files.
The example of this file is enclosed.
line 1 - name of file with parameters of matrix (Fparam)
line 2: name1 - name of input file with matrix
        name2 - name of input file with either TEC or TEC-difference
            ('Finput')
        name3 - name of output file with results of multiplications
            of input matric and reconstructed structure ('Fout')
line Nrec+2: name of file with number of all rays which cross
        the corresponding discret of model
line Nrec+3: name file with model, name file with guess,
        name file with reconstruction
line Nrec+4: name file with errors
Npi - array of contants (2pn) for each receiver
er_n - level of noise in %
Npi, er_n are input from the screen
Nsolve - the method of solution, it is input from the screen
REL - array of relaxation parameter
LMAX - max number of nonzero matric elements for each receiver
AZ - array of nonzero matric elements for all receivers
NST - array of corresponding column nonzero matric elements for
      all receivers
LST - array of number of all rays which cross the
      corresponding discret of model (SIRT   algorithm)   from
      input file <F_ST>, it is similar to LST in program <mat_rth1.for>
Niter - number of iterations, it is input from screen
Subroutine <DEFSYS> - solution of linear system equations for
                      one ray.
Subroutine <ercl2> calculates errors in metric C and L2
Subroutine <VMINM> calculates min and max of array
Function <RAN> calculates random values in [0,1]
Function <GUESS> - for initial guess
RMAX, RM, Zmax, ZSM, B1, B2 - parameters for function <GUESS>
Output files:
File <F_REC> - file with the reconstruction
File <er_solv> - errors of right items and reconstruction in
                metric C and L2
Files <Fout> - results of multiplications of the matric
                and reconstructed structure

Execution
mf77 slv_rth1.for -ol -486
RUN
ndprun slv_rth1.ltl

Part 2

Algorithms and Programs for Nonlinear Radiotomography.

2.1. The Solution of the Direct Problem of Radio Wave Propagation for Nonlinear Radiotomography.

The presence of strong gradients of electron concentration leads to the necessity of using the ray refraction in the problems of ray radiotomography. The ignoration of refraction can give wrong results of RT reconstructions, and also limits the resolving power of RT system. Taking the refraction into account it transforms to more complex problems of RT. Supposed that the set of integrals over refractable rays, which curvature is determined by propagating medium are known.

$$TEC = \int_{L[N]} Nd\sigma = L[N] \tag{1}$$

Where, as it was mentioned earlier, $\int Nd\sigma$ denotes the integration of the electron density N along the signal path. However in general case the ray paths L[N] now depend on the distribution of electron concentration and are determined by ray equations. The theory and methods of linear RT reconstructions has been given in our earlier papers [1-3,6,8]. Similar tomographic problems on linear integrals have been solved in other fields of science and the methods of solving such problems are well-known. In the case of ionospheric diagnostics, however, the major difficulty is that the linear integral of the electron concentration is proportional to the absolute phase Φ, whose accurate determination is practically impossible, therefore we have suggested [1-3,6,8,25] to apply the phase-difference (or Doppler) RT approach, which has given quite satisfactory results. Note that to date most works on the ray RT have been based on the phase approach, which can not provide high-quality and reliable results. It was not until quite recently that an acceptable alternative has been suggested, that of reconstruction by the relative phase (relative TEC) data [26,27]. Such an approach is possible, but we belive, however, that the sensitivity of this method would be lower than that of the phase-difference (or Doppler) RT [25]. Such an approach also can be usefull in a case of nonlinear RT. Than we will use similar system of equations where data will not be TEC or absolute phases, but difference of phases or Doppler frequences $D(\alpha_0)$,

which are proportional to derivative of TEC with the respect to the angle of satellite α_0, that changes lineary for cyclic orbits with the respect to time.

In this article we will consider the direct problem of ray path calculation according to electron concentration N. As it was mentioned earlier we will use the coordinate system (h, τ). To calculate ray paths, differential equation system should be used [28-29]. Here it would be convenient for us to use the following equations for calculations:

1. Equations that calculate the ray path directly with the respect to "angle of refraction"θ.

$$\begin{cases} \dfrac{d\tau}{dh} = \dfrac{R}{h}\tan\theta \\ \dfrac{d\theta}{dh} = \dfrac{1}{nh}\left(R\dfrac{\partial n}{\partial \tau} - \dfrac{h}{R}\dfrac{\partial(nh)}{\partial h}\dfrac{d\tau}{dh} \right) \end{cases}$$

(3)

2. "dinamic equations" , describing the ray path by the "time" parameter t, which physical meaning is the optical lenght.

$$\begin{cases} \dfrac{d\dot{h}}{dt} = \dfrac{(h+R)*\dot{\tau}^2}{R^2} + \dfrac{1}{2}\dfrac{\partial n^2}{\partial h} \\ \dfrac{d}{dt}\left(\dfrac{(h+R)^2}{R^2}\dot{\tau} \right) = \dfrac{1}{2}\dfrac{\partial n^2}{\partial \tau} \end{cases}, \dot{h} = \dfrac{dh}{dt}, \dot{\tau} = \dfrac{d\tau}{dt}.$$

(4)

Here R - radius of the Earth, h - the height over the Earth's surface, n - coefficient of refraction, $n = \sqrt{1 - \dfrac{\alpha}{f^2}N}$; (if N is given in units $10^{12}m^{-3}$, f - in MHz, $\alpha \approx 80.611$), τ - distance along the Earth's surface, (remember that h, τ are analog of polar coordinates, connected with the center of the Earth).

To estimate the area of using of this methods, which help to draw the ray path, test and comparison of both methods were made. To model the ray path, the quasireal models of ionosphere N (shown in fig.1) were used. In fig.1 shown are the through and local irregularities ,$h \in [0,1000], \tau \in [-1000,2200]$ km. Here and later all the pictures in shades of grey are illustrated in Cartesian coordinates, so that coordinates (h, τ) look as curvalinear coordinates, and unrefractable rays are linear.
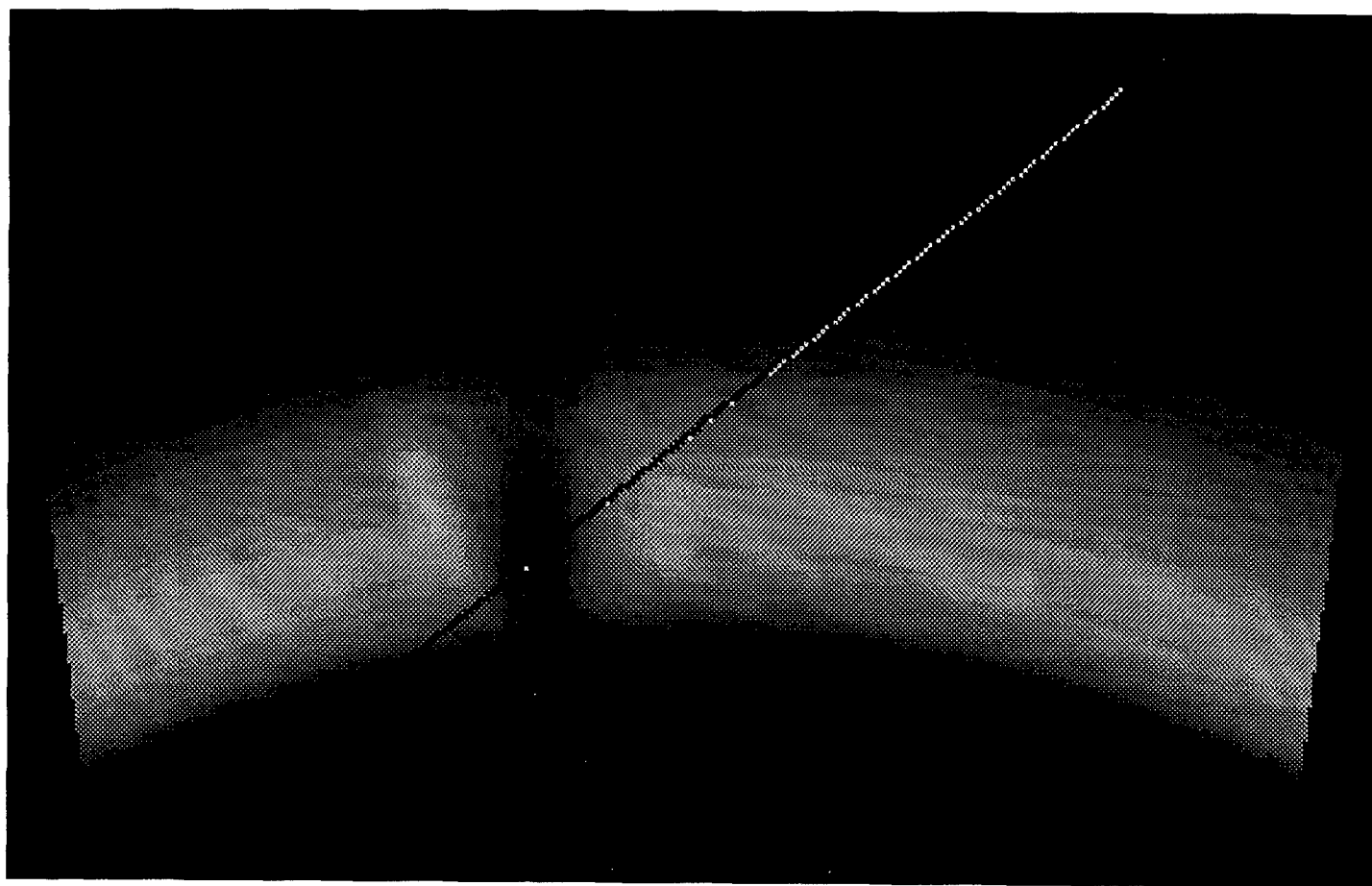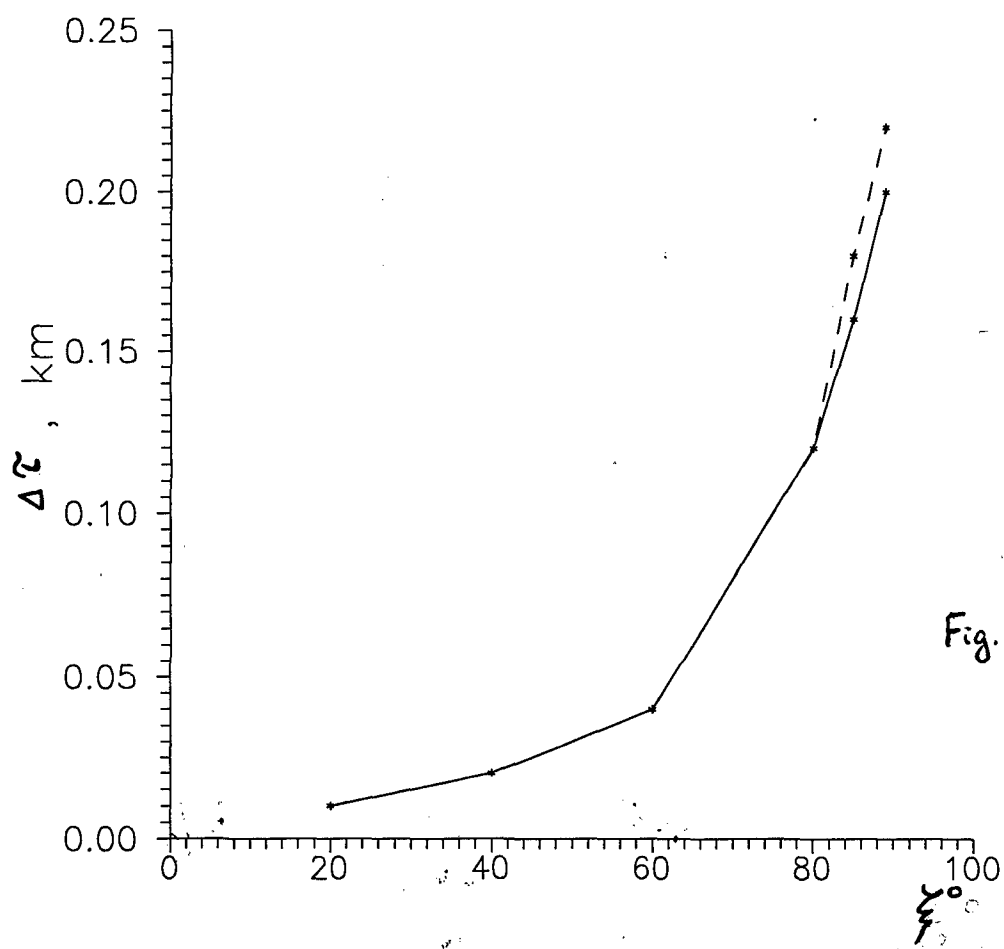
Fig.1

Fig.2

The notes of corresponded distances over h and τ in the pictures, illustrating the paths , are not shown, as the only essential things here are the distortion and divergence of rays. Let us cite the results of investigations for three essentially different cases of RT probing of ionosphere (concentration is cited in units $10^{12}\,m^{-3}$, frequency of probing f in MHz).

1. "Lower" electron concentration (with lower and average solar activity, max $N = 0.5*10^{12}\,m^{-3}, f = 150MHz$).

2. "High" electron concentration (with high solar activity, max $N = 5*10^{12}\,m^{-3}, f = 150MHz$)

3. High electron density max $N = 5*10^{12}\,m^{-3}$ and lower frequency of probing f=50 MHz.

Charts of $\Delta h(\tau), \Delta \tau(h), \Delta TEC(\tau_0), \Delta D(\tau_0)$ dependences were dedused to illustrate path calculations. Here, Δ - deflection of reflected ray from "direct" ray (may be negative, because the magnitude for "direct" ray was subtracted from the corresponded magnitude for real case), constructed with no respect to nonlinear effects, D-Doppler data. There are pictures which have ray paths with the illustration of ionosphere in grey shades, where the influence of inhomogeneities and parameters of the problem (N, f) on the ray path is seen.

To test methods of ray calculations it is expedient to use so to say "quasiexact solution" for layered ionosphere. Easy to see, that in a case of spherically layered ionosphere, equations (4) can be integrated and it is possible to get expressions for ray path $\tau(h)$ and integral I over h.

$$\tau_i - \tau(h) = \int_R^{R+h} \frac{R^2 \cos \beta dr}{r\sqrt{r^2 - R^2 \cos^2 \beta - \frac{\alpha}{f^2}(N(r) - N(R))r^2}}$$

(5)

$$I = \int_R^{R+h_0} \sqrt{\frac{r^2 - \frac{\alpha}{f^2}[N(r) - N(R)]r^2}{r^2 - \frac{\alpha}{f^2}[N(r) - N(R)]r^2 - R^2 \cos^2 \beta}} N(r)dr$$
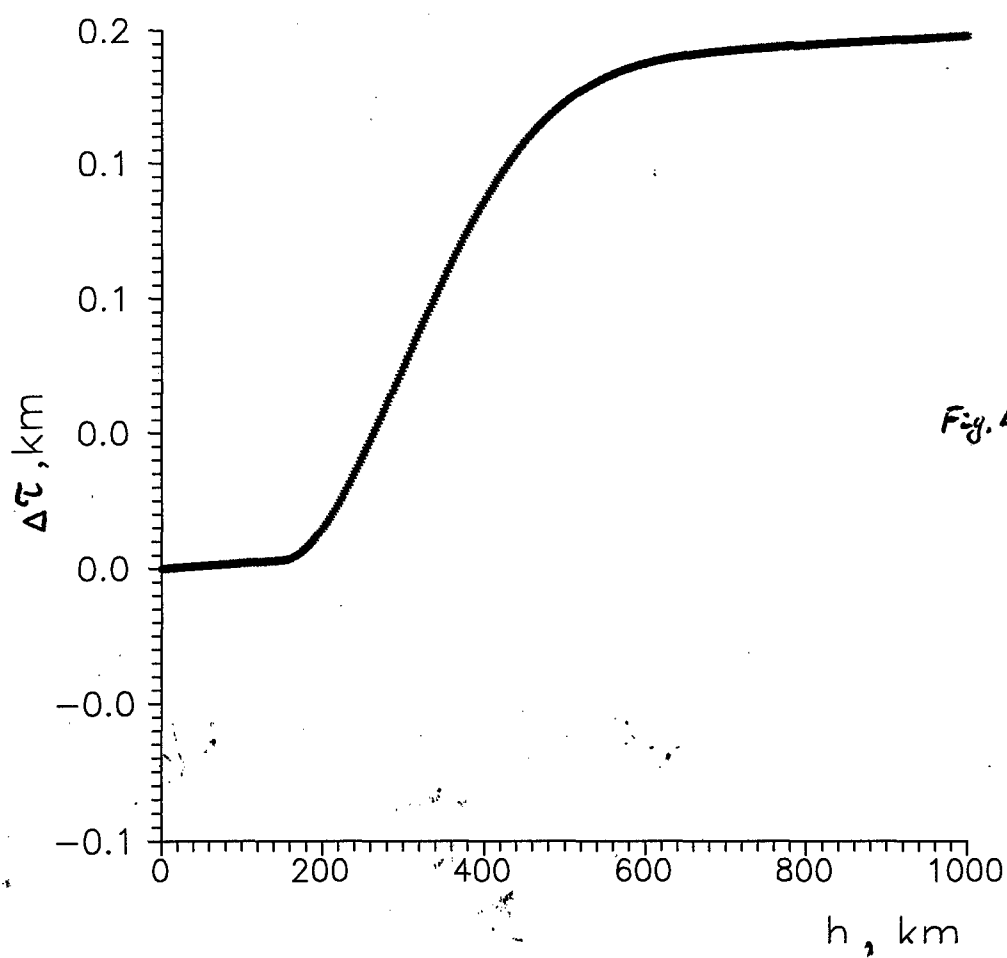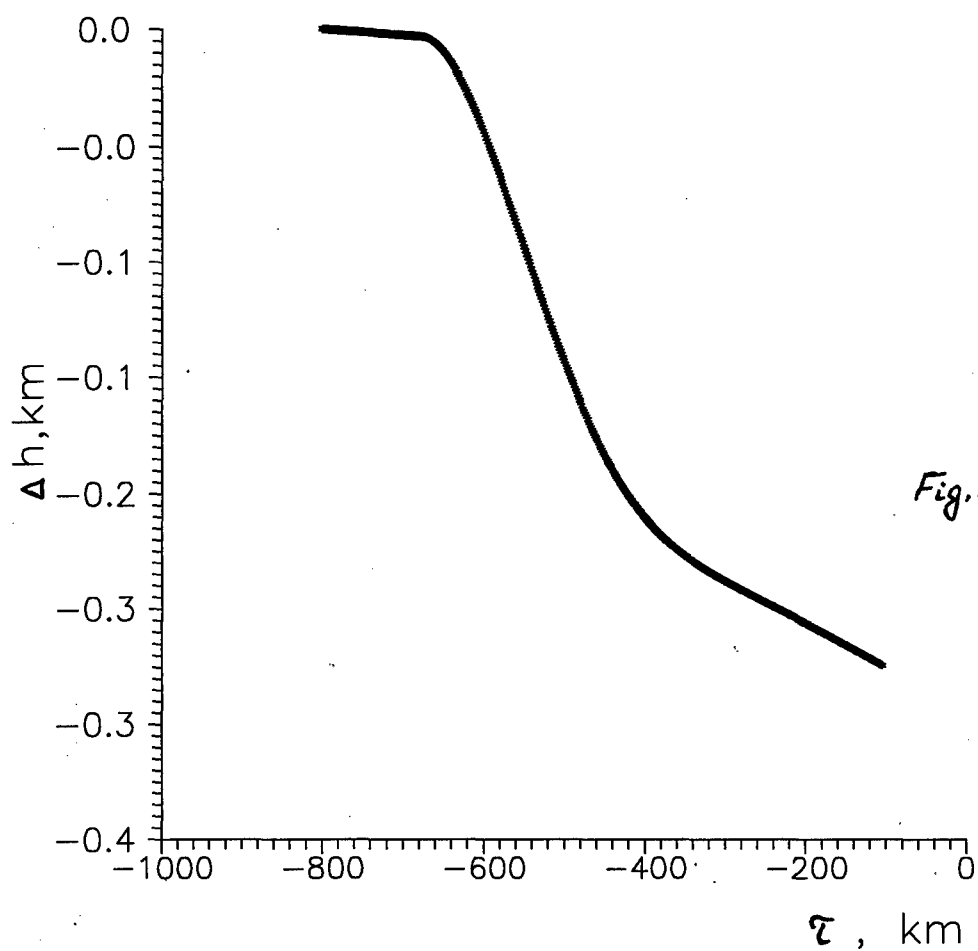
The calculation of such "quasiexact solution" were carried out for quasireal layered ionosphere (the model of fig.1, without the through and irregularities). In table 1 the

values of maximum deflection of $\tau(h_0)$ in km on the height of satellite are shown. It was found by means of both methods from differential equation system with "quasiexact solution" for one case of layered ionosphere and at various angles ξ from vertical line. Moreover the deflection over τ has the multiplicity of 100 m at fall angle $\xi = 80°$, what is quite satisfactory because at such angles the ray passes the distance multiplicity of 3000km in ionosphere. A step of solution of differential equation system by method 1 or 2 here is equal to 100m along the ray lenght, so the deflection has the multiplicity of 1 step. It is seen that the second method gives better results.

To compare the deflections of τ of solutions $\tau(h)$, which were received by two methods "in emptiness" (n=1), from exact solution "in emptiness" (fig.2), the first method , illustrated by dotted line in picture, led to maximum deflection, especially at large fall angles of ray. It is connected with the fact, that the step by step solution of differential equation system was accompanied many times by operation tan. This leads to essential supply of mistakes because of the finite bit-word lenght of computer machine. And though the second method doesn't allow to chose fixed step over h and , with the solution of differential equation system, it doesn't lead to multiple calculations of trigonometrical functions, and that is why it is more suitable for the solution of RT nonlinear problems from the point of view of accuracy and speed.

As it was expected in the case of lower electron concentration at maximum $0.5*10^{12} m^{-3}$ and f=150 MHz (case 1) the influence of ionosphere on ray path is insignificant (fig.1). Fig.3-6 show the charts of the dependences $\Delta h(\tau), \Delta\tau(h)$ for fall angles $\xi = 40,80°$ from vertical line (pic.3,5 $\Delta h(\tau)$ for $\xi = 40,80°$ correspondly, pic.4,6 $\Delta\tau(h)$ for $\xi = 40,80°$ correspondly). Pic.7 shows the values of $TEC(\tau_0), TEC_0(\tau_0)$, and fig.8 shows $D(\tau_0), D_0(\tau_0)$, where $TEC_0(\tau_0), D_0(\tau_0)$ - magnitudes of TEC and Doppler for "direct" ray (illustrated by dotted line). It is seen that with the increasing of the fall angle (what is corresponded to greater distance of ray in ionosphere), deflection of ray from the "direct" one over τ increases (compare fig.4 and 6), and, correspondly, the difference between magnitudes of TEC increases. But even for $\xi = 80°$ the difference between $TEC(\tau_0)$ and $TEC_0(\tau_0)$ doesn't exceed 0,1% for this case, and $\Delta\tau$ doesn't achieve 2km (fig.6).

In the case of high electron concentration ($N = 5*10^{12} m^{-3}, f = 150 MHz$ - the second case) the influence of nonlinear effects on ray path is essentially stronger. Fig. 9-12 show the charts of dependences $\Delta h(\tau), \Delta\tau(h)$ for fall angles $\xi = 40,80°$ from vertical line (fig.9,11- for $\Delta h(\tau)$ for $\xi = 40,80°$ correspondly, fig.10,12 $\Delta\tau(h)$ for
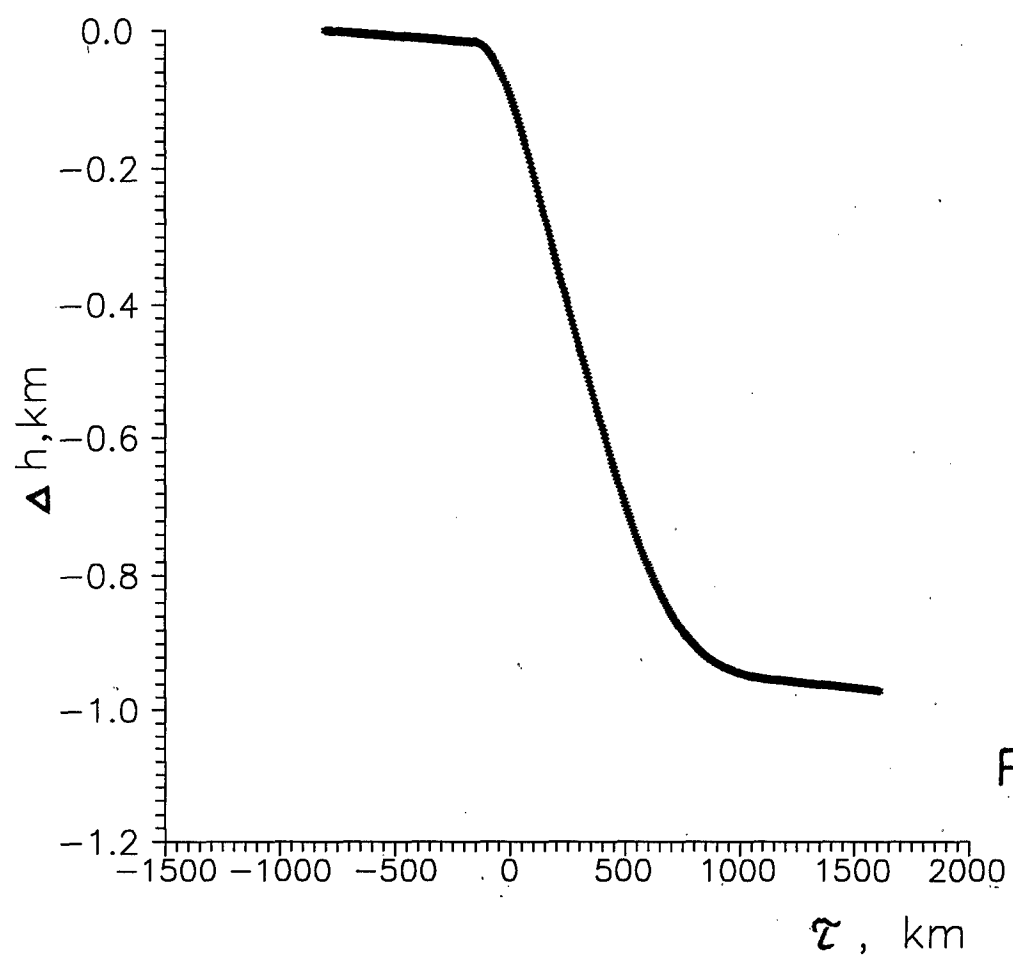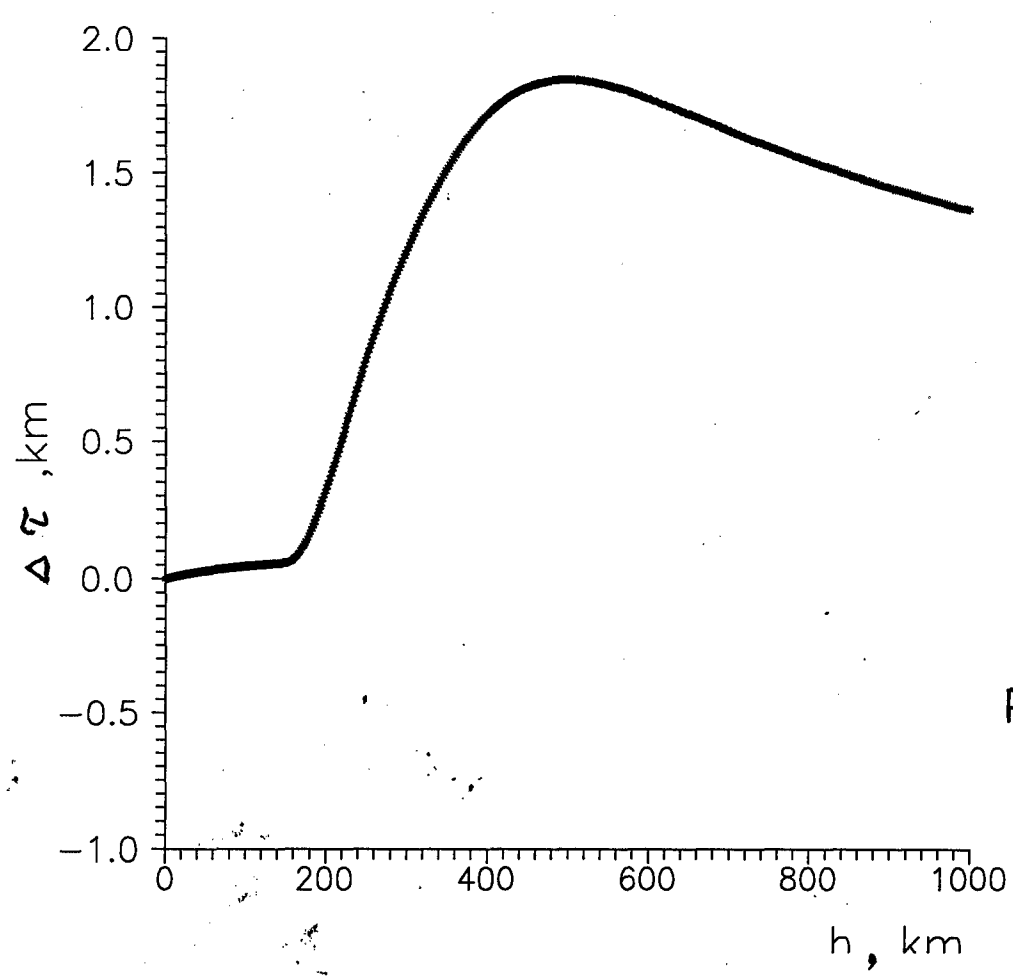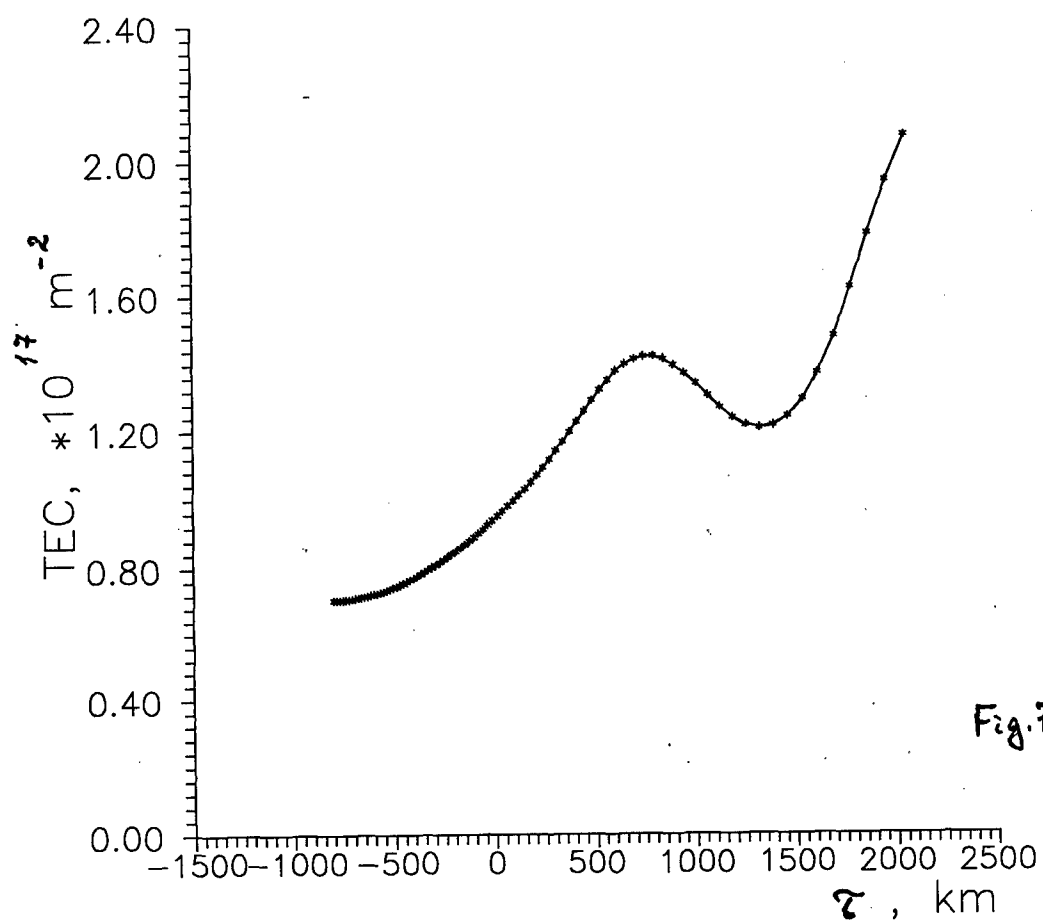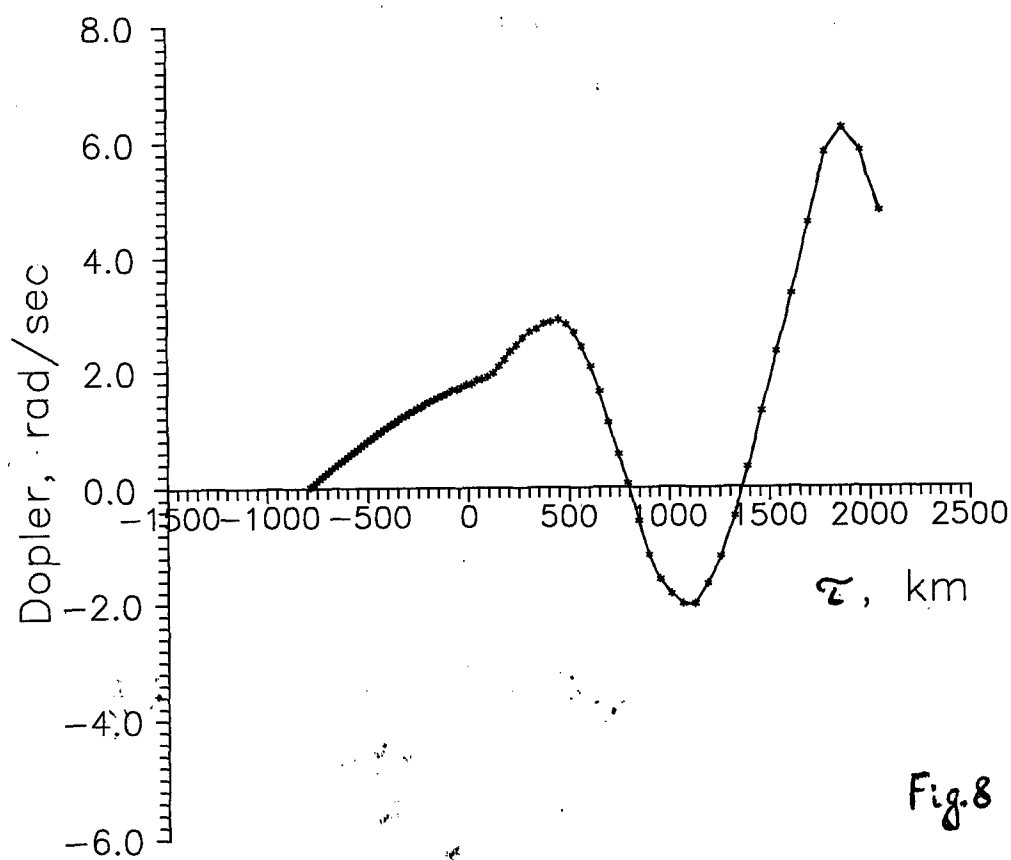
Fig. 3

Fig. 4.

Fig. 5

Fig. 6

Fig.7

Fig.8

Fig. 9

Fig. 10

Fig. 11

Fig. 12

Fig. 13

Fig. 14

$\xi = 40,80°$ correspondly). Fig.14 shows the values of $TEC(\tau_0)$ and $TEC_0(\tau_0)$, and pic.15 - the same for $D(\tau_0), D_0(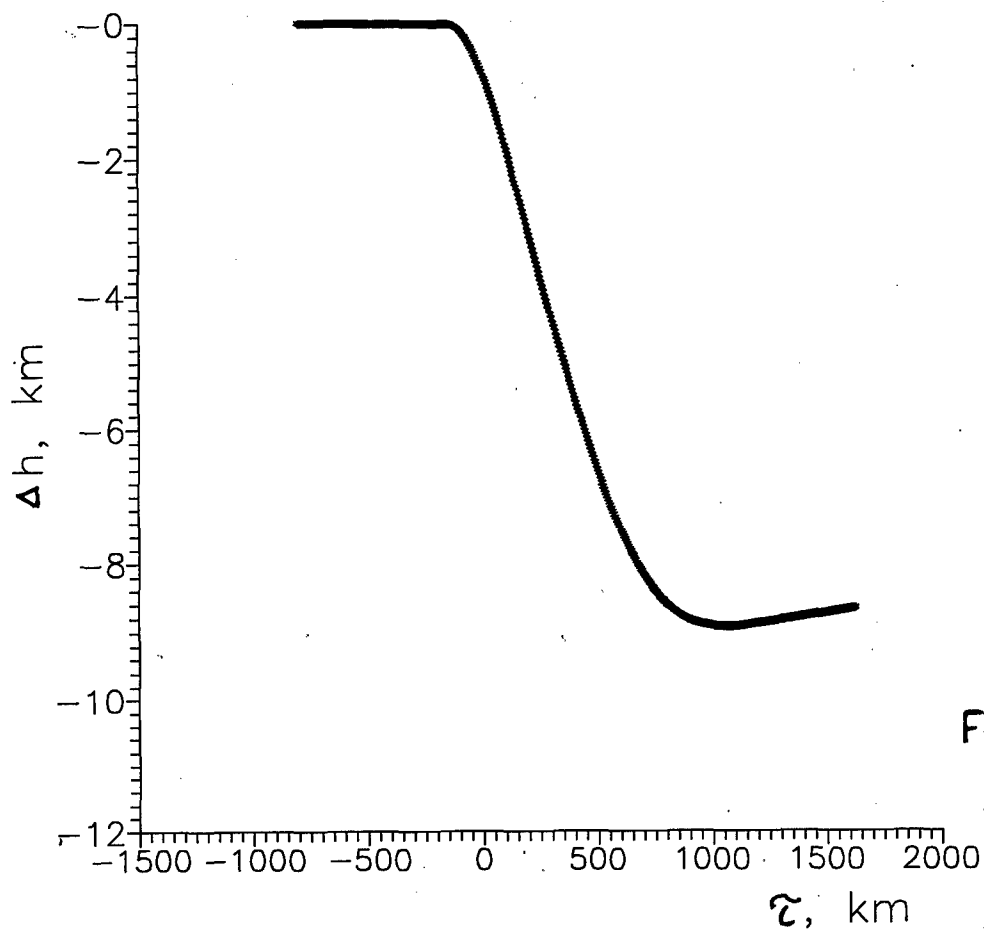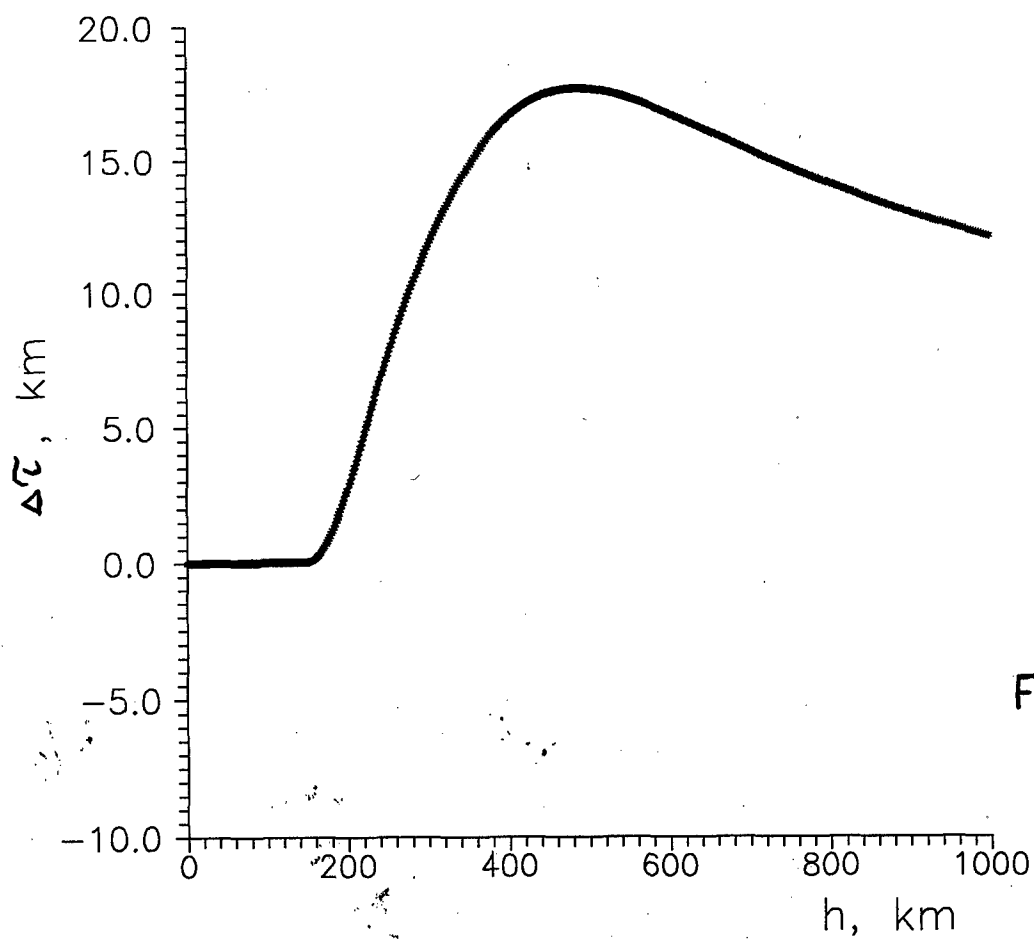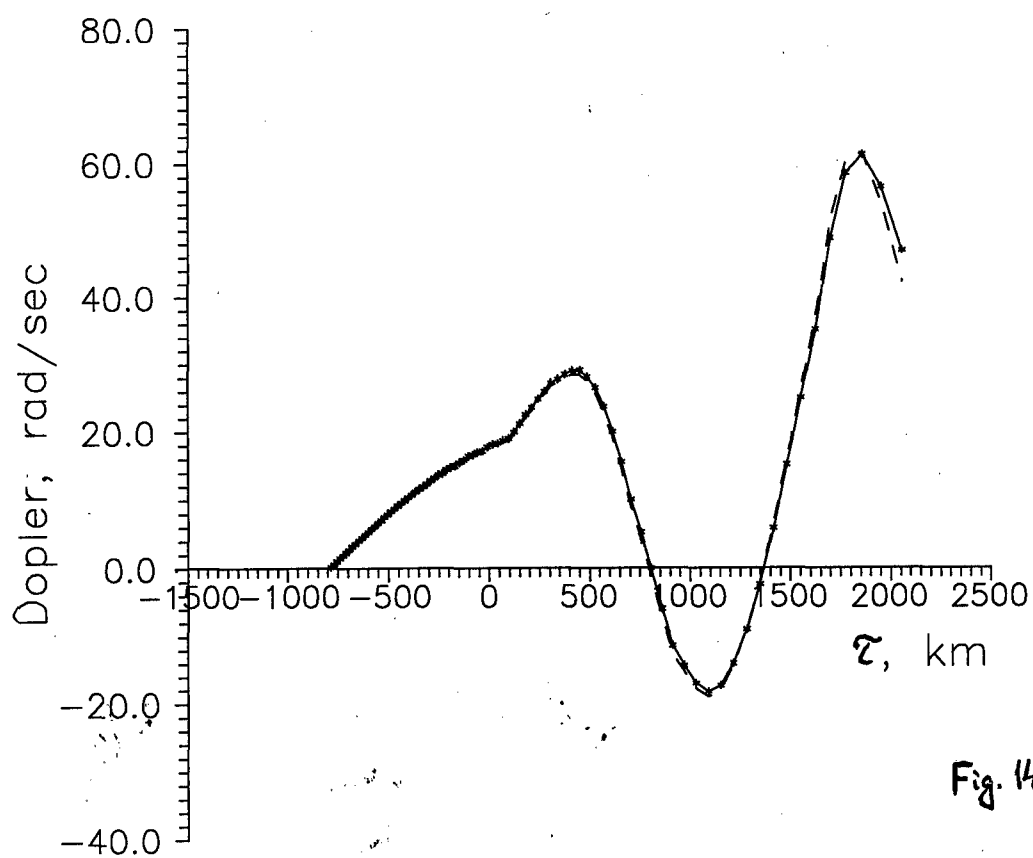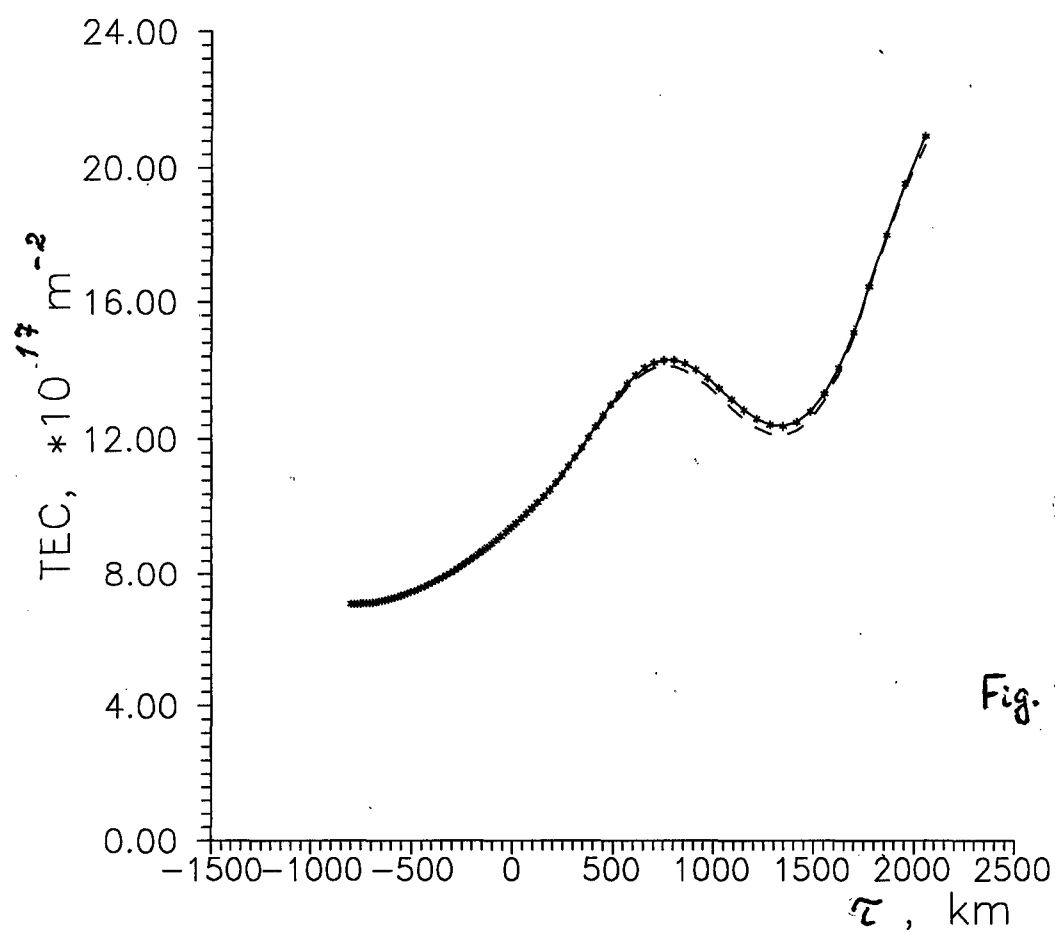\tau_0)$. In addition the mistake in data (TEC) at a fall angle equal to 80 degrees is now essential and it reaches 3% (fig.13) and $\Delta\tau(h)$ is attaining to 18 km (fig.14).

The estimations of small deflections from ray path in emptiness can be received without any difficulties from equations (4). Let us consider the vertical ray fall. It can be shown that the estimations of angles of vertical deflections and deflections themselves would be the same for another direction of ray fall. The angle χ of vertical deflection for normal ray fall $\chi = \Delta p_\tau / p$ is expressed by the analog of impulse for "dinamic" equations (4).

Let us remember that $P_h = \overset{\bullet}{h}, P_\tau = (r / R)\overset{\bullet}{\tau}, P^2 = P_h^2 + P_\tau^2 = n^2 \approx 1$, and for quasivertical ray $P_h \approx P_h(t = 0) = 1$. The increase of impulse according to τ is determined by second equation (with the respect to ignoration of difference between (R+h)/R and 1).

$$\Delta\chi \approx \Delta P_\tau \approx \frac{1}{2}\frac{\partial n^2}{\partial \tau} \Delta t \approx \frac{1}{2}\frac{\partial n^2}{\partial \tau} a \approx \frac{\alpha}{2f^2}\frac{\partial N}{\partial \tau} a \approx \frac{\alpha}{2f^2}\frac{\Delta N}{a/2} a \approx \frac{\alpha \Delta N}{f^2} \quad (6)$$

Supposed that $\Delta t \approx a$ (because $dt = dl / n \approx \Delta l$), the size of inhomogeneity, and concentration gradient is equal to ratio of its overfall ΔN and the half of total size of inhomogemeity. Then the transverse ray deflection (distance between rays) would be propotional to the passed distance L.

$$\Delta\chi \approx \chi L \approx \frac{\alpha}{f^2} \Delta N L \quad (7)$$

What is (for probing frequency 150 MHz) equal to:

$$\Delta\chi \approx 3,6*10^{-3} \Delta N L \quad (8)$$

Here ΔN is measuring in units of $10^{12} m^{-3}$. It is notable that the relations (6,7) do not involve the sizes of irregularity, everything is determined by overfall of electron concentation. For typical overfalls $\Delta N \approx (1 - 3)10^{12}$ and ray lenght

$L \approx (1 - 3)10^3 km$ the deflection (8) would be varyed in the range between one and tens of kilometers.

Fig.15 shows the deflection $\Delta\tau(h)$ (when $\xi = 80°$), calculated for the same layer (fig.1) in the third case of high concentration and lower frequency probing. For the second and the third cases the parameter $\alpha\Delta N / f^2$ differs in 9 times, that is why the deflection $\Delta\tau(h)$ behaves like the deflection from fig.6, but nearly ten times more. In the scale fig.1 the deflections equal to 10 km , which are typical for the second case, are unnoticable, that is why to illustrate path calculations the figures for the third case are cited. Fig.16 shows well the "focusing" of ray by the electron concentration trough . Fig.17-18 show, that the local irregularities can deflect the ray in various directions from the straight ray, and it depends on from what side relatively to irregularity maximum the ray passes.

As it follows from the results of this section, the small angular and linear deflections of real rays from linear approximation are propotional to variations ΔN of electron concentration and do not depend on the size of irregularities. For probing frequancy 150 MHz, these deflections are estimated less than a kilometer for variations $\Delta N \le 10^{12} m^{-3}$, that is when the solar activity is not high. For example, these deflections can reach tens of km for $\Delta N \ge (2 - 3)10^{12} m^{-3}$, when the solar activity is high. Hence, it follows that for RT investigations on 150 MHz the respect of refractable corrections is necessary only for high solar activity and for the sizes of digitization elements less than 20-30 km. The use of lower frequency radiowaves $f \le (50 - 100)MHz$ for RT investigations requires the respect of refraction.

Table 1.

$\xi, °$	$\Delta\tau_{max}(h)$, кm. METHOD 1	$\Delta\tau_{max}(h)$, кm. METHOD 2
0	3.78E-5	3.78E-5
20	3.08E-2	4.47E-3
40	-7.14E-2	1.17E-2
60	-0.12	3.03E-2
80	-0.27	0.11

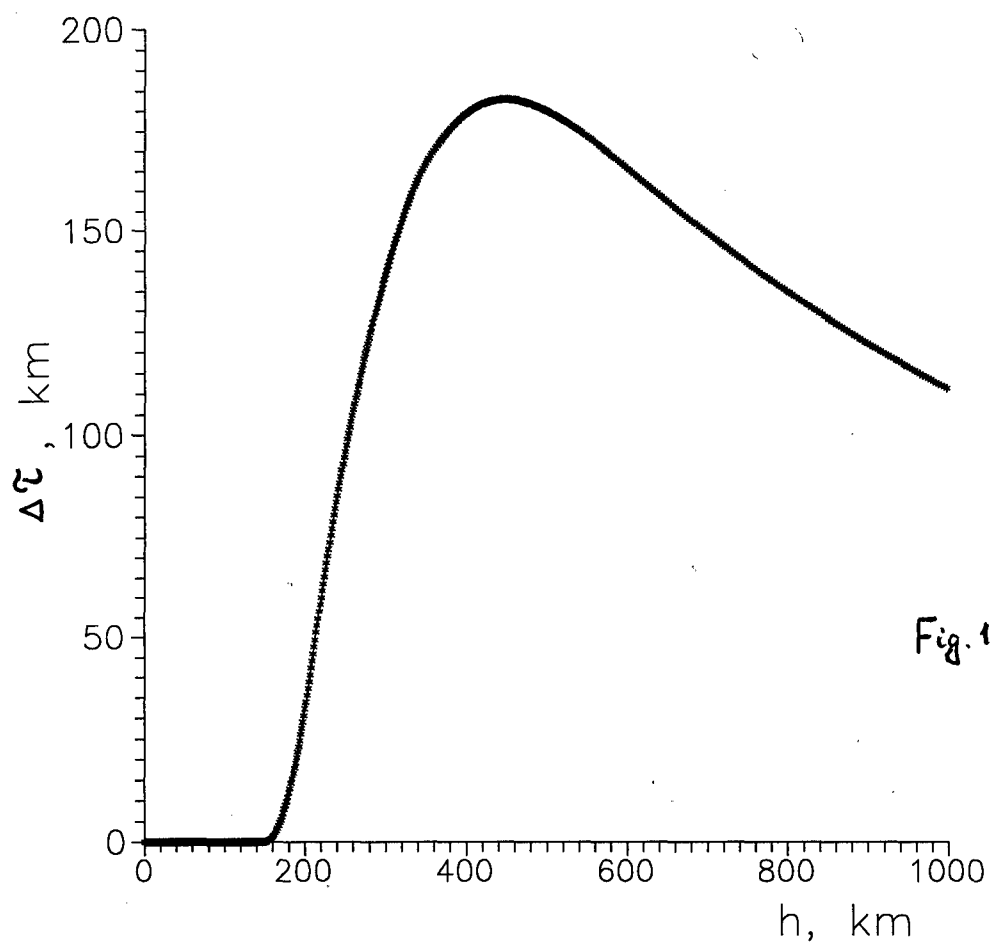## Description of the programs for calculation TEC, Phase and Phase-difference measurements for Nonlinear RT.
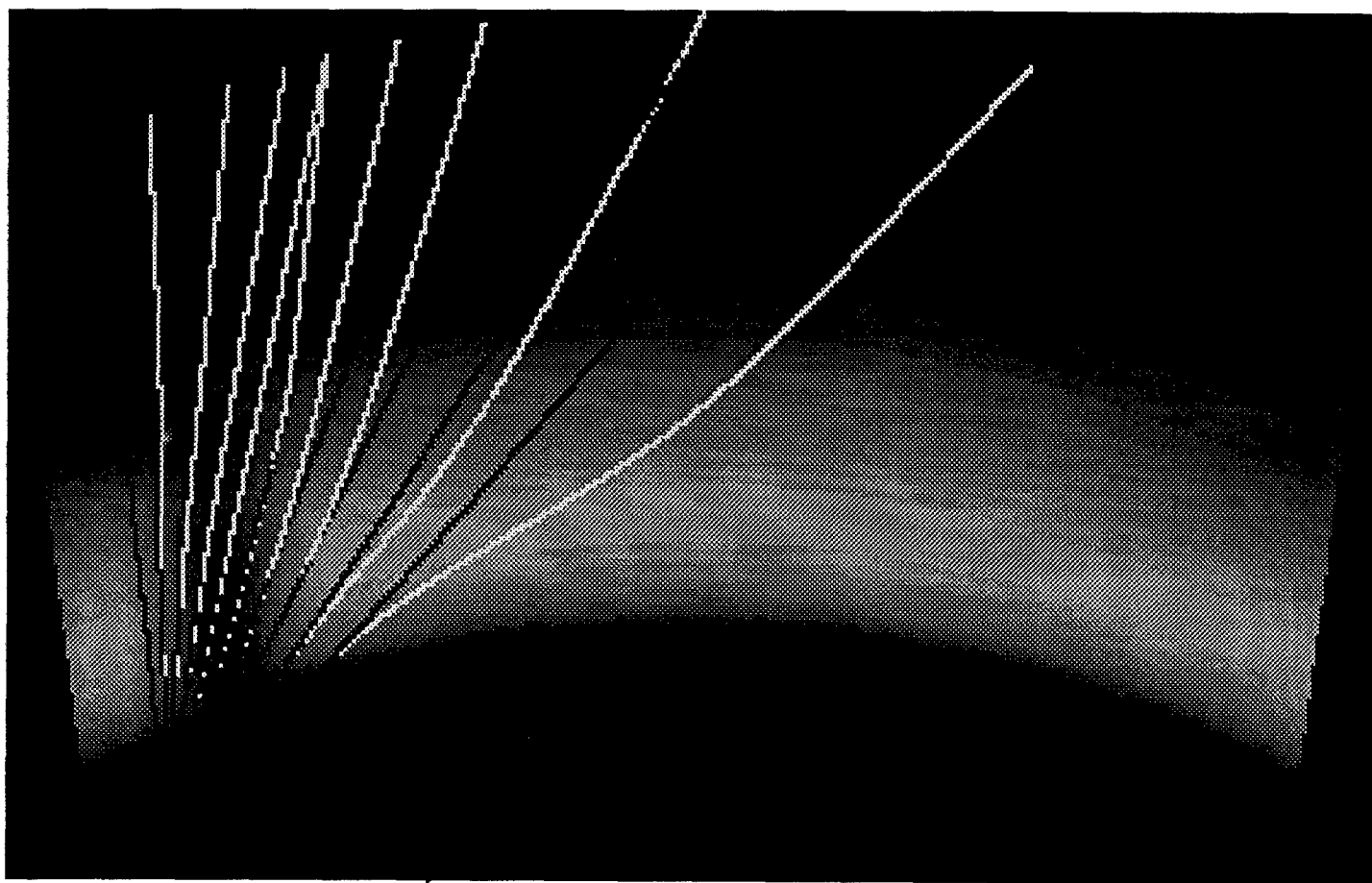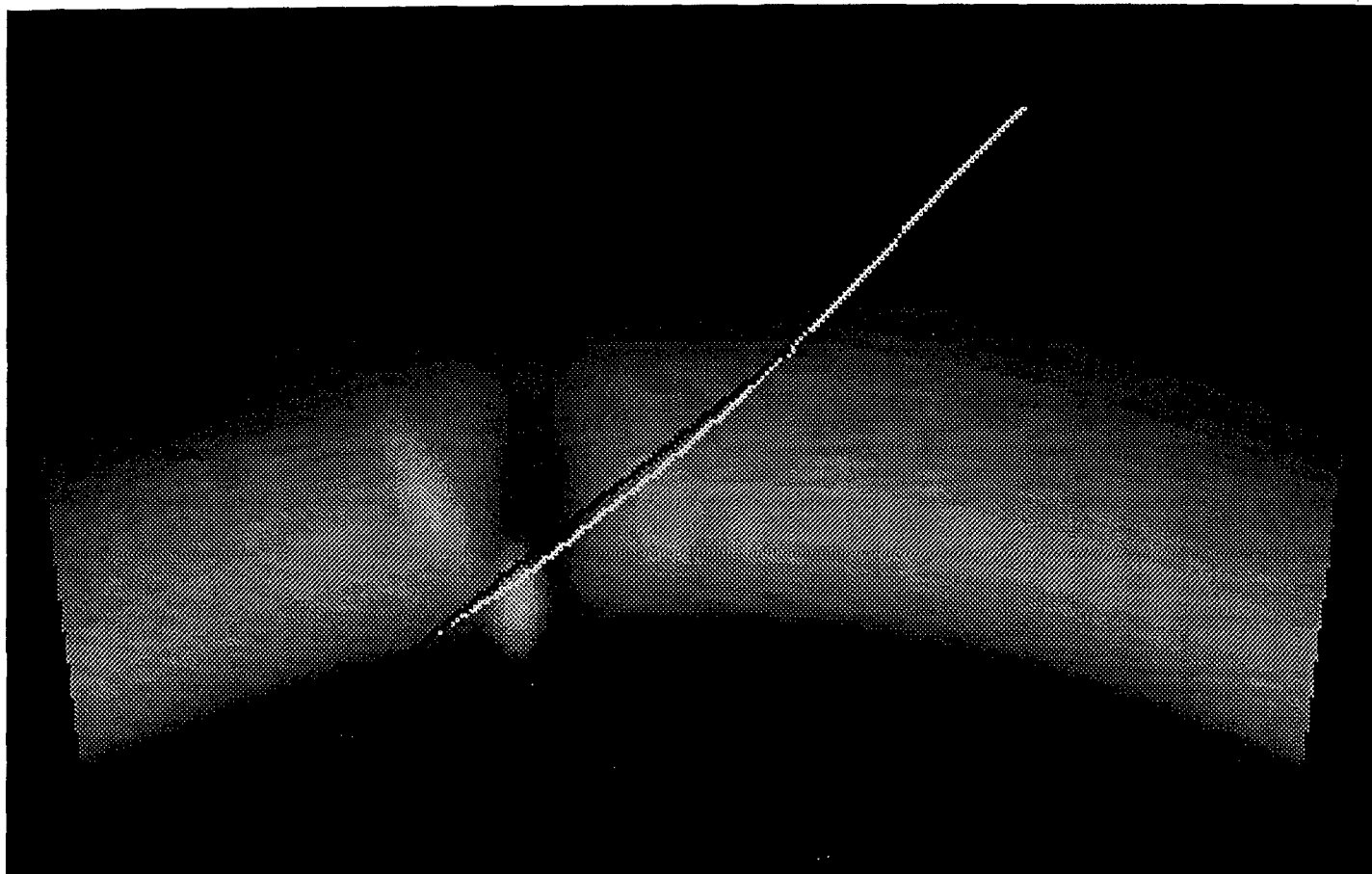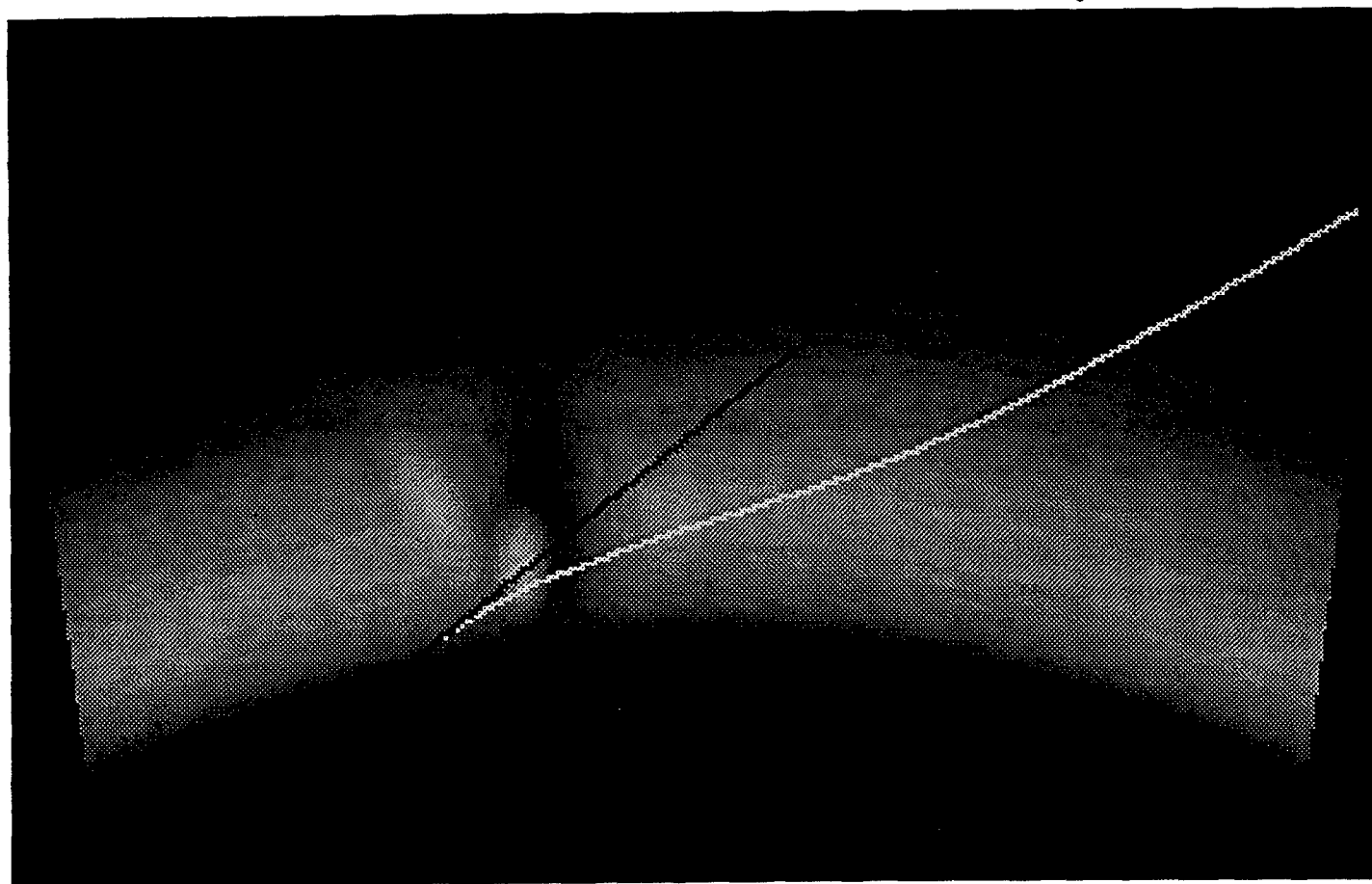
Fig. 15

Fig. 16

Fig. 17

Fig. 18

System Requirements

- Computer: IBM AT-486 or compatible (with coprocessor)
- Operating System: MS-DOS or PC-DOS version 3.0 and later
- Memory: at least Extended memory 8 Mbytes
                    (depends on geometry and type of
                    approximation reconstructed function)
- Hard Disk Space: 35 Mbytes
- Software: NDP-FORTRAN-486 Compiler Ver.3.1
                    NDPLink Ver.3.0 (C) MicroWay, Inc.

Program <dir_nl.for>

   This program solves direct problem for Nonlinear and Linear RT measurements, namely, determines the model structure and calculates the TEC, Phase and Phase-difference integrals on the model structure.

Input parameters and files:

   When starting program, you may choose the type of RT (Nonlinear or Linear) and RT measurements (TEC, Phase or Phase-difference). This program calculates Phase-difference measurements only for linear RT. Then program asks about integrals to calculate. If you need only model structure you can answer 'No'.

   Input file <task.dir> contains information about RT measurements geometry and defines the names for output files. The example of this file is enclosed. It contains the following lines:

'F_Nmod' - input file that describes parameters of model structure.
       The example of this file is enclosed.

'F_model' - output file with model structure (GRD-format)

NF, NR - number of discrets on the horizontal and vertical grid

Nrec   - number of receivers

FP, TSAT0, TSAT1, RAY - Nrec lines with coordinates of receivers,
                    initial and final positions of satellite
                    in km and number of rays for each receiver

HFIST, HFIN - vertical size of reconstructed area in km

TFIST, TFIN - horizontal size of reconstructed area in km

NJ - number of the discrete steps along the ray

'FINT' - Nrec lines with the names of output files for integrals
        for each receiver

Freq - the probing frequency (MHz)

ts, ddt, ddh - parameters for subroutine <INTERG>

The model structure is determined by function <FMODEL> which uses functions <FUNC1>, <FUNC2>, <HOMPAR>, <HOMCOS>. The combinations of these functions make it possible to obtain different model structures.

Subroutine <DEFPSI> determinates the angles of rays on the satellite's cooordinates.

Subroutine <DEFINT> calculates the integrals for all rays for each receiver and uses subroutine <INTERG> which calculates the integral for one ray.

Output files:

MODEL.GRD - file with model structure (GRD-format)

Files <lin_int> - arrays of either TEC, Phase or Phase-difference integrals

Compilation

mf77 dir_nl.for -ol -486

RUN

ndprun dir_nl.ltl

Program <dpl_nl.for>

    This program calculates Phase-difference measurements for nonlinear RT for one receiver.

Input parameters and files.

'SFILE' - input file with phase array

NZ - dimension of phase array

Subroutine <rd> reads of input file

Subroutine <dpl> calculates doppler by means of approximation of phase of polynomial of the power 3 and uses subroutines <regres> and <gauss>.

Subroutine <wr> writes in output file.

Output file.

'NFILE' - output file with doppler

Compilation

mf77 dpl_nl.for -ol -486

RUN

ndprun dpl_nl.ltl

Program <tblint.for>

   This program calculates linear interpolation of input array.

Input file.

'interp.ts' - input file contains number of receivers and

      Nrec lines with names of input and output files,

      with dimensions of input and output arrays.

The example of this file is enclosed.

Output file.

'F_appr' - output files with interpolated arrays.

Compilation

mf77 tblint.for -ol -486

RUN

ndprun tblint.ltl

2.2. Design of the different versions of the RT operators for nonlinear Radiotomography.

   The problems of the design of the different versions of the RT operators (matrices) are considered in this section. At first it is necessary to perform digitization of the linear integrals (1.1) according to the position of the satellite, which is dependent on the coordinates τ_{0j} or the angle $\alpha_{0j} = \tau_{0j} / R$. The dependences $\tau(h)$ or $h(\tau)$ are determined from ray equations (4). A series of elevation β_{ij} of the satellite for i-receiver are determined from relation (1.6) which define a series of discrete values of the linear integrals $I_{ij} \equiv I(\beta_{ij}, \tau_i)$. The

discretization procedure is fully described in [3, 25].　　As it was shown earlier in [3,.8,.25], analogously we obtain the system of linear equations, which may be either overdetermined or sub-definite.

$$L_{i,j}^{m,n} F_{m,n} = I_{i,j} \ , \ \text{or} \ L_{MJ} F_M = I_J. \tag{9}$$

Here, "renumbering" of the ray $(i,j) \rightarrow J$ and the sells of the ionosphere $(m,n) \rightarrow M$ is performed in the second equation. The problem of ionospheric RT according to phase-difference or Doppler measurements require higher-order interpolation than the piecewise-constant representation of the function. The Doppler frequency $\Omega = d\phi / dt$ measured in the experiment is determined by the phase derivative (2), namely:

$$\Omega = \frac{V_0}{R + h_0} \frac{d\phi}{dt}$$

where V_0-velocity of a satellite moving uniformly along a circular orbit. As it was shown in [3,.10], if the matrix of the direct problem $L_{JM} : F_M \rightarrow I_J$ is continuous with respect to the angle of the satellite α_0, it is possible to obtain a system for phase-difference or Doppler data by differentiating (9) with respect to the angle α_0:

$$A_{JM} F_M = D_J. \tag{10}$$

Here, $D_J \equiv \Delta I_J / \Delta \alpha_0$ are Doppler data and $A_{JM} \equiv \Delta L_{JM} / \Delta \alpha_0$ is finite -difference ratio (or derivative) of the matrix L_{JM} to the increment of the angle.

The methods of constructing the projection operators or L_{JM} matrices for the phase RT and also for the phase-difference RT are similar to the methods presented in details earlier in [3, 25], but it is necessary to take into account the dependence $\tau(h)$ or $h(\tau)$. The following operators (matrices) for solving the RT problems are described:

A - is built with the piece-constant approximation,

B - is built with the piece-planar approximation,

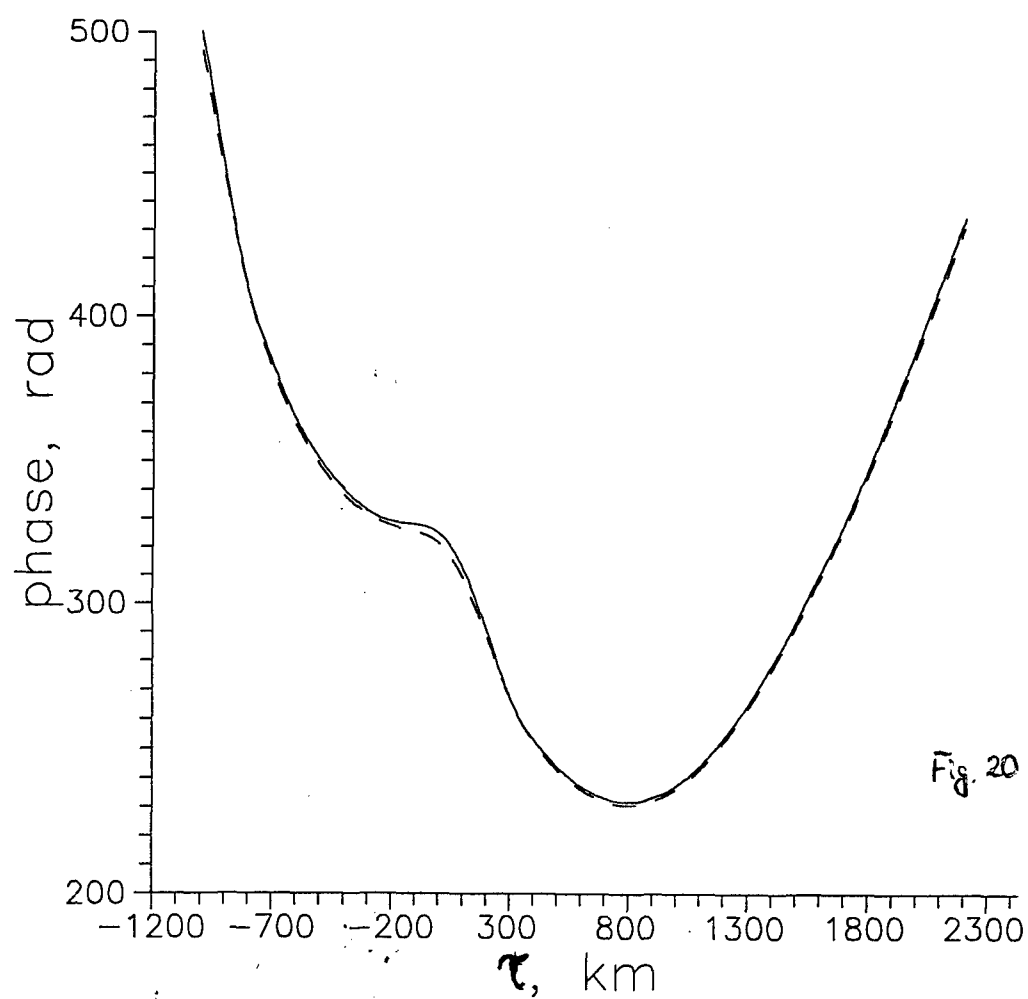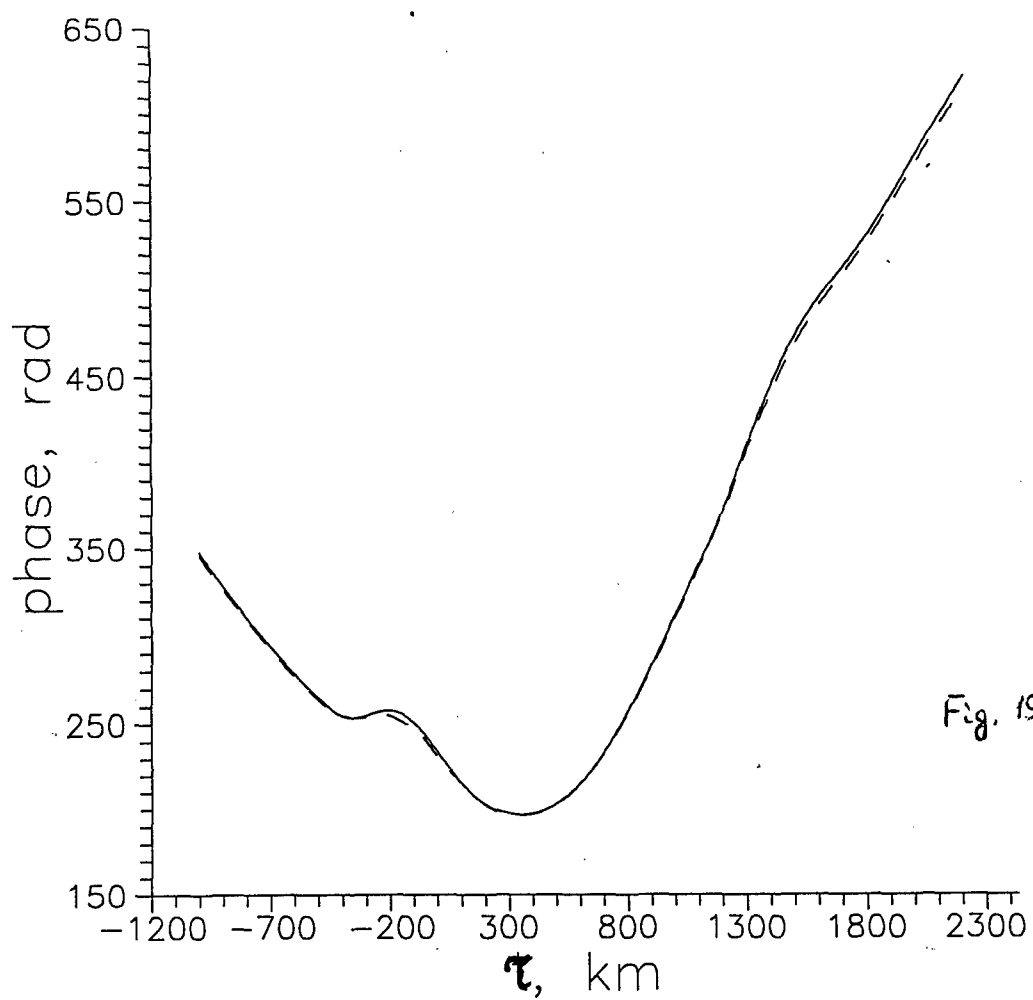C - is built with the linear product approximation,

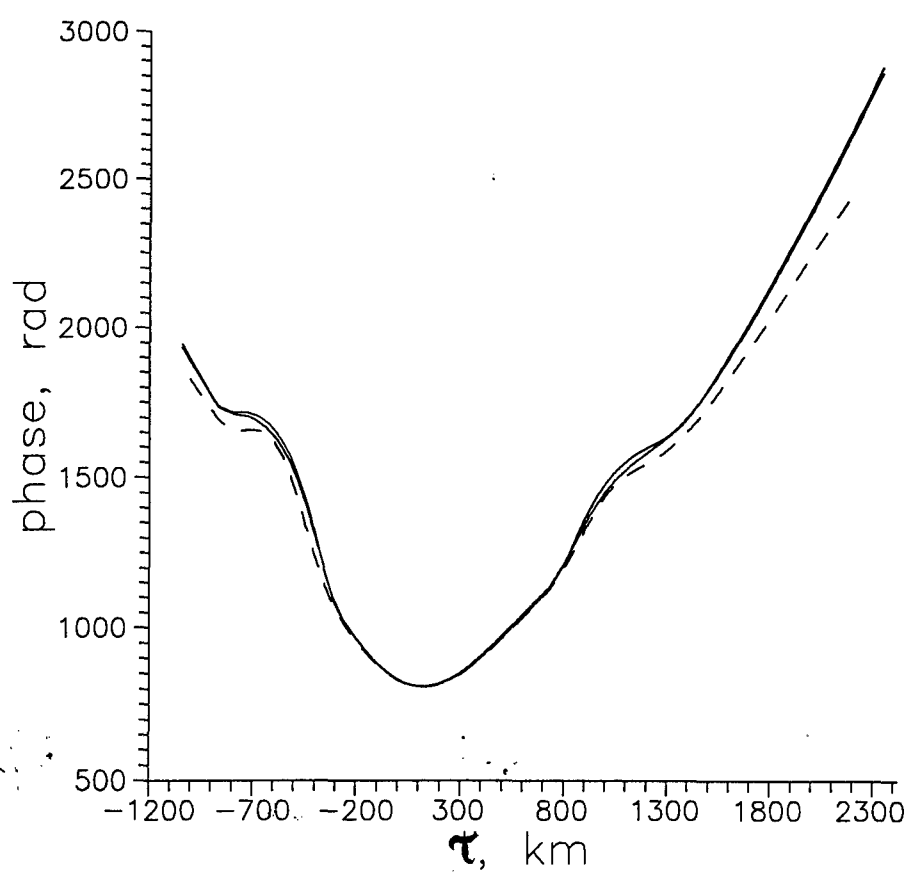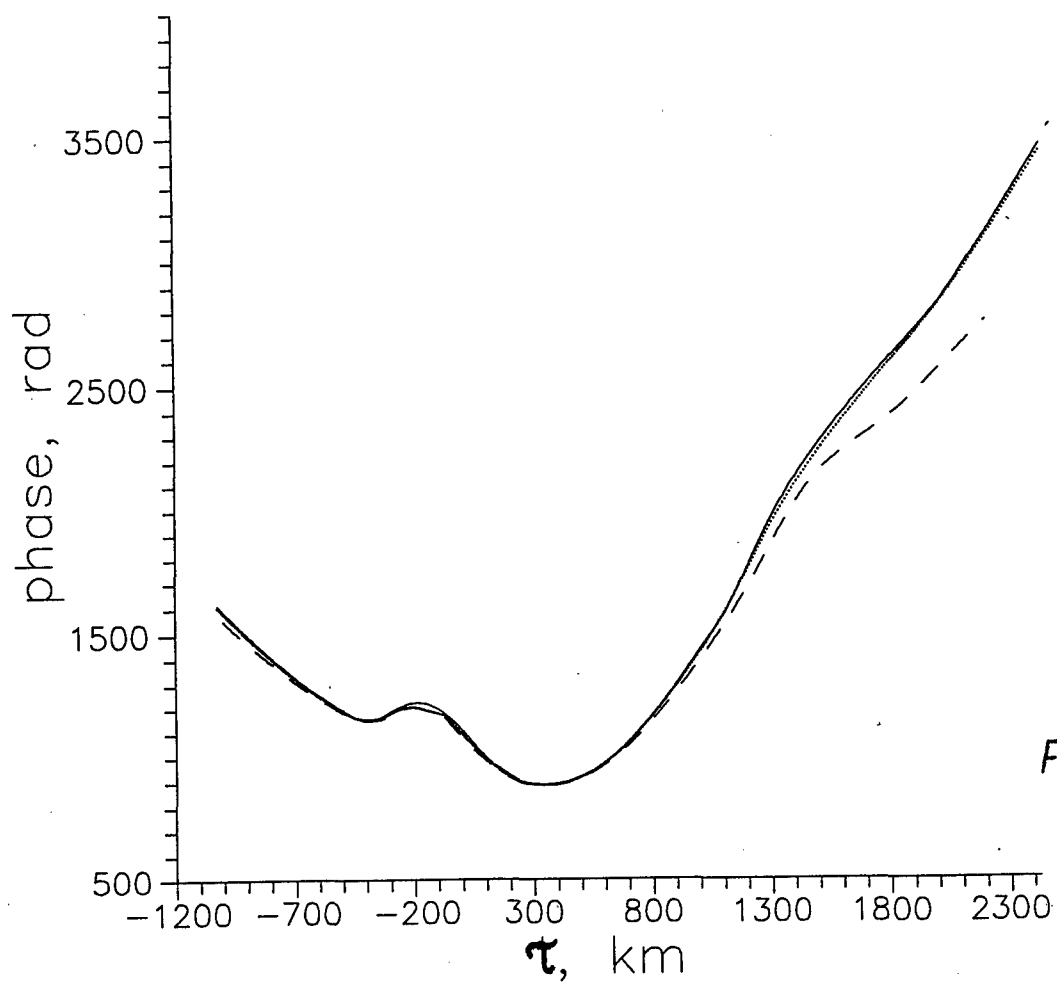D - is built with the cubic spline product approximation.

Projection operators with approximations of higher orders allow a better approximation of the operator of the direct problem, i.e. they enable us to come closer to the true operator of the direct problem. It is necessary to note that formally in the shape of equations (9-10), the problems of linear and nonlinear RT are identically. But it is not so, when designing of operators in the problems (9-10) we use direct rays in the linear RT, on the other hand in the nonlinear RT we use the rays are determined by system (4). Therefore the equations (9-10) relatively sought function F (the distribution of the electron density) are nonlinear, because the distribution of the electron density defines the structure of operators A and L in (9-10). Of course, if the curvature of the rays is not great, than the operators of linear and nonlinear RT will be practicallly coincided.
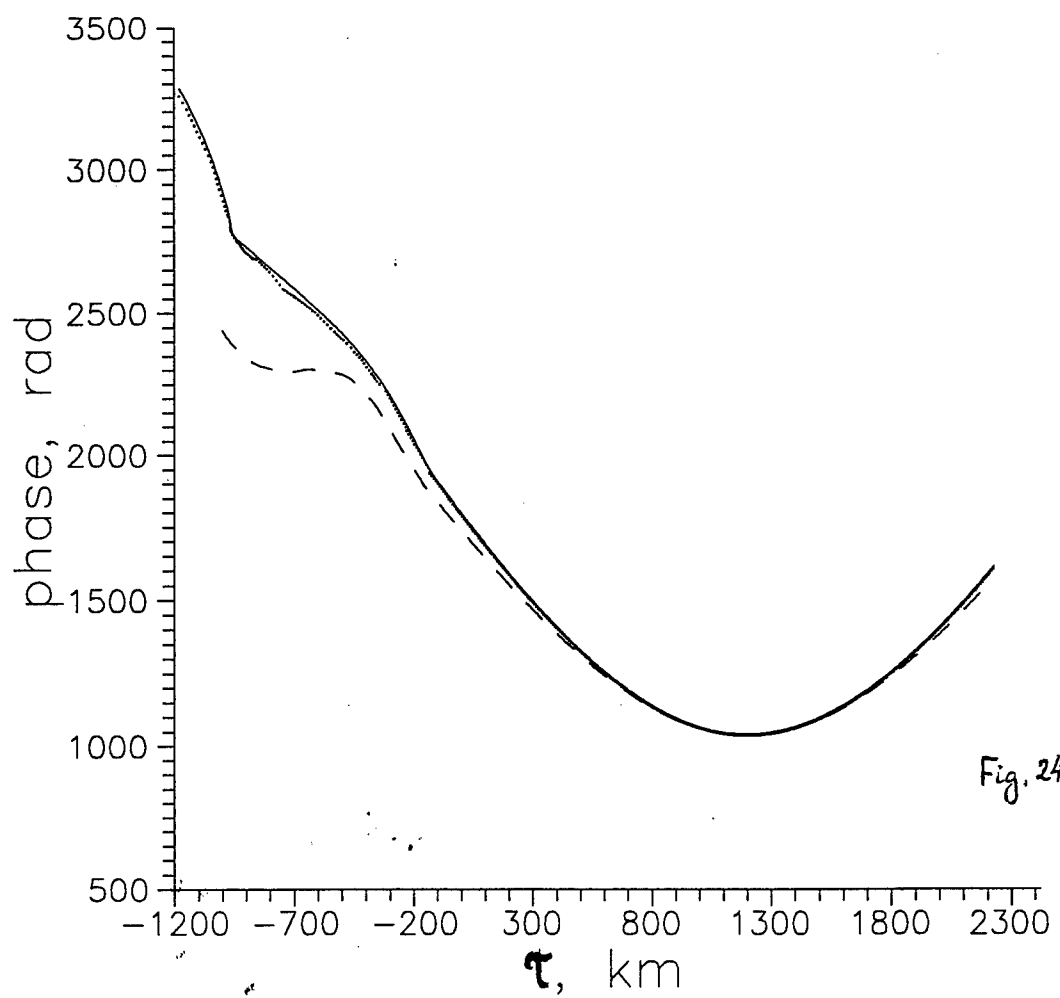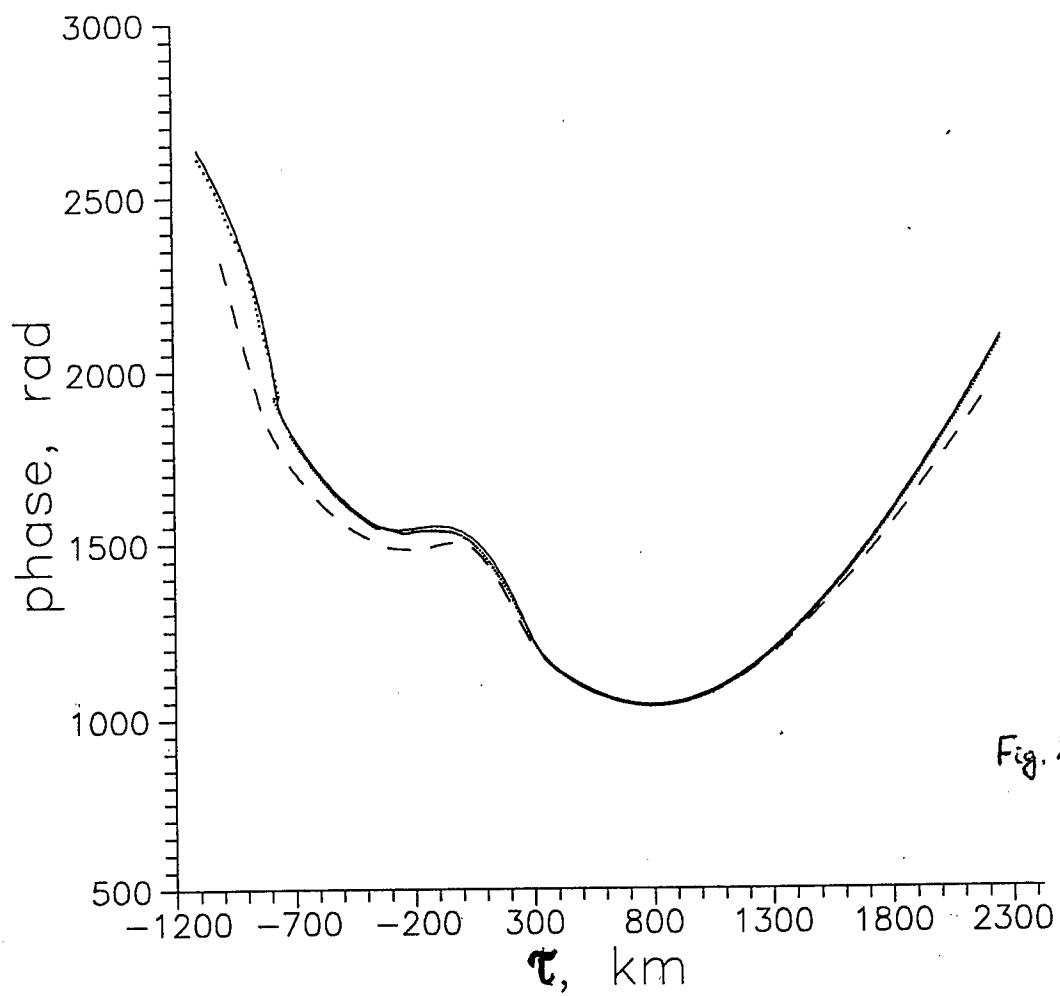
Table 1,2 show examples of errors of calculations of the phase (integrals- I_J) for each of receiving site (in this case a chain of four receiving sites with cooordinates τ: 0, 300, 800 and 1200 km are used) with refraction and without refraction for model 1: two irregularities are on the edge of the trough (this model will be discribed in the next section) with the help of different operators: B, C. For model 1 the electron density ΔN changes from $1*10^{12} m^{-3}$ (tabl.1) to $5*10^{12} m^{-3}$ (tabl.2) at probing frequency 150 MHz. Errors of the numerical simulation can appropriately be characterized by number δ, which shows the deviation of the calculated function (being reconstructed) $\overline{F}$ from the true function F: $\delta = \|F - \overline{F}\| / \|F\|$. The norms of the spaces l^2 and l^∞ can be helpfully used ($\delta_2 \equiv \delta(l^2)$ and $\delta_\infty \equiv \delta(l^\infty)$).

As it is seen from tabl.1 if ΔN is about $10^{12} m^{-3}$ the errors of calculation of the direct problem operator with and without refraction are commensurately and consist of part of percent. In other words true phase little differs from the phase calculated without refraction, that is illustrated in Fig.19 (first receiver) and Fig.20 (third receiver). The true phase is shown by solid line, and dashed line is the phase calculated without refraction in these figures. The curves are practically coincided. The phase calculated with refraction is not presented, because it is indistinguishably from true phase.

We have another situation if ΔN is about $5*10^{12} m^{-3}$. As it is shown in tabl.2, the errors of calculation of the direct problem operator without refraction δ_∞ are 25% in space l^∞ at the same time the refraction corrections allow to decrease these errors up to units of percent. The curves of true phase (solid line), phase calculated with

Fig. 19

Fig. 20

Fig. 21

Fig. 22

Fig. 23

Fig. 24

refraction (dotted line) and phase calculated without refraction (dashed line) are presented in Fig.21-24 for all four receiving sites. One can see essential difference between true phase and phase calculated without refraction. In particular, the phase calculated without refraction has different behaviour than true phase in Fig.21 (receiver 1) and in Fig.24 (receiver 4), and the difference of values is about 700-800 radian (Fig. 24). In other hand, the phase calculated with refraction has not essential differences from true phase. Hence, as it was mentioned in section 2.1, it is necessary to take into account the refraction corrections for RT at probing frequency 150 MHz when $\Delta N \geq 2 - 3*10^{12} m^{-3}$, i.e. in years of high solar activity.

Table 1
Accuracy of construction of the direct problem operator

Model 1, $\Delta N \approx 10^{12} m^{-3}$

Operator type	Receiver	Nonlinear RT δ_∞	δ_2	Linear RT δ_∞	δ_2
B	1	0.0084	0.0061	0.0131	0.0096
	2	0.0079	0.0057	0.0111	0.0081
	3	0.0068	0.0051	0.0123	0.0073
	4	0.0070	0.0052	0.0134	0.0087
C	1	0.0071	0.0057	0.0130	0.0093
	2	0.0081	0.0059	0.0110	0.0082
	3	0.0067	0.0051	0.0121	0.0071
	4	0.0069	0.0051	0.0115	0.0086

Table 2
Accuracy of construction of the direct problem operator

$$\textit{Model 1,} \quad \Delta N \approx 10^{12} m^{-3}$$

Operator type	Receiver	Nonlinear RT		Linear RT	
		δ_∞	δ_2	δ_∞	δ_2
B	1	0.0115	0.0081	0.2056	0.1192
	2	0.0098	0.0070	0.1486	0.0769
	3	0.0106	0.0061	0.1241	0.0683
	4	0.0135	0.0065	0.2591	0.1242
C	1	0.0092	0.0073	0.2041	0.1191
	2	0.0101	0.0072	0.1471	0.0767
	3	0.0099	0.0060	0.1219	0.0679
	4	0.0109	0.0064	0.2558	0.1238

Description of the program for calculation of the different versions of the matrix (operators) for Nonlinear RT

System Requirements

- Computer: IBM AT-486 or compatible (with coprocessor)
- Operating System: MS-DOS or PC-DOS version 3.0 and later
- Memory: at least Extended memory 8 Mbytes
              (depends on geometry and type of
              approximation reconstructed function)
- Hard Disk Space: 35 Mbytes
- Software: NDP-FORTRAN-486 Compiler Ver.3.1
              NDPLink Ver.3.0 (C) MicroWay, Inc.

Program <mat_nl.for>

This program designs different versions of the operators (matrics) for phase RT or phase-difference RT.

Input parameters and files:

When starting program, you may choose the type of RT (Nonlinear or Linear) and RT measurements (TEC, Phase and Phase-difference).

Input file <task.dir> is same as in program <DIR_NL.FOR>

Parameters <NF, NR, NREC, NJ, FP, TSAT0, TSAT1, RAY, HFIST, HFIN, TFIST, TFIN, Freq, ts, ddt, ddh> are similar to same parameters of program <DIR_NL.FOR>.

File <name_F.mat> contains NREC lines with names of output files.

'F_model' - input file of model structure (program <DIR_NL.FOR>)

APTYPE - type of approximation of reconstructed structure, it is introduced from the screen

Subroutine <DEFPSI> determinates the angles of rays on the satellite's coordinates.

Subroutine <DEFMAT> determinates the matrix elements with corresponding approximation for one receiver and uses subroutine <RAYINT> and subroutine <APPROX>.

Output files:

Files <F_matr> - arrays of matric of corresponding approximation for each receiver

File <Fparam> - parameters of matrices for each receiver

Files <F_int> - results of multiplications of calculated matrix and model structure

File <F_st> - array (LST) of number of all rays which cross the corresponding discret of model

Compilation

mf77 mat_nl.for -ol -486

RUN

ndprun mat_nl.ltl

2.3 The solution of the inverse problem for satellite nonlinear Radiotomography.

In this section we will cite the results of solution of inverse nonlinear RT problem. As we noted earlier, equation systems (9-10) are nonlinear equatons relatively to electron density distribution, because electron density distribution determines also the structure of operators A and L themselves in (9-10). The successive approximation method is the most suitable method to solve such linear equation systems. This approach is correct because the ray distortion is not strong in the majority of practically interesting cases and operators of linear and nonlinear RT are close. On the first stage of successive approximation method matrixes L and A are calculated using the initial approximation N. Then one of the linear equation systems is solving (9 or 10 correspondly) and the first approximation of electron density distribution N is finding. On the second stage the following approximations for matrixes A or L are calculating using the first approximation N. Then again the corresponding linear equation system is solving and the second approximation of electron density distribution N is finding. Further this process can be repeated. Thus, here, on every stage , the linear equation system is solving, using the operator matrix, which was constructed according to previous approximation N.
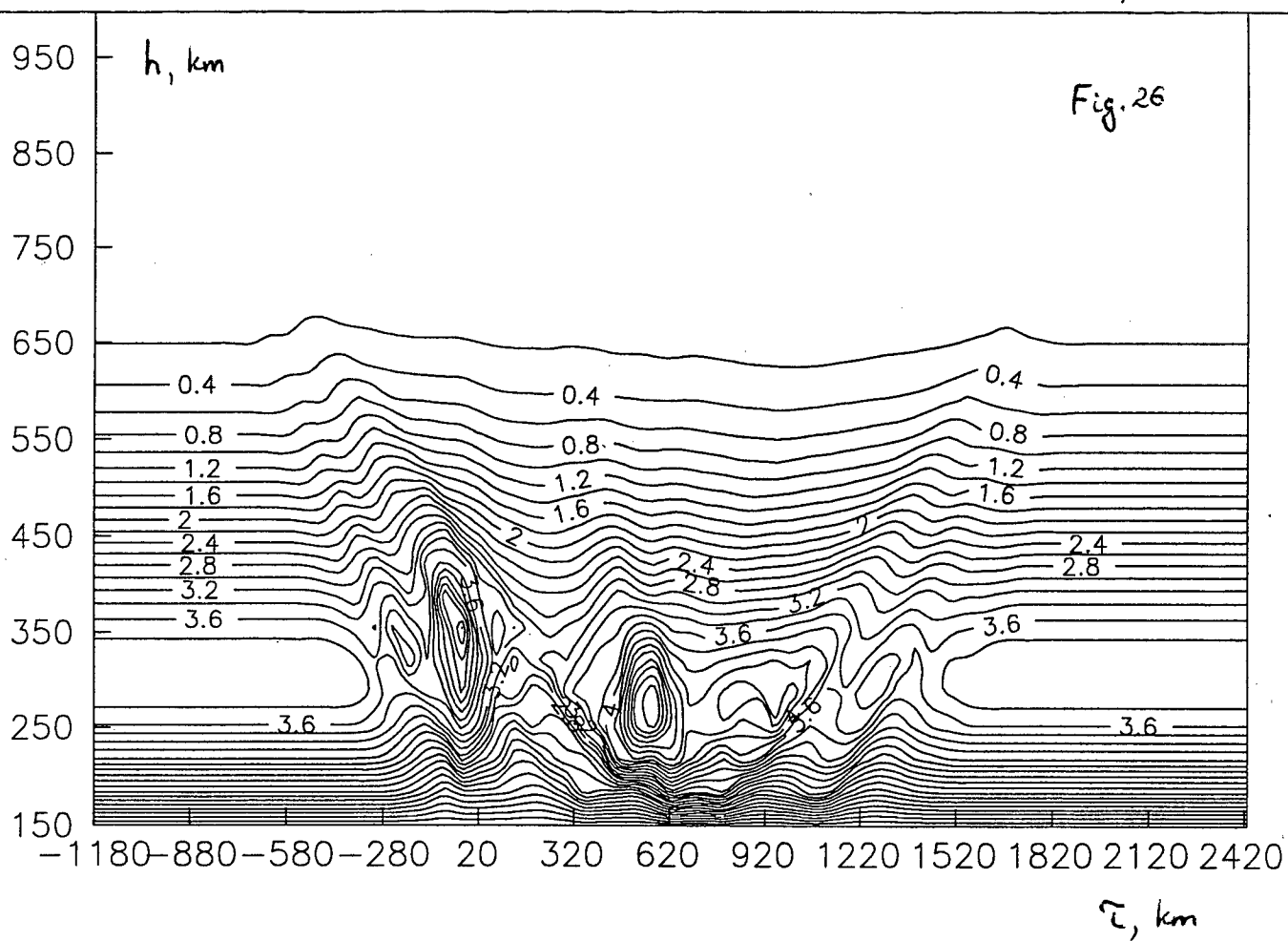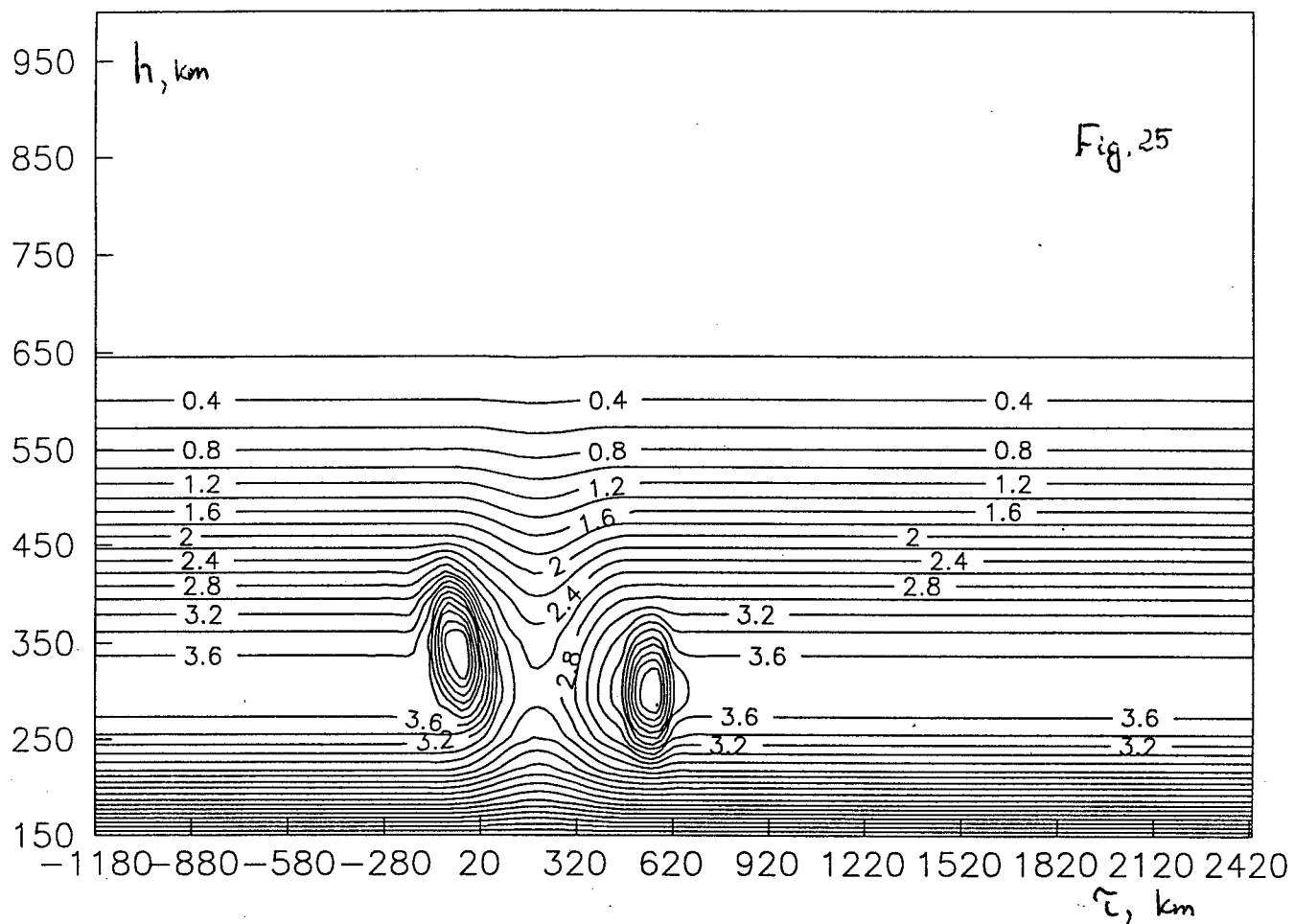
There ixist a lot of variants of solution of linear RT problem, which give different results. To illustrate the solution of nonlinear RT problem it is correct to use the same method in a case of linear RT, to make it possible to distinguish the difference between linear and nonlinear RT for our analysis. In the following examples, the method C of building the operators of direct problem was used. (C is built with the linear product approximation). The use of other methods of building the operators of direct problem, the same for linear and nonlinear case, gives the same results. Here, to solve the RT problems, the phase 9 and phase-difference or Doppler (10) approach will be used. Though the use of phase approach over TEC is appeared to be unperspective (we repeatedly criticized this method), however, here, it is usefull to cite the results of the influence of refractable corrections on both approaches.
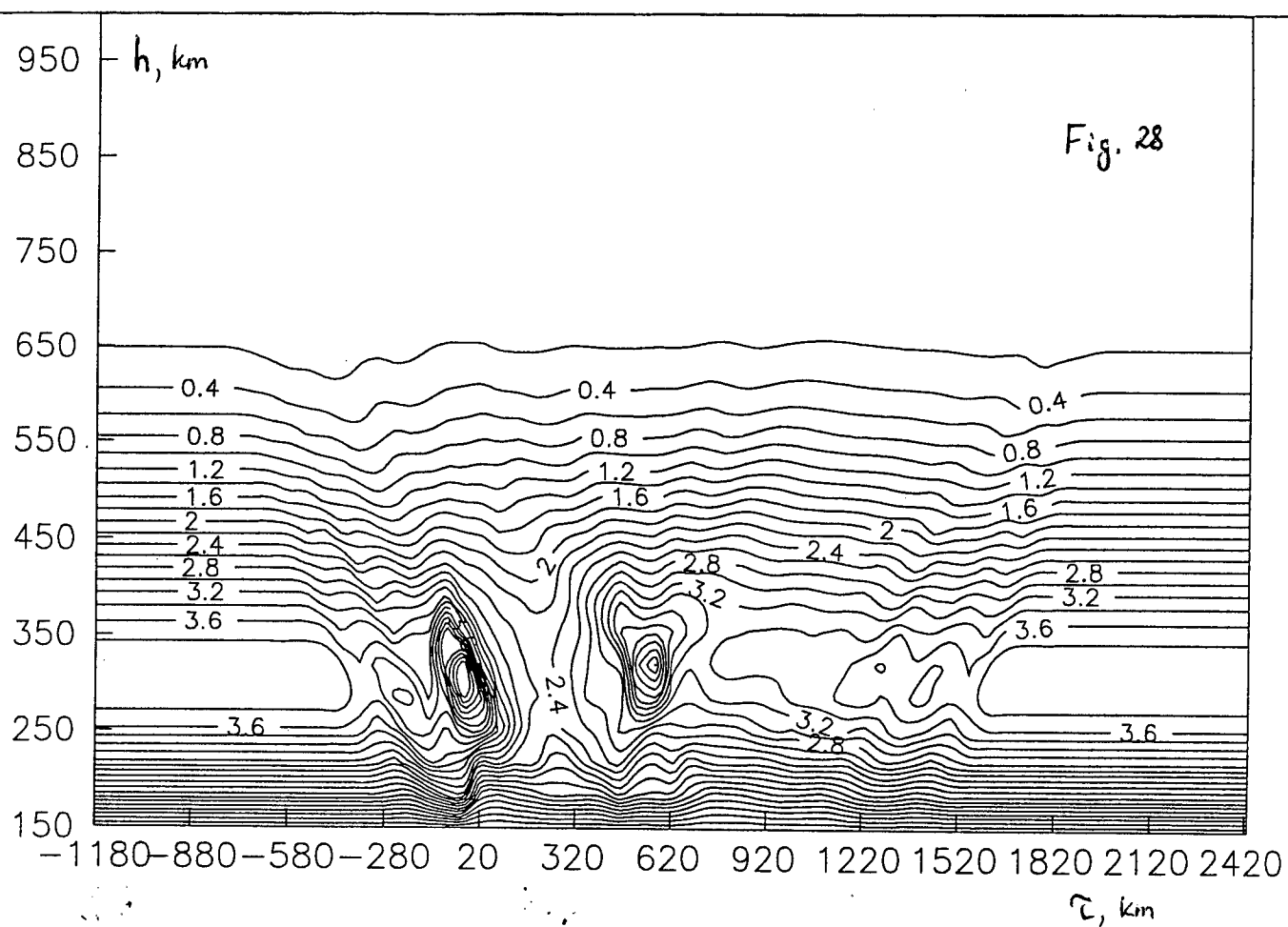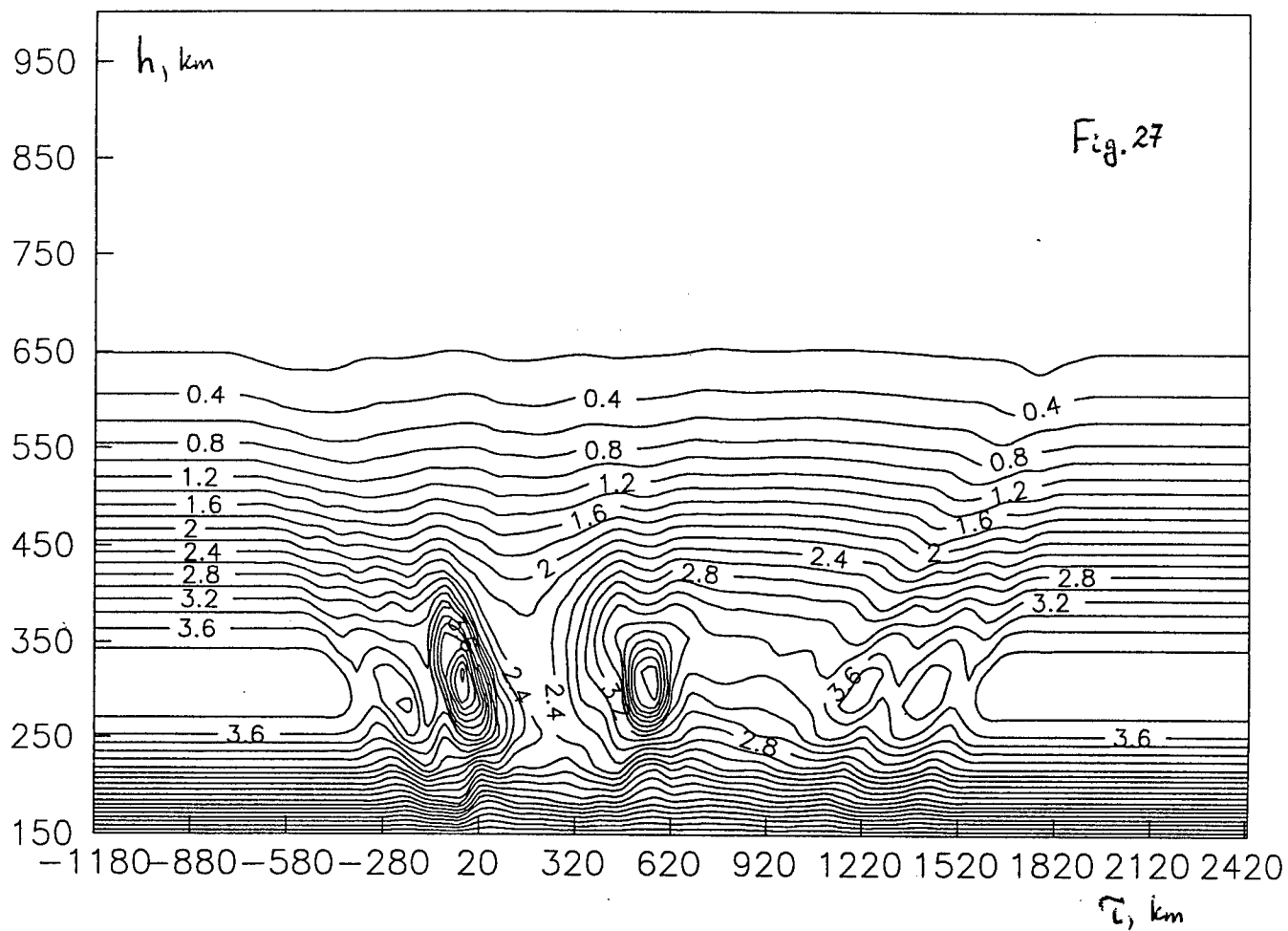
To estimate the power of the influence of refractable corrections on the solution of RT problems we will use several simple ionospheric models. It is obvious, that the qualitative sight of the influence of refractable corrections on the solution of RT problems slightly depends on the model, and it (sight) is determined mainly by the parameter $a\Delta N / f^2$ (9,10) which characterizes the variations of electron density.

As a first model, the model of quasilayered ionosphere with a trough and two irregularities on the border of the trough (fig.25), with maximum of electron density equal to $5*10^{12} m^{-3}$ (f=150 Mhz) was used. Phase curvatures of this model were already cited in the previous section (fig.19-34). Fig.26-28 show the radiotomographic reconstruction results of given model: fig.26 - reconstruction by linear RT method,

fig.27 - reconstruction by nonlinear RT method after the first stage, fig.28 - reconstruction by nonlinear RT method after the second stage. It is notable that the reconstruction quality became better. This is also demonstrated by reconstruction mistakes, for example, for linear RT the mistakes $(\delta_2 = 12.4\%$ and $\delta_\infty = 37.9\%$), and for nonlinear RT after the first stage $(\delta_2 = 8.4\%$ and $\delta_\infty = 20.8\%)$. Also the congruence of the magnitude of electron density maximum for nonlinear case 5.08 (in units $10^{12} m^{-3}$) against 5.59 in linear case is essentially better. This essential improvement of reconstructions is not amasing, because the operator approximation of direct problem essentially improves at high electron density $\Delta N \approx 5*10^{12} m^{-3}$ with the use of nonlinear RT approach (fig.21-24). In a case of lower electron density $\Delta N \approx 0.5*10^{12} m^{-3}$ the operators approximation of direct problem are closed for linear and nonlinear RT (fig.19-20) and the solution results of inverse problem practically coincide.

As a second ionospheric model the model of quasiwave structure on the background of the layered ionosphere (fig.29) with electron density maximum $3*10^{12} m^{-3}$ was used. On such maximum level the results of RT reconstructions by linear and nonlinear RT methods are closed, however the mistakes in nonlinear case $(\delta_2 = 9.5\%$ and $\delta_\infty = 24.4\%)$ are slightly less that the linear case mistakes $(\delta_2 = 10\%$ and $\delta_\infty = 27.2\%)$. The closeness of RT reconstruction results is explained by quite good linear operator approximation, what is illustrated in fig.32, where the real phase is illustrated by intire line, calculated with the respect to refractable corrections and the result of product of operator (9) linear approximation and the model is illustrated by dashed line. The situations in reconstructions notably changes with the increasing of electron density maximum of quasiwave structure to $5*10^{12} m^{-3}$ (fig.33). The difference between linear and nonlinear RT now is becoming more essential. The reconstruction quality received by means of linear RT method is not satisfying: in fig.34 it is difficult to guess where the quasiwave structures are $(\delta_2 = 13.4\%$ and $\delta_\infty = 32.5\%)$. The result of the first stage of nonlinear RT reconstruction is cited in fig.35, the second stage in fig.36. Seen is, with the use of nonlinear RT approach the situation became notably better, what is demonstrated by the reconstruction mistakes $(\delta_2 = 8.19\%$ and $\delta_\infty = 24.4\%)$ after the first stage, $(\delta_2 = 8\%$ and $\delta_\infty = 24\%)$ after the second stage. In the last case the difference between linear (dashed line in fig.37-38) and nonlinear (entire line, which practically coincides with real phase) approximation is more essential compared with the less
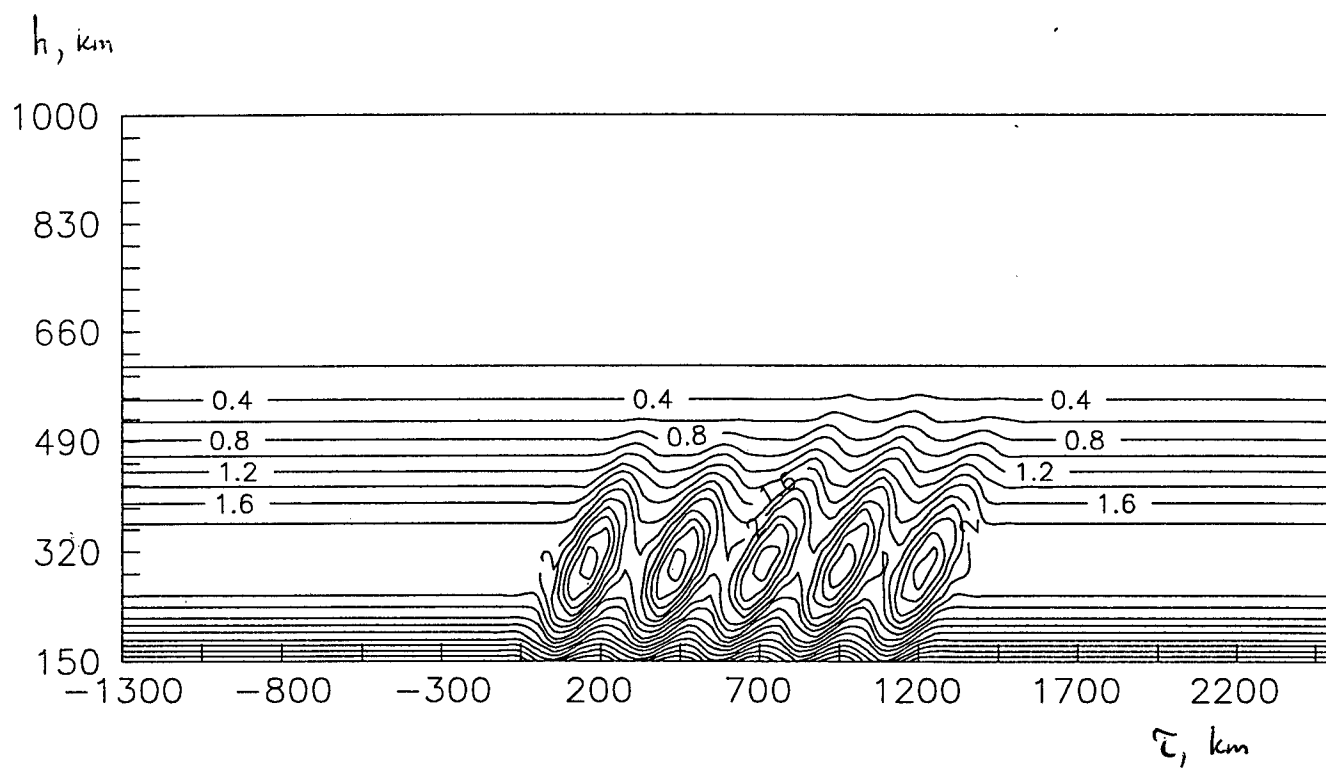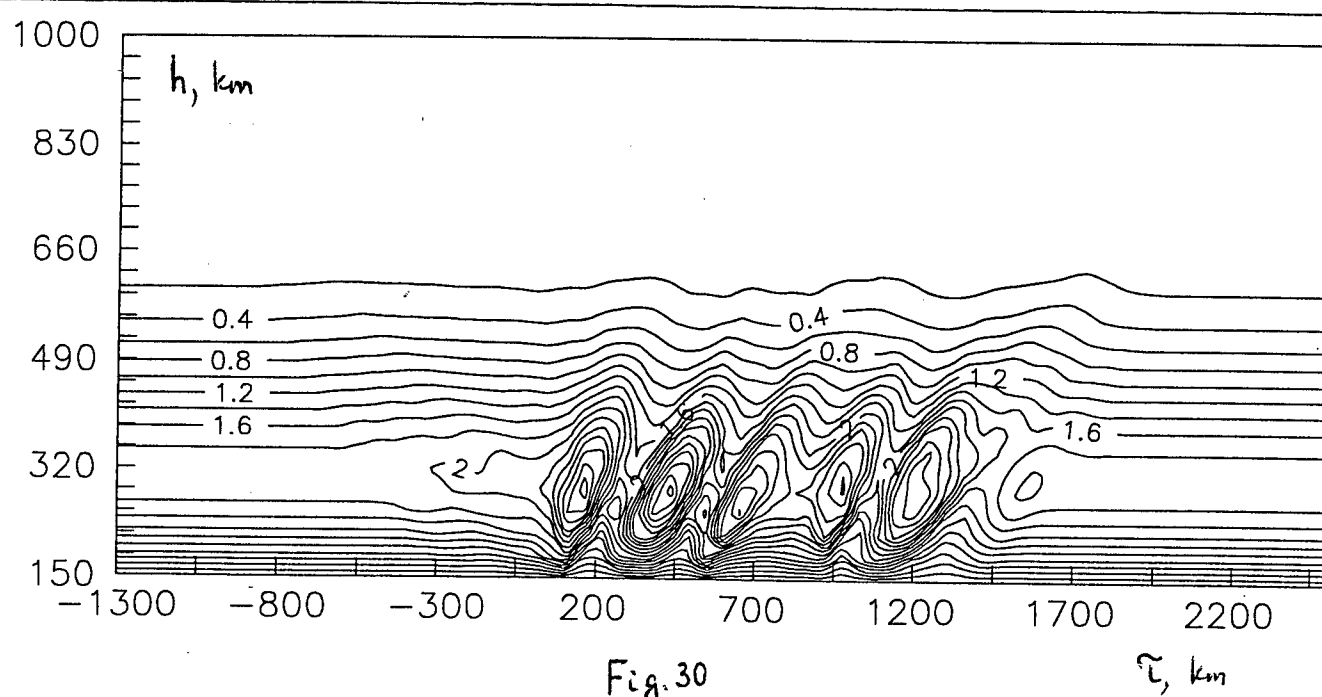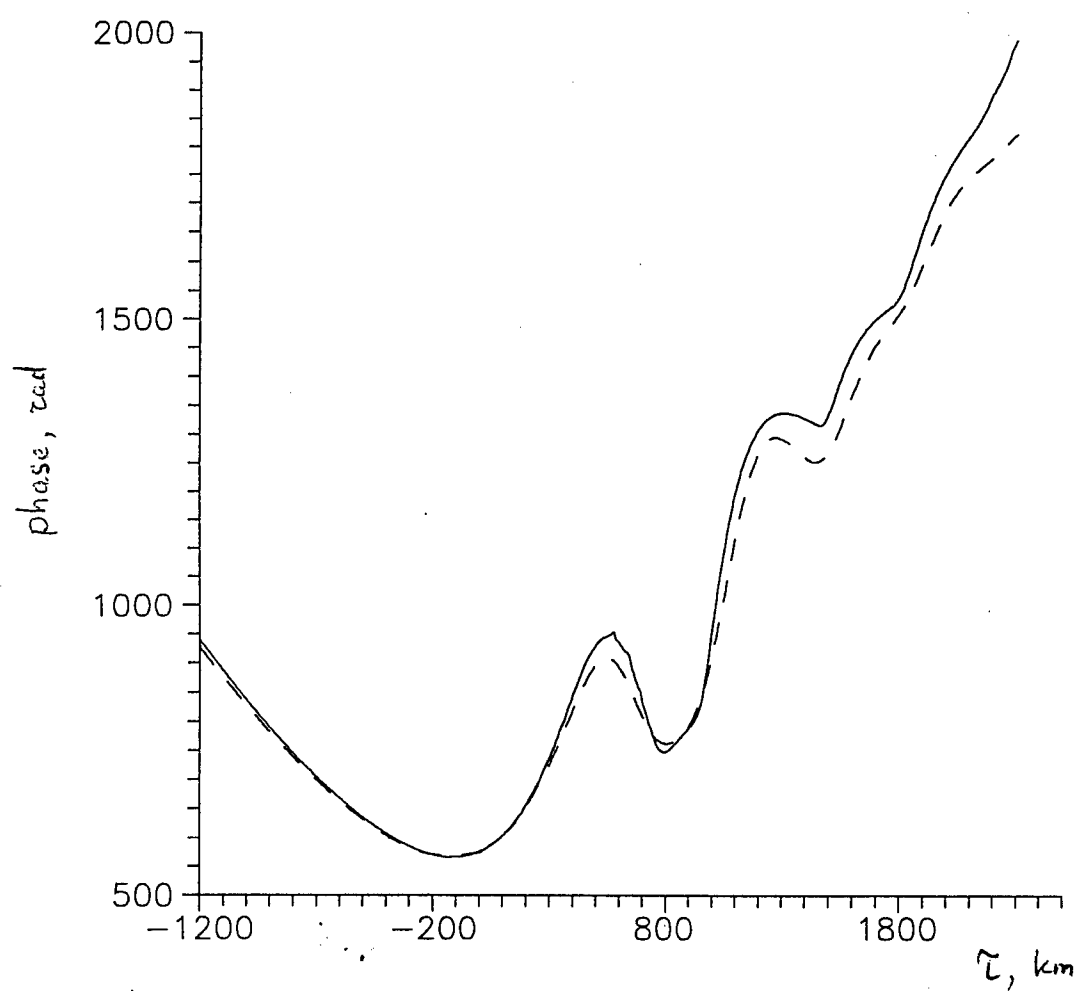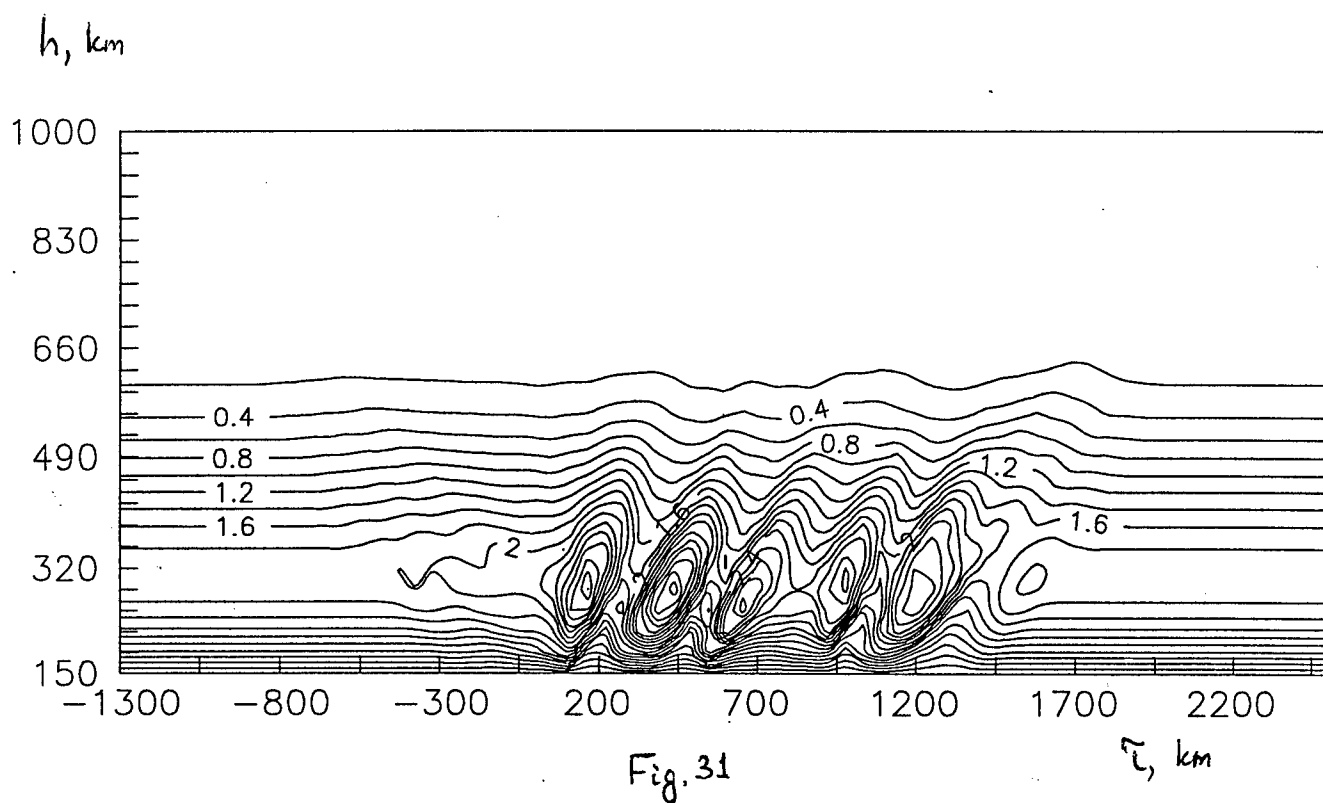
Fig. 25

Fig. 26

Fig. 27

Fig. 28

Fig. 29

Fig. 30

h, km

Fig. 31

phase, rad

Fig. 32

Fig. 33

Fig. 34

Fig. 35

Fig. 36

Fig. 37

Fig. 38

maximum, what is seen well in fig.37-38, where this difference is cited for first two receivers.

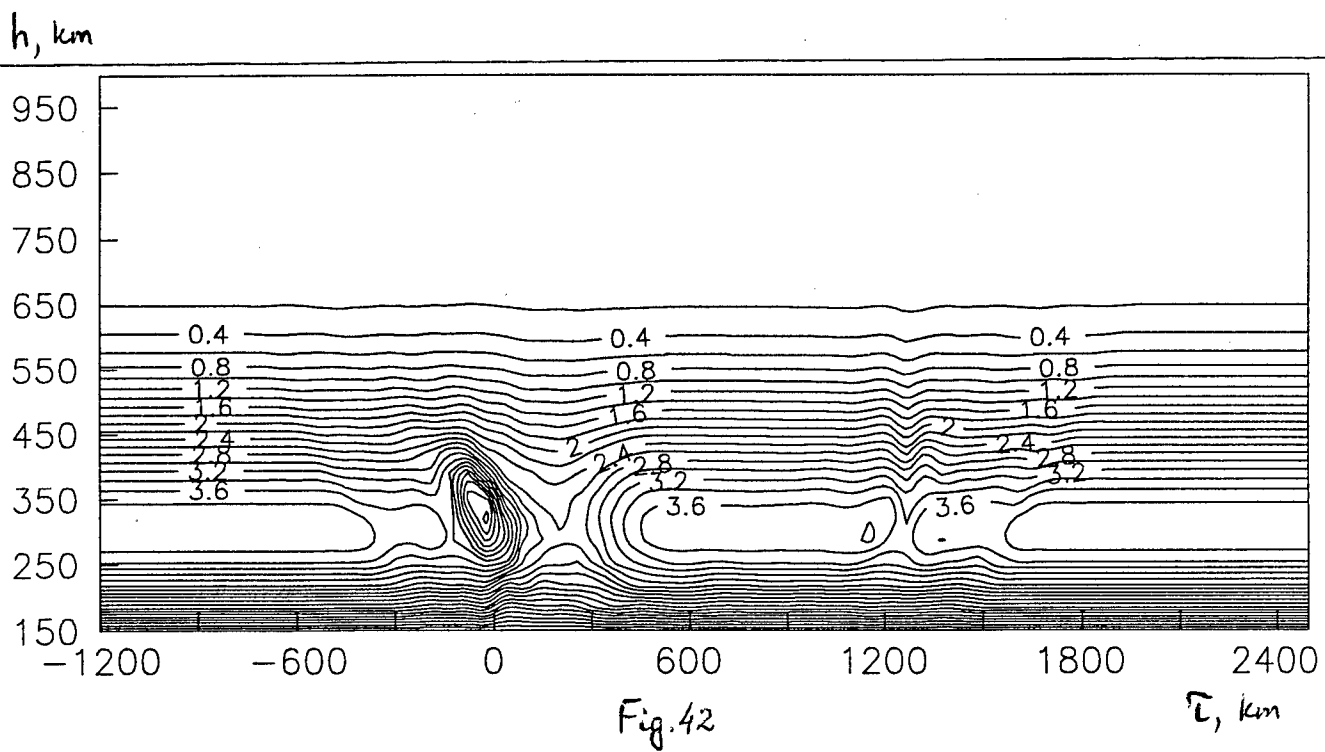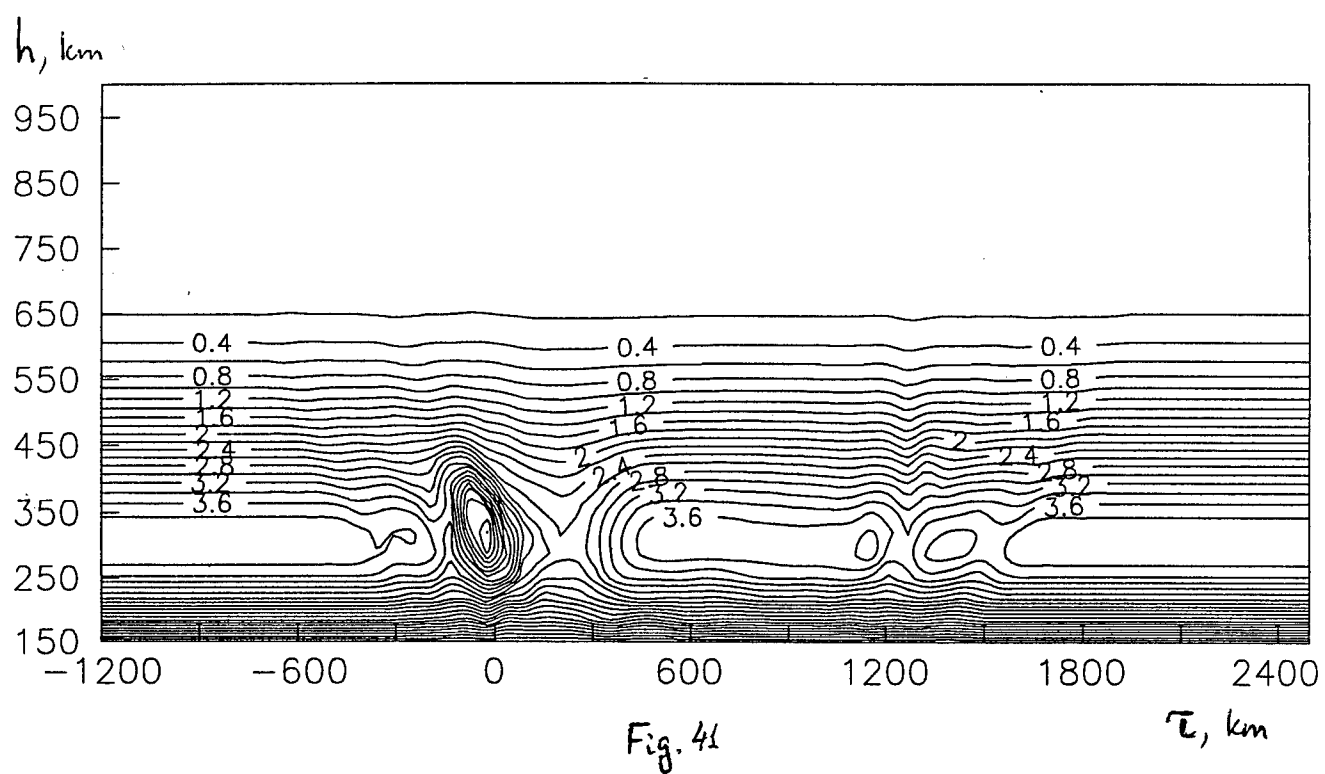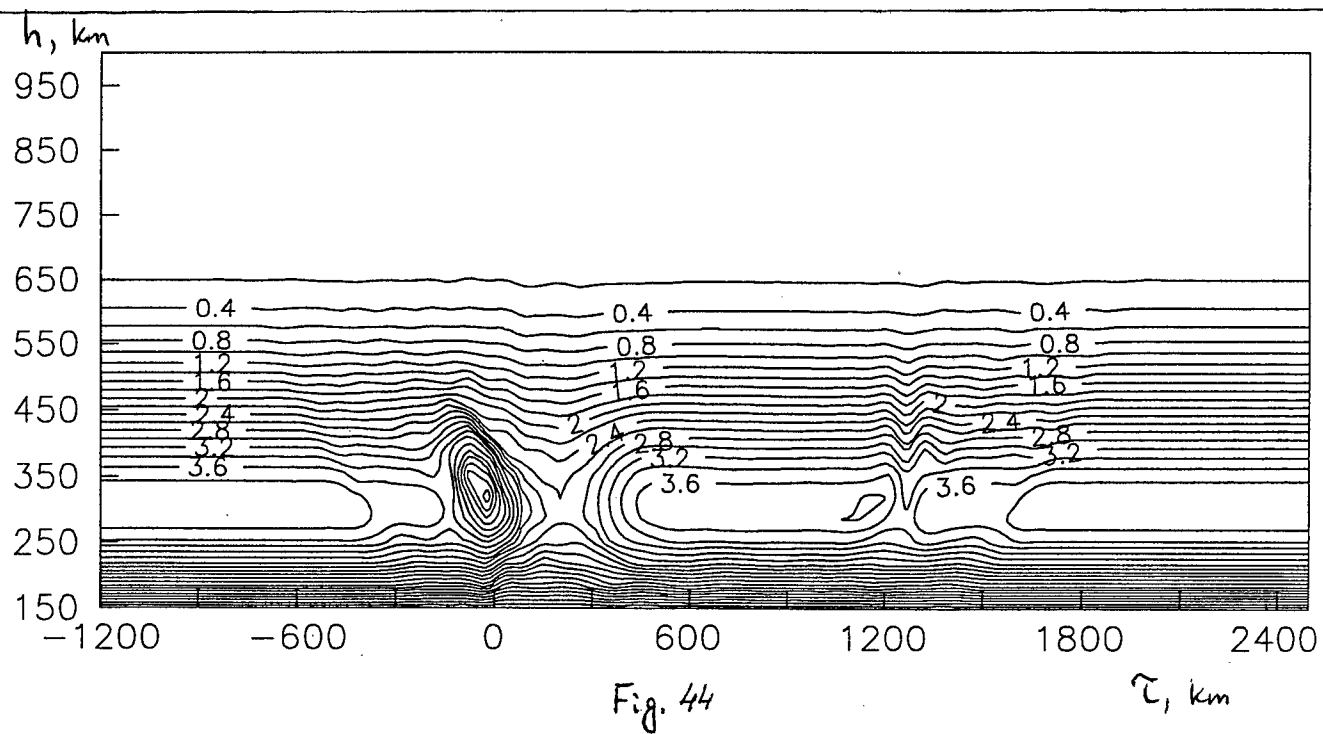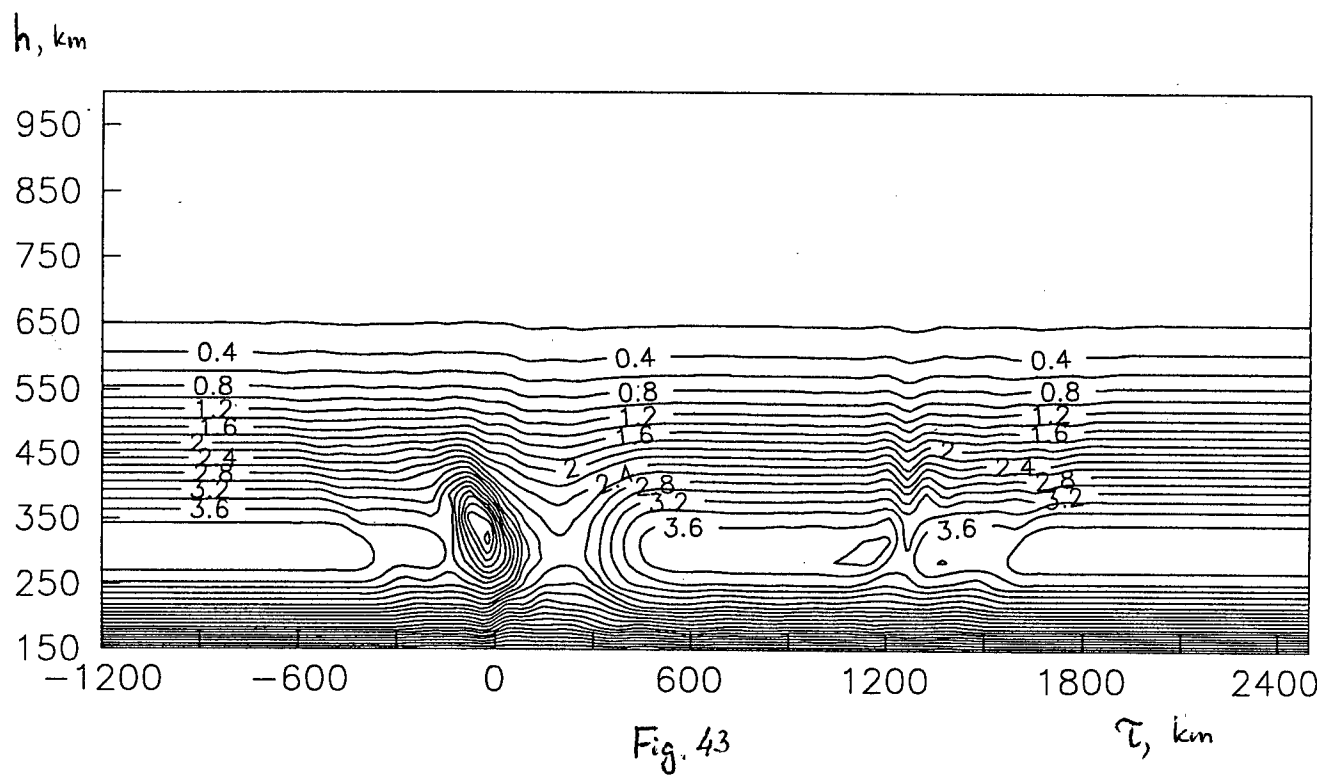The results, cited earlier, are related to reconstructions over phase and TEC. As it would be seen lower, the same results in a meaning of influence of refractable corrections, are obtaining also under the reconstruction over phase difference (TEC or Doppler difference). In fig.39 shown is the following ionospheric model with a trough, possitive irregularity from the left border of trough and negative irregularity from the right . The lower reconstruction quality in linear approach according to phase measurings ($\delta_2 = 12.7\%$ and $\delta_\infty = 38.4\%$) is illustrated by fig.40, where strong artefacts and distortions do not allow to select initial irregularities. The use of sequential stages of nonlinear RT method over phase differences gives better results: I stage (fig.41, $\delta_2 = 9.3\%$ and $\delta_\infty = 46.5\%$), II stage (fig.42, $\delta_2 = 9.18\%$ and $\delta_\infty = 48.8\%$), III stage (fig.43, $\delta_2 = 9.1\%$ and $\delta_\infty = 46.7\%$), IV stage (fig.44, $\delta_2 = 9.12\%$ and $\delta_\infty = 46.8\%$),. The use of three stages is enough here as the quality improvement doesn't take place with the following stages. The use of Doppler method essentially improves the reconstruction results both in linear and nonlinear cases, what is explained by higher sensitivity [25] of difference Doppler method. The Doppler reconstruction results are given in fig.45 (linear case, $\delta_2 = 7\%$ and $\delta_\infty = 20\%$) and fig.46 (nonlinear case, $\delta_2 = 5.6\%$ and $\delta_\infty = 19\%$) , where high reconstruction quality is seen well.

The last fourth model which illustrates the nonlinear RT methods is shown in fig.47. It is a quite complete structure with a trough and four irregularities (two "positive" $\tau \approx 0km, \tau \approx 1300km$ and two "negative" $\tau \approx -50km, \tau \approx 1000km$). Such combinations of "positive" and "negative" irregularities, overlaping each other for different receivers, usually are the most difficult for RT reconstructions. The electron density level is supposed to be high enough $\Delta N \approx 5*10^{12} m^{-3}$, to make refractable effects exhibit notably. The result of RT reconstruction by the linear Doppler RT method is shown in fig.48. ($\delta_2 = 7.8\%$ and $\delta_\infty = 18.7\%$). Here, the possitive irregularities are seen well, but the negative practically are not exhibited. The results of RT reconstruction made by nonlinear Doppler RT method are much better, the are shown in fig.40 (after the first stage $\delta_2 = 6.5\%$ and $\delta_\infty = 16.5\%$) and in fig.41 (after the second stage $\delta_2 = 5.5\%$ and $\delta_\infty = 13.8\%$). The attention should be payed to quite high reconstruction quality in fig.41, where the main qualitative pecularities of reconstructed structure are exhibited well. Let us note that here and earlier during the step by step RT reconstruction only small quantity of iterations 2-4
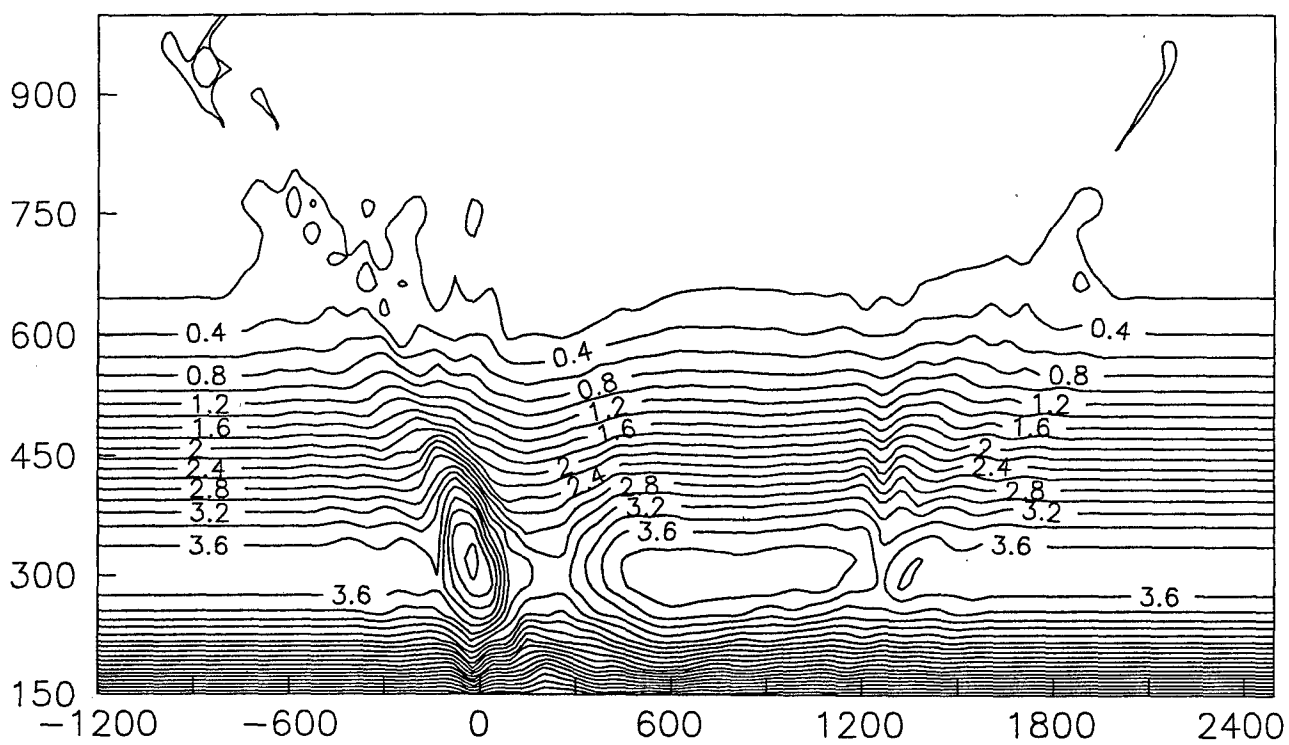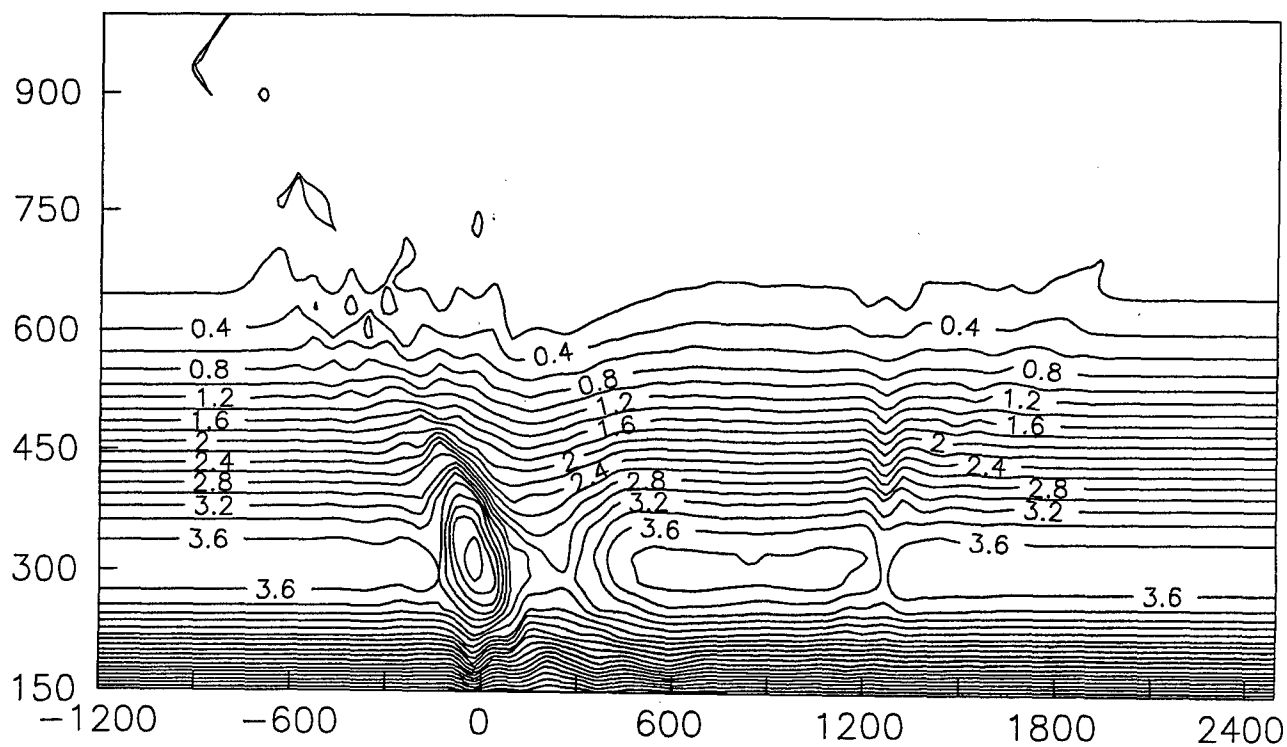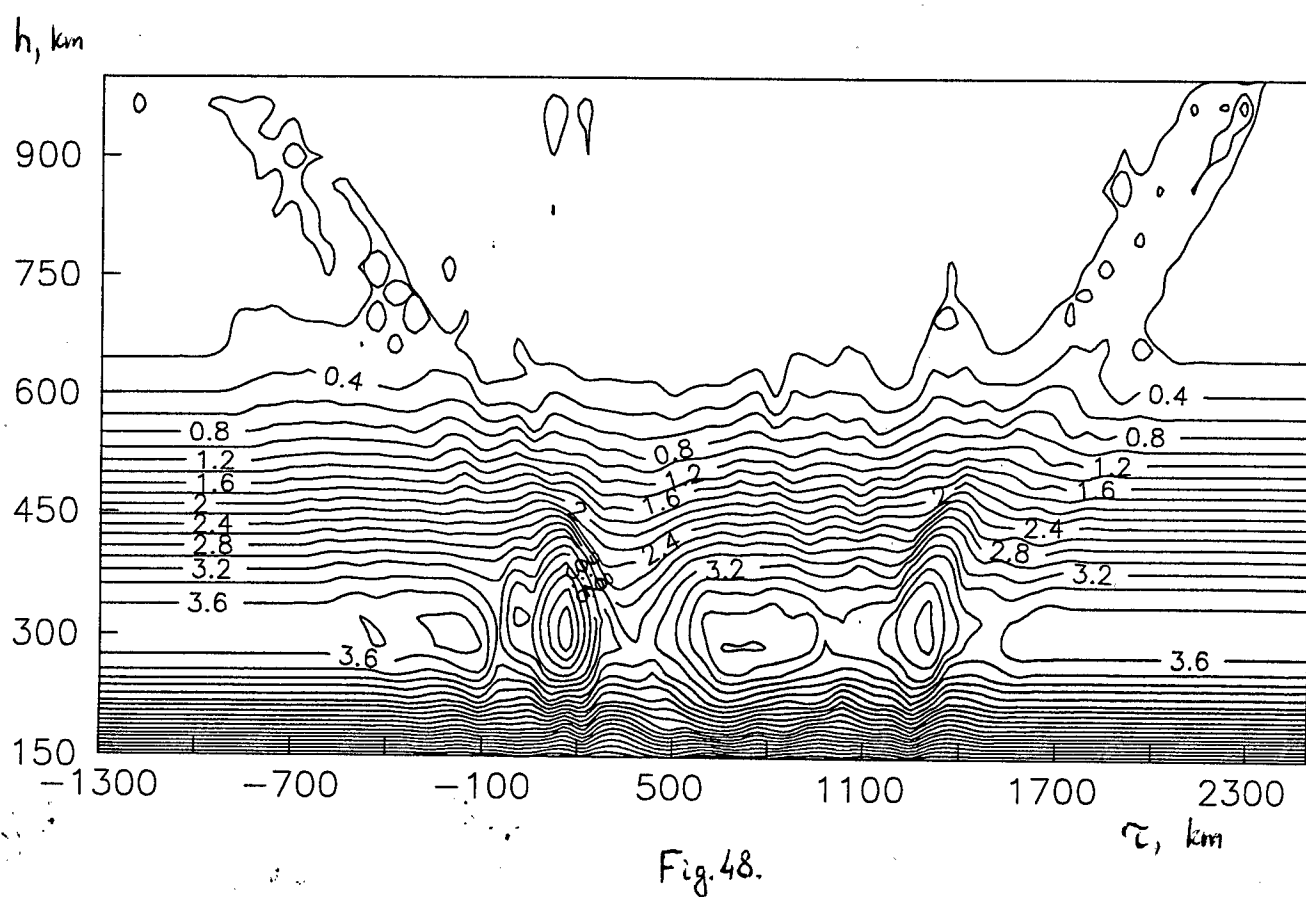
Fig. 39

Fig. 40

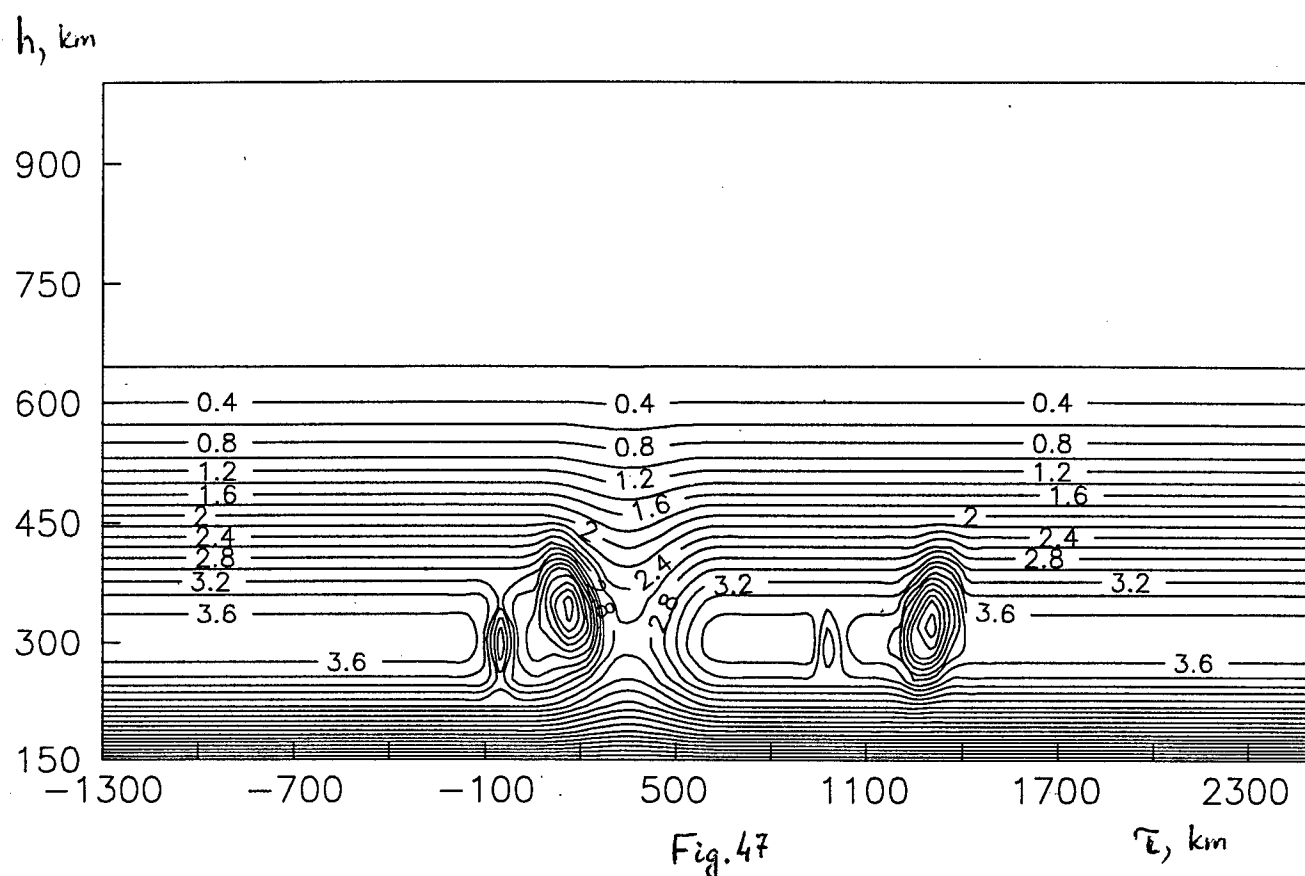Fig. 41

Fig. 42

Fig. 43

Fig. 44

Fig. 45

Fig. 46

Fig. 47

Fig. 48.

Fig.49

Fig.50

93

Fig. 51

Fig. 52

by ART and MART methods were used. The mistake , compared with the mistake of operator approximation sould be left in the first part of equations (9-10). Than, if we increase the iteration quantity and dicrease the mistake in the right part (the mistake according to data I or D) the solution will go away from the real and they (solutions) will diverge. Than the matrix operator calculation for the next stage will have the large mistakes and the sequential stage will not lead to the improvement of results. However such a small iteration quantity gives usually good coincidence of the right part of equations (9-10). As an example, let us cite the result of comparison of Doppler frequencies for the second and the third receivers after only the two iterations of the second stage (relative mistakes of Doppler frequencies $\delta_2 = 11\%$ and $\delta_\infty = 24\%$). F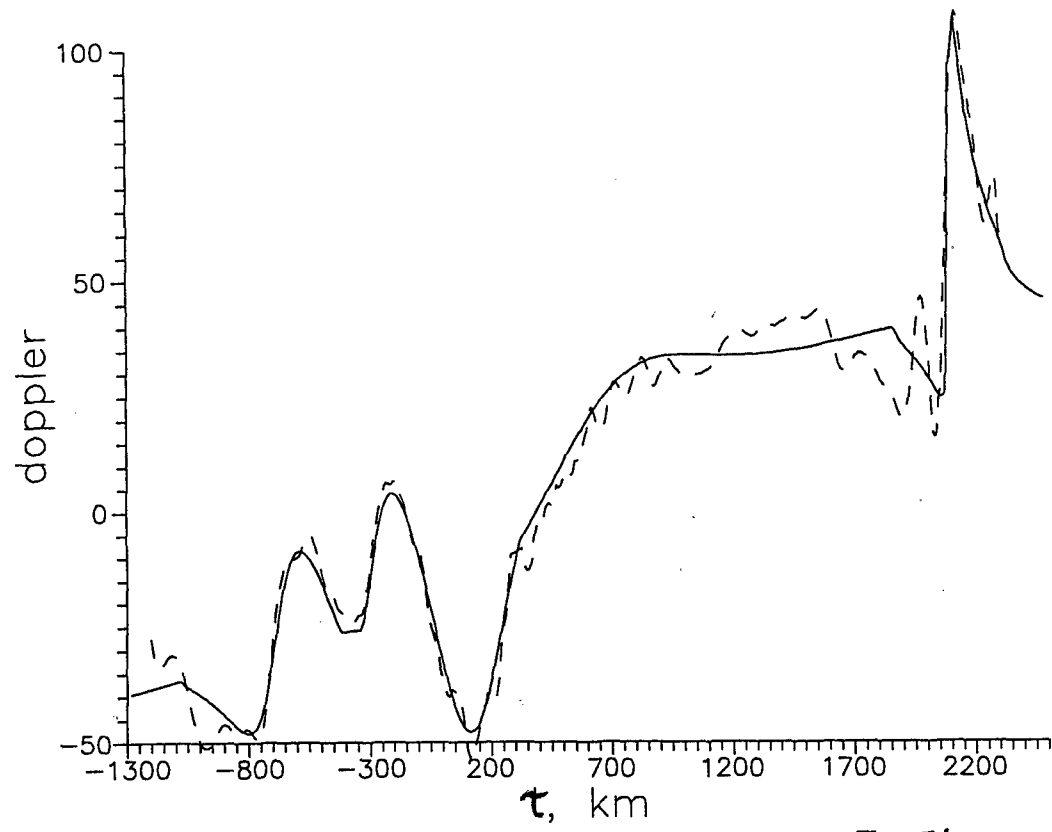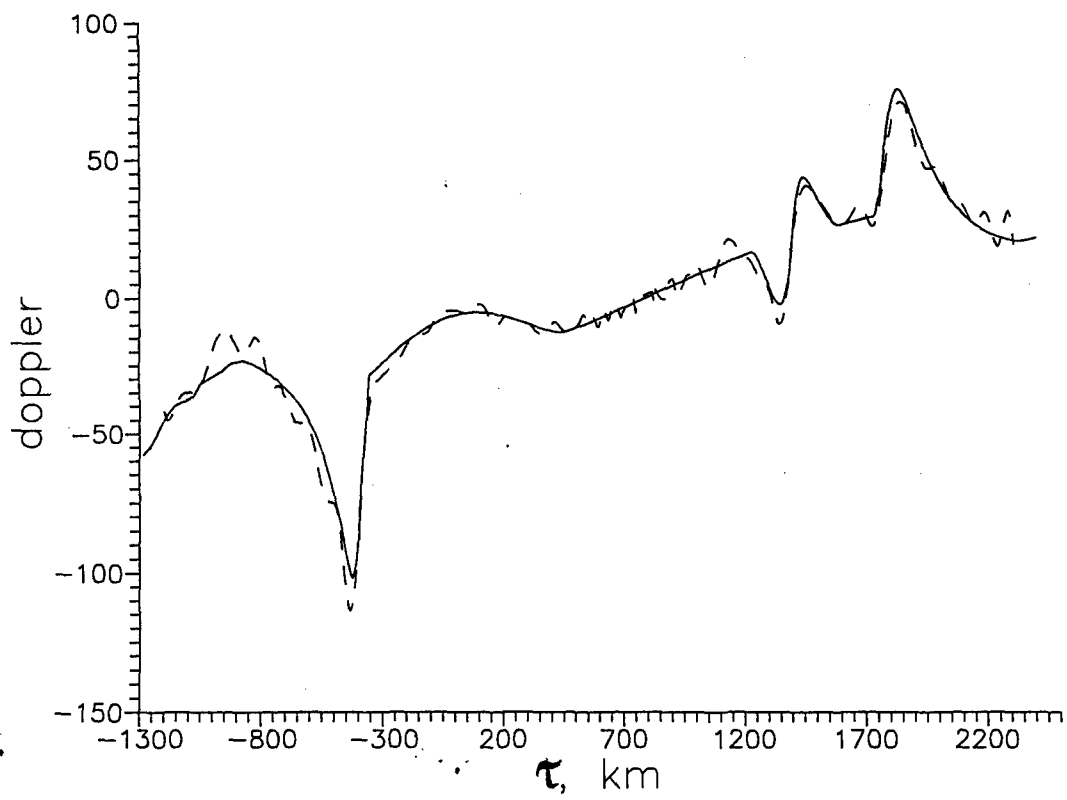ig.51 and fig.52 show the real Doppler frequencies for by entire line, and Doppler frequencies after RT reconstructions from fig.50 - by dashed line.

Generally it should be stated that the refractable effects becomes essential when the deflection of refractable rays from direct becomes comparable with the size of element digitization in RT problem. The deflections of refractable rays are determined mainly by electron density difference ΔN. On the probing frequencies equal to hundreds of MHz, usually, the refraction is ignored for $\Delta N \leq 1*10^{12} m^{-3}$ and for size of element digitization more than 20 km. The refraction should be respected for large $\Delta N \geq (2-4)*10^{12} m^{-3}$, for example, in the years of solar activity, and also for probing on frequencies equal to 50-100 MHz. More precise estimations , for intermediate cases, can be obtained from 6-8, and also by computer modelling with the help of programs presented here.

Description of the program for solution of inverse problem Nonlinear RT

Program <slv_nl.for>

This program solves inverse problem for TEC, Phase or Phase-difference RT by means of different algorithms: ART, MART, SIRT. It calculates errors of reconstruction in metric C and L2 in dependence upon data errors and noises.

Input parameters and files.

When staring program, you may choose the type of RT measurements

Answer = 1 - Phase RT: Tec_ph = 1 ---> TEC measurements

Tec_ph = 2 ---> Phase measurements

Answer = 2 : Phase-difference RT

Answer, Tec_ph are input from the screen

NF, NR - number of discrets on the horizontal and vertical grid

NREC - number of receivers

'F_MOD' - input file of model structure (program <dir_rth1.for>)

'F_X0' - input file of initial guess

(program <dir_rth1.for> or function <guess>)

'Fparam' - input file with parameters of matrix

XIST - model structure from input file 'F_MOD'

File 'name_F.slv' containes Nrec lines with names of input and output files.
The example of this file is enclosed.

line 1 - name of file with parameters of matrix (Fparam)

line 2: name1 - name of input file with matrix

name2 - name of input file with either TEC or TEC-difference

('Finput')

name3 - name of output file with results of multiplications

of input matric and reconstructed structure ('Fout')

line Nrec+2: name of file with number of all rays which cross

the corresponding discret of model

line Nrec+3: name file with model, name file with guess,

name file with reconstruction

line Nrec+4: name file with errors

Npi - array of contants (2pn) for each receiver

er_n - level of noise in %

Npi, er_n are input from the screen

Nsolve - the method of solution, it is input from the screen

REL - array of relaxation parameter

LMAX - max number of nonzero matric elements for each receiver

AZ - array of nonzero matric elements for all receivers

NST - array of corresponding column nonzero matric elements for

all receivers

LST - array of number of all rays which cross the

corresponding discret of model (SIRT algorithm) from

input file <F_ST>, it is similar to LST in program <mat_nl.for>

Niter - number of iterations, it is input from screen

Subroutine <DEFSYS> - solution of linear system equations for

one ray.

Subroutine <ercl2> calculates errors in metric C and L2

Subroutine <VMINM> calculates min and max of array

Function <RAN> calculates random values in [0,1]

Function <GUESS> - for initial guess

RMAX, RM, Zmax, ZSM, B1, B2 - parameters for function <GUESS>

Output files:

File <F_REC> - file with the reconstruction

File <er_solv> - errors of right items and reconstruction in
            metric C and L2

Files <Fout> - results of multiplications of the matric
            and reconstructed structure

Execution

mf77 slv_nl.for -ol -486

RUN

ndprun slv_nl.ltl

References

1. Kunitsyn, V.E., E.D.Tereshchenko, E.S.Andreeva, A.V.Galinov, and M.A.Filimonov, Radiotomography of global ionospheric structures, Polar Geophys.Inst. Press, Apatity, No.90-10-78,pp. 1-30, 1990 (in Russian).

2. Andreeva, E.S., A.V.Galinov, V.E.Kunitsyn, Yu.A.Melnichenko, E.D.Tereshchenko, M.A.Filimonov, and S.M.Chernyakov. Radiotomographic reconstruction of ionization trough in the plasma near the Earth, J.Exp.Theor.Phys. Lett., 52, 145-148, 1990.

3. Kunitsyn, V.E., and E.D.Tereshchenko, Tomography of the Ionosphere, Moscow, Nauka, 1991 (in Russian).

4. Saenko,Y.S., I.I.Shagimuratov, A.N.Namgaladze, G.A.Yakimova, H.S.Hatsvalyan, O.V.Biryukov, and V.I.Kuzin, Reconstruction of electron density distribution in the ionosphere based on the tomographic processing of satellite radio signals, Geomagnetism and Aeronomy, 31, 558-561, 1991.

5. Pryse, S.E., and L.Kersley. A preliminary experimental test of ionospheric tomography, J.Atm.Terr.Phys., 54, 1007-1012, 1992.

6. Andreeva, E.S., V.E.Kunitsyn, and E.D.Tereshchenko. Phase difference radiotomography of the ionosphere, Annales Geophysic., 10, 849-855, 1992.

7. Klobuchar, J.A., P.F.Fougere, and P.H.Doherty. The Promise and the Potential Perils of Ionospheric Tomography, Abstracts IEEE/AP-S Symposium, London, Canada, 544, 1992.

8. Kunitsyn, V.E., and E.D.Tereshchenko. Radio Tomography of the Ionosphere, Antennas Rropagation Magazine, 34, 22-32, 1992.

9. Pryse, S.E., L.Kersley, D.L.Rice, C.D.Russell, and I.K.Walker, Tomographic Imaging of the ionospheric mid-lalitude trough, Annales Geophys., 11, 144-149, 1993.

10. Kunitake, M., M.Hayakawa, K.Ohtaka, T.Tanaka, H.Ishibashi, K.Igarashi, T.Ono, A.Morioka, and H.Oya. Ionospheric Tomography campaign May-July 1992 in Japan,Abstracts of XXIV Gen. Assem. of the URSI, Kyoto, 330, 1993.

11. Oraevsky, V.N., Y.Y.Ruzhin, V.E.Kunitsyn, E.S.Andreeva, A.Kh.Depueva, E.F.Kozlov, O.G.Razinkov and I.I.Shagimuratov, Radiotomographic sections of subauroral ionosphere along Moscow-Arkhangelsk trace, Institute of Terrestrial Magnetism, Ionosphere and Radio Wave Propagation Press, Preprint No. 100 (1047), 1993.

12. Raymund, T.D., S.E.Pryse, L.Kersley, and J.A.T.Heaton, Tomographic reconstruction of ionospheric electron density with European incoherent scatter radar verification, Radio Science, 28, No. 5, 811-817, 1993.

13. Kunitsyn, V.E., E.D.Tereshchenko, E.S.Andreeva, B.Z.Khudukon, and T.Nygren. Investigations of the Ionosphere by Satellite Radiotomography, Int. J. Imaging Syst.Techn., 5, No.2, 112-127, 1994.

14. Foster, J.C., M.J.Buonsanto, J.A.Klobuchar, J.M.Holt, P.Fougere, W.A.Pakula, T.D.Raymund, V.E. Kunitsyn, E.S.Andreeva, E.D.Tereshchenko, and B.Z.Kudukon. Russian-American Tomography Experiment, Int. J. Imaging Syst.Techn., 5, No. 2, 148-159, 1994.

15. Bust, G.S., J.A.Cook, G.R.Kronschnabl, C.J.Vasicek, and S.B.Ward. Application of ionospheric tomography to single site location range estimation, Int. J. Imaging Syst.Techn., 5, No.2, 160-168, 1994.

16. Pakula, W.A., D.N.Anderson, M.Beaudet, et al., Initial Total Electron Content Results from the Pan American Ionospheric Tomography Campaign, Proceedings of the Beacon Satellite Symposium, Aberystwyth UK, 266-269, 1994.

17. Oraevsky, V.N., V.E.Kunitsyn, Y.Y.Ruzhin, et al., Radiotomographic sections of subauroral ionosphere along Moscow-Arkhangelsk trace, Geomagnetism and Aeronomy, 35, 117-122, 1995.

18. Wells D., N.Beck. D.Delikaraoglou et al., Guide to GPS Positioning, Canadian GPS Assotiates, 1986.

19. Dixon T.H., An Introduction to the Global Positioning System and some Geological Applications, Reviews of Geophysics, 29, 249-276, 1991.

20. Wanninger L., Sardon E., Warnant R., et al., Determination of the Total Electron Content with GPS - Difficulties and their Solution, Proceedings of the International Beacon Satellite Symposium, Aberystwyth UK, 13-16, 1994

21. Wilson B.D. and Mannucci A.J., Instrumental Biases in Ionospheric Measurements derived from GPS data, in Proc. of the ION-GRS 93 Conference, Institute of Navigation, Salt Lake Sity, Utah, 1343-1351, 1993.

22. Hajj G.A., Ibanez-Meier R., Kursinski E.R., Romans L.J., Imaging of the Ionosphere with the Global Positioning System, Int. J. Imaging Syst.Techn., 5, No. 2, 174-184, 1994.

23. Klobuchar J.A., Doherty P.H., Bailey G.L., Davies K., Limitations in Determining Absolute Total Electron Content from Dual-Frequency GPS Group Delay Measurements, Proceedings of the International Beacon Satellite Symposium, Aberystwyth UK, 1-4, 1994.

24. Snow R.W., Romanowski P., Doherty P.H., Klobuchar J.A., A Comparison of Ionospheric Total Electron Content Measurements with Code and Codeless GPS Receivers, Proceedings of the International Beacon Satellite Symposium, Aberystwyth UK, 17-20, 1994.

25. Kunitsyn, V.E., E.S.Andreeva, O.G.Razinkov, and E.D.Tereshchenko. Phase and Phase-difference Ionospheric Radio Tomography, Int. J. Imaging Syst.Techn., 5, No. 2, 128-140, 1994.

26. Raymund T.D., Comparisons of Several Ionospheric Tomography Algorithms, Proceedings of the International Beacon Satellite Symposium, Aberystwyth, UK, 49-51, 1994

27. Fremouw, E.J., B.M.Howe, J.A.Secan, and R.M.Bussey. Simulation Results from a Tomographic Processor Emplying the WDLS Formulation of Discrete Inverse Theory, Proceedings of the International Beacon Satellite Symposium, Aberystwyth UK, 172-175, 1994

28. Solimeno, S., B. Crosignani, P. Diporto, Guiding, Diffraction and Coonfinement of Optical Radiation, Academic Press, Inc., 1986.

29. Kravtsov, Yu., Yu. Orlov. Geometrical Optics of Inhomogeneous Media, Springer-Verlag, 1993.